Summer 2005

Active Control of Large Amplitude Nonlinear Free Vibrations and Nonlinear Supersonic Panel Flutter of Beams and Composite Plates Using Piezoelectric Self-Sensing Actuators

Qinqin Li
Old Dominion University

ACTIVE CONTROL OF LARGE AMPLITUDE NONLINEAR FREE VIBRATIONS AND NONLINEAR SUPERSONIC PANEL FLUTTER OF BEAMS AND COMPOSITE PLATES USING PIEZOELECTRIC SELF-SENSING ACTUATORS

by

Qinqin Li
B.E., July 2002, Civil Aviation University of China, Tianjin, P. R. China

A Thesis Submitted to the Faculty of
Old Dominion University in Partial Fulfillment of the
Requirement for the Degree of

MASTER OF SCIENCE

AEROSPACE ENGINEERING

OLD DOMINION UNIVERSITY
August 2005

Approved by:

Chuh Mei (Director)

Jen-Kuang Huang

Brett Newman

ABSTRACT

ACTIVE CONTROL OF LARGE AMPLITUDE NONLINEAR FREE VIBRATIONS AND NONLINEAR SUPERSONIC PANEL FLUTTER OF BEAMS AND COMPOSITE PLATES USING PIEZOELECTRIC SELF-SENSING ACTUATORS

Qinqin Li
Old Dominion University, 2005
Director: Dr. Chuh Mei

This thesis employs a coupled structural-electrical finite element modal formulation for the control of nonlinear free vibrations, and supersonic panel flutter of beams and composite plates with and without thermal environment. Multiple modes of the nonlinear free vibration and supersonic panel flutter are considered in the closed loop simulations. Two different controllers are designed and investigated. The first one is the output feedback controller comprised of a Linear Quadratic Regulator (LQR) and an Extended Kalman Filter (EKF). EKF considers the nonlinear state space matrix and has a gain sequence evaluated on-line. Thus the LQR/EKF nonlinear controller has more accurate state estimation over Linear Quadratic Gaussian (LQG) controller for the nonlinear dynamics. The second controller is the output feedback adaptive LQR/EKF controller. This adaptive controller includes a modal frequency identification and state estimation algorithm. Lead Zirconate Titanate (PZT5A) is used to suppress the free vibration. PZT5A and another piezoelectric actuator: Macro Fiber Composite (MFC) are used to suppress supersonic panel flutter. The placement of actuators is based on two approaches: one is the norm of optimal feedback control gain matrix (NFCG) method and the other is H_2 norm. The placement of piezoelectric

sensors is based on the Kalman Filter feedback estimation gain (NKFEG) method. Based on the locations of both actuators and sensors, placement of self-sensing actuators is realized. Numerical simulations show that the LQR/EKF controller is hard to suppress limit cycle oscillations (LCO) for nonlinear free vibrations. The adaptive LQR/EKF gives good control for the nonlinear free vibrations, even with unknown sudden changes. Three types of responses for the nonlinear panel flutter at supersonic speeds and elevated temperatures are studied. They are the LCO, chaos and static thermal post-buckling deflections. The LQR/EKF is effective to control all the responses.

ACKNOWLEDGEMENTS

I would like to express my deepest thanks to my advisor, Dr. Chuh Mei, who gave me excellent guidance and never ending encouragement. His insight, illumination and patience provided a key role throughout my work and made the whole research a true pleasure. I would also like to give my sincere thanks to the other members of my thesis committee: Dr. Jen-Kuang Huang and Dr. Brett Newman. Their useful suggestions and valuable comments improved the thesis and are much appreciated. I am grateful for all the faculty and staff members in Aerospace Department, and also the financial support from the department.

I also extend my thanks to Dr. Xinyun Guo and Dr. Mohammed Salim Azzouz, as they helped me a lot in nonlinear structural modelling and programming.

Last, but not the least, special thanks go to my parents and my boyfriend, Mr. Hong Zhang, for their everlasting love and support, and for always encouraging me to do my best.

TABLE OF CONTENTS

LIST OF TABLES

LIST OF FIGURES

NOMENCLATURE

$\{a\}, \{b\}$	generalized coordinates
$[A], [B], [D]$	inplane, coupling and bending stiffness matrix
$[B_\phi]$	electric field & electric potential relationship matrix
$\{d\}$	piezoelectric charge constant
$[d]$	stress constant
D_{ik}	electric displacement
$[e]$	piezoelectric strain constant
E, E_1, E_2, E_p	Young's modulus
E_{ik}	electric field
g_a	nondimensional aerodynamic damping coefficient
G, G_{12}, G_p	shear modulus
$[g], [G]$	element and system aerodynamic damping matrices
$[\bar{G}]$	modal aerodynamic damping matrix
h	beam or composite plate thickness
$[k], [K]$	element and system stiffness matrices
$[K_{lin}]$	combined system linear stiffness matrix
$[k1], [k2]$	element first-order and second-order nonlinear incremental
$[K1], [K2]$	combined system first and second order nonlinear stiffness matrices
$[K_w]$	combined system linear stiffness matrix
$[\bar{K}]$	modal linear stiffness matrix
$[\bar{K}_{qq}]$	modal nonlinear stiffness matrix

L	beam or composite plate length
M_∞	free stream Mach number
$[m], [M]$	element and system mass matrices
$[\bar{M}]$	modal mass matrix
$\{N\}, \{M\}$	force and moment resultant vectors
$n1, N1$	element and system first-order nonlinear incremental stiffness matrices
$n2, N2$	element and system second-order nonlinear incremental stiffness matrices
P_a	aerodynamic pressure
$\{p_\phi\}, \{P_\phi\}$	element and system electric force vectors
q	dynamic pressure
$\{q\}$	natural modal coordinate vector
$[Q]$	lamina reduced stiffness matrix
$[\bar{Q}]$	transformed lamina reduced stiffness matrix
T	temperature
$[T]$	transformation matrix
u, v	inplane displacements
V	airflow velocity
$\mathbf{V}, \mathbf{V_i}$	electrical potentials
w, W	element and system nodal displacements
x, y, z	Cartesian coordinates
z_k	Cartesian coordinates due to thickness of the kth layer

α	coefficient of thermal expansion (CTE)
β	$\sqrt{M_\infty^2 - 1}$
Δ	increase value
$\{\varepsilon\}$	strain vectors
$[\epsilon]$	permittivity matrix
ϕ	fiber orientation angle
$\{\phi\}, \{\Phi\}$	element and system eigenvector
$\{\bar{\phi}\}$	modal electric force vector
$[\Phi]$	system eigenvector matrix
$\{\kappa\}$	bending curvature vector
λ	nondimensional dynamic pressure
μ	air-panel mass ratio
$\nu, \nu_1, \nu_2, \nu_{12}, \nu_{21}, \nu_p$	Poisson's ratio
$[\Theta]$	slope matrix
ρ, ρ_p	mass density
$\{\sigma\}$	stress vector
ω	frequency

Subscripts

a	air
b	bending
cr	critical
m	membrane / composite matrix
NB	stiffness matrices due to $\{N_b\}$

Nm	stiffness matrices due to $\{N_m\}$
$\Delta Tb, \Delta Tm$	stiffness matrices due to $\{N_{\Delta T}\}$
u, v, w	in-plane and transverse displacements
ΔT	thermal
ε	strain
ϵ	dielectric permittivity
σ	stress

CHAPTER I

INTRODUCTION

I.1 Motivations

There are two main parts in this thesis. One is adaptive control of nonlinear free vibration, the other is active control of supersonic panel flutter with or without thermal environment. The first part is a learning process of active control of nonlinear vibration, and it is also a preparation for the second one. As a self-excited, dynamic instability phenomenon, panel flutter is often encountered in the supersonic and hypersonic flight vehicles, which can lead the fatigue failure of the skin panels. Suppression of panel flutter has been paid much attention in the past 40 years. Aerodynamic heating also affects the panel flutter of high speed flight vehicles. Under thermal loads, the surface panel may be subjected to flutter at lower critical dynamic pressure; large temperature increase may also cause large thermal deflections. And such thermal deflection of the skin panel may change the configuration of the vehicles, which leads to poor flight performance. So it's necessary that thermal effects are considered in panel flutter suppression.

In most literatures, panel flutter caused by only the aerodynamic pressure is discussed. Limit Cycle Oscillation (LCO) will occur beyond the critical dynamic pressure. Suppression of the LCO has been discussed by Zhou et al. [1, 2]. Under thermal effects, three types of responses are considered: LCO (including periodic motions), chaotic and static thermal post-buckling deflections. LCO (including periodic motions) has been successfully controlled in many literatures [1–4]. Suppression

of the latter two responses are seldom discussed. This thesis will research the suppression of the chaotic motions and static thermal post-buckling deflections with Linear Quadratic Regulator (LQR) and Extended Kalman Filter (EKF). Successful suppression results of all the three responses will be shown later.

I.2 Survey of Literature

I.2.1 Nonlinear Vibration of Beams

The active control of vibration of flexible structure has important applications in engineering especially in aerospace and automotive fields. Most literature used linear or nonlinear control method for a linear model. However, nonlinearity is easily included due to large elastic motion, which influences the structure tremendously but has been seldom considered in controls. The first literature in large amplitude vibration of beam can be traced to Woinowsky-Krieger [5], who considered the free vibration of a simply supported beam with axial force, which introduced a nonlinear cubic term into the Euler-Bernoulli equation of the beams. Using a single-mode approach and the elliptic function, the relationship between displacement amplitude and ratio of nonlinear frequency to natural frequency was obtained. Chu and Herrmann [6] used the perturbation method and the principle of energy conservation to solve the nonlinear free vibration of simply supported plates and compared their results with the elliptic function approach. Srinivasan [7,8] employed the Ritz-Galerkin technique to obtain the algebraic equation of nonlinear free and forced vibrations of simply supported beams and plates, then used Newton and Bigradient Matrix method to get the numerical solution. Ray and Bert [9] supplied three different methods to

investigate the nonlinear free vibration of a simply supported beam: Assumed Space Mode (ASM), Assumed Time Mode (ATM) and Ritz-Galerkin method. Bennett and Eisley [10] used a three-mode Galerkin method to analyze large amplitude motion of a beam with clamped ends. Pandalai and Sathyamoorthy [11] obtained the modal equations for the nonlinear vibrations of beams by Lagrange's Equation.

After all these classic methods, finite element method gradually was employed in this area. Mei [12–14] presented finite element analysis for nonlinear vibrations of beams and plates, obtained remarkable agreement with the results of Burgreen [15] and Srinivasna [7], Chu and Herrmann [6], Evensen [16], experimental data. Nayfeh, Mook and Lobitz [17] developed a numerical-perturbation method for the nonlinear analysis of beam vibrations by using finite-difference or finite-element techniques to solve linear spatial problem, and the method of multiple scales to solve nonlinear temporal problem. Since the former work didn't consider the inplane effects, when using Rayleigh-Ritz Method to get the frequency-amplitude relationship of vibrations of slender beams, thin circular and rectangular plates, Raju et al. [18] included the inplane modes into the analysis and found that inplane inertia is negligible but the inplane deformation is to reduce the nonlinearity. Then Bhashyam and Prathap [19] presented a Lagrange-type and a Galerkin finite element approach for studying the nonlinear vibrations of clamped-clamped and simply supported beams with immovable ends. They neglected the inertia terms due to inplane displacement u, using a condensation procedure to eliminate u and obtain matrix equations in transverse displacement w alone. Then the eigenvalue problem can be examined for the behavior of w alone. In 1994, Srirangarajan [20] presented two methods: multiple scales and the ultra-spherical polynomial approximation procedure to solve nonlinear free

vibrations of simply supported uniform beams, comparing with another nine previous methods [21–23]. Then in 1997, Shi et al. [24] presented a time-domain multiple modal formulation based on the finite element method for large-amplitude free vibration of thin composite plates. They found that finite element method is able to obtain the Duffing-type modal equations more easily than the classic continuum partial differential equations (PDE) and Galerkin's method. They concluded that for simply supported beams, the single-mode solution is accurate; for beams with other support condiyions, multiple modes are needed.

I.2.2 Nonlinear Vibration of Plates

For the plate, Chlandi [25] first studied plate vibrations experimentally in 1787. She observed nodal patterns on square plates at their natural frequencies. Then many studies followed. For large amplitude nonlinear vibration of the plate, von Karman [26] first considered the inplane effect and give an analytical solution for a simply supported plate. Then there are many approximation methods [27] derived in this area. Mei [13] was the first one who applied finite element method in the problem. Especially for the geometrically nonlinear behavior of composite plates, Vhuen-Yuen Chia [28] gave a good review in 1988. Shi et al. [24] presented a time-domain multiple modal formulation based on the finite element method for large-amplitude free vibration of thin composite plates. Recently Alhazza and Alhazza [29] gave a review on the recent progress in plate and shell vibrations. Most recently, Harada and Yamada [30] used finite element method to derive reduced-order nonlinear modal equations of plates, and they obtained dominant nonlinear in-plane pseudo-modes by an approximate approach using the Newton-Raphson method. Saha et al. [31] formed the

large amplitude nonlinear free vibration of isotropic plate by a variational method, then solved the corresponding static problem first through an iterative scheme using a relaxation parameter, and solved the dynamic problem as a standard eigenvalue problem.

I.2.3 Active Control of Vibration

Mostly, active vibration controllers can be designed in terms of the two description of vibration: modal modes and wave motion. Generally, modal control aims to control the global behavior of the structure, while wave control aims to control the flow of vibrational energy through the structure [32]. There are lots of literatures for wave control [32–34]. However, when wave control efficiently suppressed vibration on one parts, global response of the control may introduce vibration on other parts since wave control did not consider the global motion of the structures. To avoid the drawback of the wave control, modal control becomes another interesting method. Although modal control may have the main disadvantage, spillover, with the appearance of smart structures, the problem can be manageable. Currently, modal control has been realized by many methods. Meirovitch et al. [35] compared coupled control and independent control methods for flexible system by using pole placement and linear optimal control techniques, showing that independent control is superior than coupled control by offering a larger choice of control techniques and requiring less computational efforts. Inman [36] extended independent modal space control to non-conservative structures. Later he [37] also explained although independent control is attractive, sometimes it will be difficult to get, because the model is an approximation, and the effect of controller on the unmodeled modes, that is, the spillover

needs to be considered. Then he also applied smart structures to give two solutions to the problem. Above methods mainly used pole placement as control techniques. Actually, other techniques were also implemented in modal control. Meirovitch et al. [35] also used linear optimal control technique by solving Riccati equation for the steady-state case. Zhang [38] analyzed the optimal vibration control problem by using the natural second-order form of the equations of motion, then obtained optimal rectangular control feedback matrices by solving a set of linear differential equations but not nonlinear Riccati equation. Robust control also is used in this area. Wang and Huang [39] designed an H-infinite controller with the model error compensator to suppress the beam vibration, and the framework of the control algorithm is still the independent modal space control. Xie el al. [40] used H-infinite control method to suppress the low-frequency modal vibration of the thin plate covered with a controllable constraint, and rejected the modal spillovers. For the application of adaptive control in the field, Abdel-Motagaly and Mei [41] used adaptive feedback linearization to control the nonlinear free vibrations of a simply supported beam modeled in a single-mode, and they had a better result than linear controller (LQR and H-infinite). Yu and Zhang [42] applied an adaptive backstepping design to synchronize two uncertain chaotic systems including a duffing oscillator. Last but not the least, intelligent control algorithm are taken into this topic as well. de Abreu and Ribeiro [43] proposed an on-line self-organizing fuzzy logic controller to control of vibrations in flexible structures. This method minimized the role of human experience by updating the rule base using self-organizing procedure. Later they [44] presented a design of adaptive fuzzy controller for the control of the same objects. Based on Lyapunov's stability theory, they synthesize a stable adaptive system. Both methods

have been verified effectively in experiments of steel cantilever test beams. Hossain et al. [45] used Genetic Algorithm (GA) and Adaptive Neuro-Fuzzy Inference system to develop mechanisms of the active control of a flexible beam in transverse vibration. Significant level of vibration cancellation has been achieved with these methods in the tests. In this research, sudden changes of the frequency for some unknown reason will be considered for the free vibration control case. An LQR/EKF controller with system identification will still suppress such vibration successfully.

I.2.4 Piezoelectric Sensor and Actuator

To realize active control, sensors and actuators are the necessary parts of the whole control system. Recently, smart structures have been broadly used as the part. Piezoelectric material is the most commonly used one in the field. At first, monolithic piezoelectric elements such as PZT, PLZT, PVDF are used to control vibration of beams [46–50] and plates [51–54]. Recently, piezoelectric fiber composite materials such as the 1-3 Composites, Active Fiber Composites (AFC), Macro Fiber Composites (MFC) have been developed [55–57]. With the fiber-reinforced composite nature, and interdigitated electrodes, they could increase actuation authority, flexibility and the ability to impose twisting deformation onto a structure. Many applications of these piezocomposite materials have been presented [58–60]. In fact, piezoelectric materials not only can be used as actuators or sensors in vibration active control, but also, can combine both functions on one device, that is self-sensing actuator, which is perfectly collocated and can be effectively modelled and implemented in vibration suppression [48, 61]. To suppress vibration efficiently, the location of actuators and sensors are very important. Many methods for the optimal placement of

actuators and sensors have been developed. For example, the controllability method, including the modal controllability [62], modal and system controllability [63], spatial controllability [64], and H_∞ analytical bound approach [65]. Another classic method is the performance index method [66, 67]. Other special algorithms, such as Genetic Algorithm (GA) [68] and simulated annealing optimization algorithm (SA) [69] are also used. Most of the methods are efficient for linear models. In this thesis, both PZT5A and MFC will be applied to suppression free vibration and panel flutter with or without thermal stresses. Results will show that MFC will give better control results.

I.2.5 Panel Flutter

In 1970, E. H. Dowell [70] gave a review for the experimental and theoretical research in panel flutter. He summarized four analysis categories for panel flutter, considering nonlinearities in structural or aerodynamic theories. Then he listed five approaches in deriving the equations of motion: Galerkin's method, finite difference method, finite element method, separation of variables method and traveling wave method. Mei et al. [71] provided a comprehensive review of nonlinear panel flutter at supersonic and hypersonic speeds in 1999. They summarized five panel flutter theories and four classic analytic methods. Then they showed that using the finite element method, limitations of the classic method can be overcame and effects of aerodynamic damping, complex panel configurations and support conditions, laminated composite anisotropic panel properties, flow angularities, inplane stresses and thermal loads can be included in the formulation. In 2000, Abdel-Motagaly et al. [72] considered the acoustic excitation of nonlinear panel flutter at supersonic speeds. He gave various

results for isotropic and composite panels at many combinations of sound pressure level and dynamic pressure. In 2003, Guo and Mei [73] applied aeroelastic modes to study the nonlinear panel flutter at arbitrary supersonic yawed angle. Their results showed that, at zero or arbitrary yawed flow angle, only two aeroelastic modes or six to seven modes are needed for designing the controllers for flutter suppression instead of six or thirty six normal modes. Recently, Azzouz et al. [74] studied the nonlinear flutter of shallow shell panels under yawed supersonic flow angle using finite element method.

Since nonlinear supersonic panel flutter under thermal loads is studied in this thesis, a brief survey of panel flutter under temperature effects is provided. Mei et al. [71] gave a detailed review of the thermal effects for the nonlinear panel flutter at supersonic and hypersonic speeds. They showed there exists five types panel behaviors: flat, buckled, limited-cycle oscillation (LCO), periodic and chaotic motions. In 2001, Duan and Mei [75] analyzed the nonlinear response of the supersonic panel flutter under thermal and acoustic loads. Their results showed that only thermal and acoustic loads need to be considered for the design of surface panel under moderate sound pressure level (SPL), but all three loads including aerodynamic pressure need to be considered at high SPL. Cheng et al. [76] studied the combination of aerodynamic damping, thermal effects and flow angle on the stability boundaries of supersonic panel flutter. Their results concluded that, for isotropic square plates heated uniformly, flow angle has less effects than thermal effects, but for composite plates, flow angle can not be ignored. They also found that the interaction between the stiffening caused by temperature gradients and the softening caused by thermal expansion results in a slowly decreasing stability boundary. Recently, Cheng and

Mei [77] analyzed the thermal effects on the hypersonic panel flutter using a finite element modal method. They found that at low or moderate dynamic pressure, the fluttering panel under thermal effects evolves into chaos by the period-doubling route, but at high dynamic pressure, it takes the intermittent transitions route.

I.2.6 Suppression of Panel Flutter

For the suppression of panel flutter, the review of Mei et al. [71] listed that the optimal control, the rate feedback control and the active compensation of aerodynamic stiffness (ACAS) control are the main active control methods to suppress the linear and nonlinear panel flutter. Most passive control methods induce inplane loads to make the panel stiffer, then they could increase its critical dynamic pressure and suppress the fluttering. They also summarized that, for linear panel flutter, bending moment induced by piezoelectric materials is not effective since there is no bending behavior in the linear case. But for nonlinear case, bending moment is effective in flutter suppression. Sadri et al. [78] applied linear quadratic Gaussian design (LQG) controller to suppress the linear panel flutter. Rayleigh-Ritz method is used to obtain the model and the GA is used to determine the optimal locations of the piezoeletric actuators. Recently, Kim et al. [79] applied a neuroadaptive controller to suppress the flutter of a swept-back cantilevered composite panel using fiber bragg grating (FBG) sensors. The controller consisted of the neuroidentification model which is to obtain the mathematical representation of the real plant, and a neurocontroller which is to apply the real-time control of the system.

Considering the thermal effects, Zhou et al. [1, 2] applied an optimal controller to suppress the nonlinear supersonic panel flutter under uniform thermal loads. And

the papers showed good results for suppression the LCO and periodic fluttering. Moon and Kim [4] suppressed the nonlinear composite panel flutter under thermal effects with active/passive hybrid piezoelectric networks. This approach has both advantages of high performance and feedback action of active control and less control effort and more stable of passive control. Also the controller successfully suppressed the periodic fluttering. Duan et al. [80] used shape memory alloy (SMA) to suppress the supersonic panel flutter under thermal loads considering the flow yaw angle. With SMA, the critical buckling temperature for the panel can be increased, and the thermal postbuckling can be completely suppressed. Also the critical dynamic pressure is increased, then the panel flutter due to aerodynamic pressure is reduced or suppressed. Park and Kim [3] applied MFC actuators to suppress the nonlinear panel flutter under uniform temperature distribution. They showed that inplane actuation of MFC can increase critical temperature and critical dynamic pressure and decrease the large thermal deflection. And out-of-plane actuation of MFC can suppress the aero-thermal large deflection, but snap-through behavior can occur when the applied voltage reaches the critical snap-through voltage. In most of these literatures, LCO and periodic motions of panel flutter can be controlled successfully but not for chaotic motion. Panel flutter with or without thermal stresses will be suppressed in the thesis by the LQR/EKF controller. The results will show that the controller can handel both LCO and chaotic conditions. And when the number of actuators is not enough, static deflection can be obtained. With more actuators, the thermal static postbuckling deflection can be suppressed completely.

I.3 Scope of Thesis

Finite element formulations for the nonlinear large amplitude free vibrations and the nonlinear supersonic panel flutter will be developed in chap. 2. von Karman's large deflection theory is applied in the strain displacement relations. Quasi-steady first-order piston aerodynamic theory is implemented to develop the aerodynamic pressure and aerodynamic damping in the finite element formulation for supersonic panel flutter. Modal transformation is applied to obtain the modal equations of the system.

In chap. 3, state space equations of the system will be developed for the output feedback control. Several controllers will be described: Linear Quadratic Gaussian (LQG) controller, the LQR/EKF controller which is comprised of a linear quadratic regulator (LQR) and an extended Kalman Filter (EKF). The EKF uses linear approximation over every step of the iteration for nonlinear systems, then solves the Riccati equation to get the EKF gains. Thus the EKF includes nonlinearity of the system and can provide better estimation than linear Kalman Filter. A system frequency identification will be applied to provide a good start estimation value for EKF and Kalman Filter. The auto regressive exogenous (ARX) model is employed in frequency identification.

Three optimal location methods for the two types of piezoelectric actuators and sensors, PZT5A and MFC, are described in chap. 4. The three placement methods are the norm of optimal feedback control gain matrix (NFCG) method, the H_2 norm method and the norm of Kalman Filter estimator gain (NKFEG) method. The first two methods are for optimal actuator locations and the last one is for optimal sensor

placement. For all approaches, if the particular location has higher values, then this location has higher control authority or controllability.

Chap. 5 will present all the numerical results of the modelling and control for the nonlinear free vibrations. A 2-D beam and a 3-D composite plate will be studied. LQR/EKF control results will be shown. Also, before and after using the system ID, the control results will be compared. For different actuator placement methods, results will be displayed for each control object. Analysis and control results: the maximum deflection time history, phase plot, modal participation, controlled vibration and control efforts will be presented.

Supersonic panel flutter control results will be shown in chap. 6. A 2-D isotropic panel and a 3-D composite panel will be discussed. The performance of LQR/EKF controller will be presented. Control effects of different piezoelectric actuators will be compared. Also, with or without thermal stresses, supersonic panel flutter will produce different responses. Successful control results of LCO, static responses and chaotic motions will be presented here. The same results of analysis and control listed in chap. 5 for free vibrations will also be shown in this chapter for nonlinear panel flutter.

In chap. 7, conclusions, contributions and future work will be given.

CHAPTER II

FINITE ELEMENT FORMULATION

II.1 Strain Displacement Relations

The isotropic beams and rectangular plates and composite plates can be modelled by using the Bogner-Fox-Schmit (BFS) [81] C1 conforming rectangular elements. Each BFS element consists of 16 bending degrees of freedom (DOF) $\{w_b\}_{16\times1}$ and 8 in-plane DOF $\{w_m\}_{8\times1}$ as described below:

$$\{w_b\} = \{w_1\ w_2\ w_3\ w_4\ w_{x1}\ w_{x2}\ w_{x3}\ w_{x4}\ w_{y1}\ w_{y2}\ w_{y3}\ w_{y4}\ w_{xy2}\ w_{xy3}\ w_{xy4}\}^T$$

$$\{w_m\} = \{u_1\ u_2\ u_3\ u_4\ v_1\ v_2\ v_3\ v_4\}^T. \tag{1}$$

The element transverse displacement function w, and the inplane displacement functions u and v can be expressed as:

$$\begin{aligned} w &= a_1 + a_2x + a_3y + a_4x^2 + a_5xy + a_6y^2 + a_7x^3 + a_8x^2y + a_9xy^2 + a_{10}y^3 + a_{11}x^3y \\ &+ a_{12}x^2y^2 + a_{13}xy^3 + a_{14}x^3y^2 + a_{15}x^2y^3 + a_{16}x^3y^3 \\ &= [H_w(x,y)]\{a\} \\ u &= b_1 + b_2x + b_3y + b_4xy \\ &= [H_u(x,y)]\{b\} \\ v &= b_5 + b_6x + b_7y + b_8xy \\ &= [H_v(x,y)]\{b\}, \end{aligned} \tag{2}$$

where the displacement function row matrices are

$$
\begin{aligned}
[H_w(x,y)] &= \{1\ x\ y\ x^2\ xy\ y^2\ x^3\ x^2y\ xy^2\ y^3\ x^3y\ x^2y^2\ xy^3\ x^3y^2\ x^2y^3\ x^3y^3\} \\
[H_u(x,y)] &= \{1\ x\ y\ xy\ 0\ 0\ 0\ 0\} \\
[H_u(x,y)] &= \{0\ 0\ 0\ 0\ 1\ x\ y\ xy\},
\end{aligned}
\tag{3}
$$

and the generalized coordinate vectors are

$$
\begin{aligned}
\{a\} &= \{a_1\ a_2\ a_3\ a_4\ a_5 a_6\ a_7\ a_8\ a_9\ a_{10}\ a_{11}\ a_{12}\ a_{13}\ a_{14}\ a_{15}\ a_{16}\}^T \\
\{b\} &= \{b_1\ b_2\ b_3\ b_4\ b_5\ b_6\ b_7\ b_8\}^T.
\end{aligned}
\tag{4}
$$

The generalized coordinates $\{a\}$ and $\{b\}$ are expressed as:

$$
\begin{aligned}
\{a\} &= [T_b]\{w_b\} \\
\{b\} &= [T_m]\{w_m\}.
\end{aligned}
\tag{5}
$$

The von Karman large deflection theory is considered to account for nonlinear beam and plate analysis. The strain can be represented as

$$
\begin{Bmatrix} \varepsilon_x \\ \varepsilon_y \\ \gamma_{xy} \end{Bmatrix} = \begin{Bmatrix} \varepsilon_x^0 \\ \varepsilon_y^0 \\ \gamma_{xy}^0 \end{Bmatrix} + z \begin{Bmatrix} \kappa_x \\ \kappa_y \\ \kappa_{xy} \end{Bmatrix}. \tag{6}
$$

These strain vectors can be written in terms of the displacement functions as

$$
\begin{Bmatrix} \varepsilon_x \\ \varepsilon_y \\ \gamma_{xy} \end{Bmatrix} = \begin{Bmatrix} u_{,x} \\ v_{,y} \\ u_{,y} + v_{,x} \end{Bmatrix} + \frac{1}{2} \begin{Bmatrix} w_{,x}^2 \\ w_{,y}^2 \\ 2w_{,x}w_{,y} \end{Bmatrix} + z \begin{Bmatrix} -w_{,xx} \\ -w_{,yy} \\ -2w_{,xy} \end{Bmatrix}. \tag{7}
$$

Simply,

$$\begin{aligned}\{\varepsilon\} &= \{\varepsilon^0\} + z\{\kappa\} \\ &= \{\varepsilon_m^0\} + \{\varepsilon_\theta^0\} + z\{\kappa\} \\ &= \{\varepsilon_m^0\} + \frac{1}{2}[\theta]\{\theta\} + z\{\kappa\},\end{aligned} \tag{8}$$

where, the slope matrix and vector are defined as

$$[\theta] = \begin{bmatrix} w_{,x} & 0 \\ 0 & w_{,y} \\ w_{,y} & w_{,x}, \end{bmatrix} \tag{9}$$

$$\{\theta\} = \begin{Bmatrix} w_{,x} \\ w_{,y} \end{Bmatrix}.$$

The membrane strain and curvature vectors can be expressed in terms of the generalized coordinates:

$$\{\varepsilon_m^0\} = [C_m]\{b\} = [C_m][T_m]\{w_m\} = [B_m]\{w_m\}, \tag{10}$$

where

$$[C_m] = \begin{bmatrix} [H_u(x,y)]_{,x} \\ [H_v(x,y)]_{,y} \\ [H_u(x,y)]_{,y} + [H_v(x,y)]_{,x} \end{bmatrix} = \begin{bmatrix} 0\,1\,0\,y\,0\,0\,0\,0 \\ 0\,0\,0\,0\,0\,0\,1\,x \\ 0\,0\,1\,x\,0\,1\,0\,y \end{bmatrix}, \tag{11}$$

$$\{\varepsilon_\theta^0\} = \frac{1}{2}[\theta][C_\theta]\{a\} = \frac{1}{2}[\theta][C_\theta][T_b]\{w_b\} = \frac{1}{2}[\theta][B_\theta]\{w_b\}, \tag{12}$$

where

$$[C_\theta] = \begin{bmatrix} [H_w(x,y)]_{,x} \\ [H_w(x,y)]_{,y} \end{bmatrix} = \begin{bmatrix} 0 & 1 & 0 & 2x & y & 0 & 3x^2 & 2xy & y^2 & 0 \\ 0 & 0 & 1 & 0 & x & 2y & 0 & x^2 & 2xy & 3y^2 \\ 3x^2y & 2xy^2 & y^3 & 3x^2y^2 & 2xy^3 & 3x^2y^3 \\ x^3 & 2x^2y & 3xy^2 & 2x^3y & 3x^2y^2 & 3x^3y^2 \end{bmatrix}, \tag{13}$$

and

$$\{\kappa\} = [C_b]\{a\} = [C_b][T_b]\{w_b\} = [B_b]\{w_b\}, \tag{14}$$

where

$$[C_b] = \begin{bmatrix} [H_w(x,y)]_{,xx} \\ [H_w(x,y)]_{,yy} \\ [H_w(x,y)]_{,xy} \end{bmatrix} = -\begin{bmatrix} 0 & 0 & 0 & 2 & 0 & 0 & 6x & 2y & 0 & 0 \\ 0 & 0 & 0 & 0 & 0 & 2 & 0 & 0 & 2x & 6y \\ 0 & 0 & 0 & 0 & 2 & 0 & 0 & 4x & 4y & 0 \end{bmatrix}$$
$$\begin{bmatrix} 6xy & 2y^2 & 0 & 6xy^2 & 2y^3 & 6xy^3 \\ 0 & 2x^2 & 6xy & 2x^3 & 6x^2y & 6x^3y \\ 6x^2 & 8xy & 6y^2 & 12x^2y & 12xy^2 & 18x^2y^2 \end{bmatrix}. \tag{15}$$

The strain-displacement relations can be expressed as

$$\{\varepsilon\} = [B_m]\{w_m\} + \frac{1}{2}[\theta][B_\theta]\{w_b\} + z[B_b]\{w_b\}. \tag{16}$$

II.2 Piezoelectric Constitutive Equations

The electric enthalpy density is defined as

$$H = U - D \cdot E, \tag{17}$$

where D and E are the electric displacement density and electric field, whose product represents the electrostatic energy density. The enthalpy can be expressed as

$$H = \frac{1}{2}[Q]^E\{\varepsilon\} - \{E\}^T[e]\{\varepsilon\} - \frac{1}{2}\{E\}^T[\epsilon]^\varepsilon\{E\}, \tag{18}$$

and

$$\begin{aligned} \sigma_{ij} &= \frac{\partial H}{\partial \varepsilon_{ij}} \\ D_i &= -\frac{\partial H}{\partial E_i}, \end{aligned} \tag{19}$$

where σ_{ij}, ε_{ij} are the stress and strain, $[Q]^E$ is the stiffness matrix measured at constant electric field, $[\epsilon]^\varepsilon$ is the dielectric permittivity matrix measured at constant strain matrix $[e]$ is the piezoelectric strain constants.

Substitute Eq. (19) into Eq. (18), the coupled electrical-structural piezoelectric constitutive equations can be expressed as

$$\begin{aligned} \{\sigma\} &= [Q]^E\{\varepsilon\} - [e]^T\{E\} \\ \{D\} &= [e]\{\varepsilon\} + [\epsilon]^\varepsilon\{E\}. \end{aligned} \tag{20}$$

Since the stress constants $[d]$ and the free permittivity matrix $[\epsilon]^\sigma$ are easier to be obtained than the piezoelectric strain constants $[e]$ and clamped permittivity matrix $[\epsilon]^\varepsilon$, we can use the relationships below

$$\begin{aligned} [e] &= [d][Q]^E \\ [\epsilon]^\varepsilon &= [\epsilon]^\sigma - [d][Q]^E[d]^T, \end{aligned} \tag{21}$$

to obtain the electric displacement density equation

$$\{D\} = [d][Q]^E(\{\varepsilon\} - [d]^T\{E\}) + [\epsilon]^\sigma\{E\}. \tag{22}$$

II.3 Electric Field and Electric Displacement Density

The electric potential $\{w_\phi\}$ for each BFS element is defined as

$$\{w_\phi\} = \{\mathbf{V_1}, \mathbf{V_2}, ..., \mathbf{V_{np}}\}, \tag{23}$$

where the $\mathbf{V_i}$ is the electric potentials applied to or detected from the piezoelectric layers of the element, and np denotes the total number of piezoelectric layers. The

voltage establishes a linear electric displacement density and electric field through the thickness of the piezoelectric material. And the electric field strength is

$$E = -\nabla \mathbf{V}. \tag{24}$$

The total electric field due to all of the piezoelectric layers can be expressed as

$$\{E_{ik}\} = -[B_\phi]\{w_\phi\}, \tag{25}$$

where $i = 3$ for traditional PZT and $i = 1$ for MFC actuators [82], which means that the electric displacement density is assumed to be generated along the polarization axis only (3-direction) or 1-direction. $[B_\phi]$ is a diagonal matrix as

$$[B_\phi] = \begin{bmatrix} \frac{1}{h_1} & \cdots & 0 \\ \vdots & \ddots & \vdots \\ 0 & \cdots & \frac{1}{h_{np}} \end{bmatrix}, \tag{26}$$

where h_r describes the thickness for traditional piezoceramics or the electrode spacing of thr interdigital electrodes for the MFC actuators.

And finally the Eq. (22) can be reduced to

$$D_3 = [d][Q](\{\varepsilon\} - E_3\{d\}) + \epsilon_{ii}^{\sigma} E_i. \tag{27}$$

II.4 Constitutive Equations

For a general k-th layer piezoelectric composite plate, the stress-strain relationships are derived from the classical laminate plate theory. Since the composite plates are thin (i.e. the ratio of length or width over thickness of the panel is greater than

50), we can neglect the shear deformation. The isotropic beam can be treated as a special case of the composite plate [68].

The stress-strain relations of a specially orthotropic composite lamina and a piezoceramic layer are

$$\begin{Bmatrix} \sigma_1 \\ \sigma_2 \\ \tau_{12} \end{Bmatrix}_s = \begin{bmatrix} Q_{11} & Q_{12} & 0 \\ Q_{12} & Q_{22} & 0 \\ 0 & 0 & Q_{66} \end{bmatrix}_s \begin{Bmatrix} \varepsilon_1 \\ \varepsilon_2 \\ \gamma_{12} \end{Bmatrix} \tag{28}$$

and

$$\begin{Bmatrix} \sigma_1 \\ \sigma_2 \\ \tau_{12} \end{Bmatrix}_p = \begin{bmatrix} Q_{11} & Q_{12} & 0 \\ Q_{12} & Q_{22} & 0 \\ 0 & 0 & Q_{66} \end{bmatrix}_p \left(\begin{Bmatrix} \varepsilon_1 \\ \varepsilon_2 \\ \gamma_{12} \end{Bmatrix} - E_{ip} \begin{Bmatrix} d_{i1} \\ d_{i2} \\ 0 \end{Bmatrix}_p \right), \tag{29}$$

where the subscripts s and p indicate the structural and piezoelectric lamina, respectively. And the stress-strain relations for the kth layer of a laminated composite is obtained by combining the above two equations as

$$\begin{Bmatrix} \sigma_x \\ \sigma_y \\ \tau_{xy} \end{Bmatrix}_k = \begin{bmatrix} [\bar{Q}_{11}] & [\bar{Q}_{12}] & [\bar{Q}_{16}] \\ [\bar{Q}_{12}] & [\bar{Q}_{22}] & [\bar{Q}_{26}] \\ [\bar{Q}_{16}] & [\bar{Q}_{26}] & [\bar{Q}_{66}] \end{bmatrix}_k \left\{ \begin{Bmatrix} \varepsilon_x \\ \varepsilon_y \\ \gamma_{xy} \end{Bmatrix} - E_{ik} \begin{Bmatrix} d_x \\ d_y \\ d_{xy} \end{Bmatrix}_k \right\}, \tag{30}$$

where $[\bar{Q}_{ij}]_k$ is the transformed reduced lamina stiffness matrix comprised of the material properties and the influence of the lamination angle. For a general orthotropic piezoelectric layer such as MFC, the generated electric displacement density along

the 3-direction or 1-direction for the *kth* layer may be written as

$$D_{ik} = \begin{bmatrix} d_x & d_y & d_{xy} \end{bmatrix}_k \begin{bmatrix} [\bar{Q}_{11}] & [\bar{Q}_{12}] & [\bar{Q}_{16}] \\ [\bar{Q}_{12}] & [\bar{Q}_{22}] & [\bar{Q}_{26}] \\ [\bar{Q}_{16}] & [\bar{Q}_{26}] & [\bar{Q}_{66}] \end{bmatrix}_k \left(\begin{Bmatrix} \varepsilon_x \\ \varepsilon_y \\ \gamma_{xy} \end{Bmatrix} - E_{ik} \begin{Bmatrix} d_x \\ d_y \\ d_{xy} \end{Bmatrix}_k \right) + \epsilon^{\sigma}_{iik} E_{ik}. \tag{31}$$

Combine the two equations together, and we can obtain the following reduced form

$$\{\sigma\}_k = [\bar{Q}]_k(\{\varepsilon\} - E_{ik}\{d\}_k) \tag{32}$$

$$D_{ik} = \{d\}_k^T[\bar{Q}]_k(\{\varepsilon\} - E_{ik}d_k) + \epsilon^{\sigma}_{iik}E_{ik}, \tag{33}$$

where $[\bar{Q}]_k$ and $\{d\}_k$ are the lamina stiffness and stress/charge constants, respectively, for the *kth* piezoelectric layer and are transformed to the global x, y coordinates. For a traditional composite layer, $E_{ik} = \{d\}_k = 0$.

II.5 Resultant Forces and Moments

The resultant forces and moments acting on a laminate are obtained by integration of the stresses in each layer or laminate through the lamina thickness,

$$(\{N\}, \{M\}) = \int_{-h/2}^{h/2} \{\sigma\}_k(1, z)dz. \tag{34}$$

Substituting Eq. (30) into above equation, the laminate constitutive equation has the form

$$\begin{Bmatrix} N \\ M \end{Bmatrix} \begin{bmatrix} [A] & [B] \\ [B] & [D] \end{bmatrix} \begin{Bmatrix} \varepsilon^0 \\ \kappa \end{Bmatrix} - \begin{Bmatrix} N_\phi \\ M_\phi \end{Bmatrix}, \tag{35}$$

where $[A], [B]$ and $[D]$ are the extensional, coupling and bending stiffness matrices of the laminate, respectively, which for an n-layer laminate are defined as

$$\begin{aligned}
[A] &= \sum_{k=1}^{n} [\bar{Q}]_k (z_{k+1} - z_k) \\
[B] &= \sum_{k=1}^{n} \frac{1}{2} [\bar{Q}]_k (z_{k+1}^2 - z_k^2) \\
[D] &= \sum_{k=1}^{n} \frac{1}{3} [\bar{Q}]_k (z_{k+1}^3 - z_k^3).
\end{aligned} \tag{36}$$

II.6 Piezoelectric Resultant Forces and Moments

The force and moment vectors resulting from the piezoelectric effect are defined as

$$(\{N_\phi\}, \{M_\phi\} = \int_{h/2}^{h/2} [\bar{Q}]_k \{d\}_k E_{ik}(1, z) dz. \tag{37}$$

Substitute Eq. (32) into Eq. (35), we have the resultant force vector

$$\begin{aligned}
\{N\} &= [A]\{\varepsilon_m^0\} + [A]\{\varepsilon_\theta^0\} + [B]\{\kappa\} - \{N_\phi\} \\
&= [A][B_m]\{w_m\} + \frac{1}{2}[A][\theta][B_\theta]\{w_b\} + [B][B_b]\{w_b\} - \{N_\phi\} \\
&= \{N_m\} + \{N_B\} + \{N_b\} - \{N_\phi\}.
\end{aligned} \tag{38}$$

Similarly, the resultant moment vector is determined as

$$\begin{aligned}
\{M\} &= [B]\{\varepsilon_m^0\} + [B]\{\varepsilon_\theta^0\} + [D]\{\kappa\} - \{M_\phi\} \\
&= [B][B_m]\{w_m\} + \frac{1}{2}[B][\theta][B_\theta]\{w_b\} + [D][B_b]\{w_b\} - \{M_\phi\} \\
&= \{M_m\} + \{M_B\} + \{M_b\} - \{M_\phi\}.
\end{aligned} \tag{39}$$

The piezoelectric layer will also contribute to the total resultant force and moment vectors. Separately, the piezoelectric force resultant vector is

$$\{N_\phi\} = \sum_{k=1}^{np} \int_{z_k}^{z_{k+1}} [\bar{Q}]_k \{d_k\} E_{ik} dz$$
$$= \left[[\bar{Q}]_1 \{d\}_1 h_1 \quad \dots \quad [\bar{Q}]_k \{d\}_k h_k \quad \dots \quad [\bar{Q}]_{np} \{np\} h_{np} \right] \{E_i\} = -[P_N][B_\phi]\{w_\phi\}, \tag{40}$$

where

$$[P_N] = \left[[\bar{Q}]_1 \{d\}_1 h_1 \quad \dots \quad [\bar{Q}]_k \{d\}_k h_k \quad \dots \quad [\bar{Q}]_{np} \{d\}_{np} h_{np} \right]. \tag{41}$$

And the piezoelectric moment resultant may be expressed as

$$\{M_\phi\} = -[P_M][B_\phi]\{w_\phi\}, \tag{42}$$

where

$$[P_M] = \left[\tfrac{1}{2}[\bar{Q}]_1 d_1 h_1 (z_1 + z_2) \quad \dots \quad \tfrac{1}{2}[\bar{Q}]_k \{d\}_k h_k (z_{k+1} - z_k) \right.$$
$$\left. \dots \tfrac{1}{2}[\bar{Q}]_{np} \{d_{np}\} h_{np} (z_{np+1} + z_{np}) \right]. \tag{43}$$

II.7 Equations of Motion

II.7.1 Element Matrices

By using the Hamilton's Principle, the finite element equations for the laminated composite plate with fully coupled electrical-structural properties can be derived from

$$\int_{t_1}^{t_2} \delta(T - U + W_e) dt = 0, \tag{44}$$

where T and U are the kinetic and strain energy of the system, and W_e expresses the electrical energy. The kinetic energy is defined as

$$T = \int_V \frac{1}{2} \rho (\dot{w}^2 + \dot{u}^2 + \dot{v}^2) dV, \tag{45}$$

where $\dot{w}, \dot{u}$ and $\dot{v}$ are the transverse and membrane velocity components, and ρ is the mass per unit volume, and V is the volume of the element. The potential and electrical energies are defined as

$$\begin{aligned} U &= \int_V \frac{1}{2}\{\varepsilon\}^T\{\sigma\}dV \\ W_e &= \int_V \frac{1}{2}\{E\}^T\{D\}dV. \end{aligned} \tag{46}$$

The Hamilton's variational statement can be written in the following general form:

$$\int_V [\rho(\delta\dot{w}^T\dot{w} + \delta\dot{u}^T\dot{u} + \delta\dot{v}^T\dot{v}) - \{\delta\varepsilon\}^T\{\sigma\} + \{\delta E\}^T\{D\}]dV = 0. \tag{47}$$

For the kinetic energy part, since in Hamilton's principle, all variations must vanish at the time $t = t_1$ and $t = t_2$, then it can be expressed as

$$\begin{aligned} &\int_V \rho(\delta\dot{w}^T\dot{w} + \delta\dot{u}^T\dot{u} + \delta\dot{v}^T\dot{v})dV \\ &= \int_V \rho(\delta\dot{w}^T\ddot{w} + \delta u^T\ddot{u} + \delta v^T\ddot{v}dV \\ &= -(\{\delta w_b\}^T[m_b]\{\ddot{w}_b\} + \{\delta w_m\}^T[m_m]\{\ddot{w_m}\}), \end{aligned} \tag{48}$$

where the $[m_b]$ and $[m_m]$ element mass matrices are expressed as

$$\begin{aligned} [m_b] &= [T_b]^T \int_A \{H_w\}h\rho[H_w]dA[T_b] \\ [m_m] &= [T_m]^T(\int_A \{H_u\}h\rho[H_u] + \int_A \{H_v\}h\rho[H_v])dA[T_m]. \end{aligned} \tag{49}$$

And the potential and electrical energy can be expressed as

$$\begin{aligned} &\int_V (\{\delta\varepsilon\}\{\sigma\} - \{\delta E\}^T\{D\})dV \\ &= \int_A [\int_{-h/2}^{h/2} (\{\delta\varepsilon^0\}^T + z\{\delta\kappa\}^T)\{\sigma\}_k dz - \int_{-h/2}^{h/2} (\delta E_{ik})D_{ik}dz]dA. \end{aligned} \tag{50}$$

Substitute Eq. (34), Eq. (8) and Eq. (33) into Eq. (50), the equation can be obtained as below

$$\begin{aligned}
&\int_V (\{\delta\varepsilon\}\{\sigma\} - \{\delta E\}^T\{D\})dV \\
&= \int_A [\{\delta\varepsilon^0\}^T\{N\} + \{\delta\kappa\}^T\{M\} \\
&- \int_A [\sum_{k=1}^{np} \int_{Z_k}^{Z_{k+1}} [(\delta E_{ik})\{\{d\}_k^T[\bar{Q}]_k(\{\varepsilon^0\} + z\{\kappa\} - E_{ik}\{d\}_k) + \epsilon_{iik}^{\sigma} E_{ik}\}]dz]dA.
\end{aligned} \tag{51}$$

Since the inplane strains and curvatures are expressed as

$$\begin{aligned}
\{\delta\varepsilon^0\}^T &= \{\delta w_m\}^T[B_m]^T + \{\delta w_b\}^T[B_\theta]^T[\theta]^T \\
\{\delta\kappa\}^T &= \{\delta w_b\}^T[B_b]^T,
\end{aligned} \tag{52}$$

by substituting Eq. (38), Eq. (39) and Eq. (52) into Eq. (51), the following equation can be obtained

$$\begin{aligned}
&\int_A [\{\delta w_m\}^T[B_m]^T([A][B_m]\{w_m\} + \frac{1}{2}[A][\theta][B_\theta]\{w_b\} + [B][B_b]\{w_b\} - \{N_\phi\}) \\
&+ \{\delta w_b\}^T[B_\theta]^T[\theta]^T([A][B_m]\{w_m\} + \frac{1}{2}[A][\theta][B_\theta]\{w_b\} + [B][B_b]\{w_b\} - \{N_\phi\} \\
&+ \{\delta w_b\}^T[B_b]^T([B][B_m]\{w_m\} + \frac{1}{2}[B][\theta][B_\theta]\{w_b\} + [D][B_b]\{w_b\} - \{M_\phi\}) \\
&+ \{\delta w_\phi\}^T[B_\phi]^T[P_N]^T([B_m]\{w_m\} + \frac{1}{2}[\theta][B_\theta]\{w_b\}) + \{\delta w_\phi\}^T[B_\phi]^T[P_M]^T[B_b]\{w_b\} \\
&+ \{\delta w_\phi\}^T[B_\phi]^T([\gamma] - [\epsilon_{ii}^{\sigma}])\{w_\phi\}]dA = 0,
\end{aligned} \tag{53}$$

where the matrices $[\epsilon_{ii}^{\sigma}]$ and $[\gamma]$ are defined as

$$[\epsilon_{ii}^{\sigma}] = \begin{bmatrix} \epsilon_{ii1}^{\sigma} & \dots & 0 \\ \vdots & \epsilon_{iik}^{\sigma} & \vdots \\ 0 & \dots & \epsilon_{iinp}^{\sigma} \end{bmatrix}$$

$$[\gamma] = \begin{bmatrix} \{d\}_1^T[\bar{Q}]_1\{d\}_1 & \dots & 0 \\ \vdots & \{d\}_k^T[\bar{Q}]_k\{d\}_k & \vdots \\ 0 & \dots & \{d\}_{np}^T[\bar{Q}]_{np}\{d\}_{np} \end{bmatrix}. \tag{54}$$

Since the isotropic beam or composite plate considered are symmetric, matrix $[B]$ equals to zero. The Eq. (53) can be expressed as

$$\int_A [\{\delta w_m\}^T[B_m]^T[A][B_m][w_m] \tag{55}$$

$$+\frac{1}{2}\{\delta w_m\}^T[B_m]^T[A][\theta][B_\theta]\{w_b\} \tag{56}$$

$$+\{\delta w_m\}^T[B_m]^T[P_N][B_\phi]\{w_\phi\} \tag{57}$$

$$+\{\delta w_b\}^T[B_\theta]^T[\theta]^T[A][B_m]\{w_m\} \tag{58}$$

$$+\frac{1}{2}\{\delta w_b\}^T[B_\theta]^T[\theta]^T[A][\theta][B_\theta]\{w_b\} \tag{59}$$

$$+\{\delta w_b\}^T[B_\theta]^T[\theta]^T[P_N][B_\phi]\{w_\phi\} \tag{60}$$

$$+\{\delta w_b\}^T[B_b]^T[D][B_b]\{w_b\} \tag{61}$$

$$+\{\delta w_b\}^T[B_b]^T[P_M][B_\phi]\{w_\phi\} \tag{62}$$

$$+\{\delta w_\phi\}^T[B_\phi]^T[P_N]^T[B_m]\{w_m\} \tag{63}$$

$$+\frac{1}{2}\{\delta w_\phi\}^T[B_\phi]^T[P_N]^T[\theta][B_\theta]\{w_b\} \tag{64}$$

$$+\{\delta w_\phi\}^T[B_\phi]^T[P_M]^T[B_b]\{w_b\} \tag{65}$$

$$+\{\delta w_\phi\}^T[B_\phi]^T([\gamma]-[\epsilon_{ii}^\sigma])\{w_\phi\}]dA=0. \tag{66}$$

First the linear element stiffness matrices can be cast into such an expression

$$\begin{Bmatrix}\delta w_b\\ \delta w_m\\ \delta w_\phi\end{Bmatrix}^T\begin{bmatrix}[k_b] & [k_{bm}] & [k_{b\phi}]\\ [k_{mb}] & [k_m] & [k_{m\phi}]\\ [k_{\phi b}] & [k_{\phi m}] & [k_\phi]\end{bmatrix}\begin{Bmatrix}w_b\\ w_m\\ w_\phi\end{Bmatrix}, \tag{67}$$

where

$$[k_b]=\int_A[B_b]^T[D][B_b]dA \tag{68}$$

$$[k_m]=\int_A[B_m]^T[A][B_m]dA \tag{69}$$

$$[k_{mb}]=\int_A[B_m]^T[B][B_b]dA=[k_{bm}]^T \tag{70}$$

$$[k_{b\phi}]=\int_A[B_b]^TdA[P_M][B_\phi]=[k_{\phi b}]^T \tag{71}$$

$$[k_{m\phi}]=\int_A[B_m]^TdA[P_N][B_\phi]=[k_{\phi m}] \tag{72}$$

$$[k_\phi]=[B_\phi]^T([\gamma]-[\epsilon_{ii}^\sigma])A. \tag{73}$$

The remaining matrices are nonlinear because the slope matrix $[\theta]$. To make the calculation more convenient, the following relationship will be very important

$$[\theta]^T\{N_i\}=\begin{bmatrix}w_{,x} & 0 & w_{,y}\\ 0 & w_{,y} & w_{,x}\end{bmatrix}\begin{Bmatrix}N_x\\ N_y\\ N_{xy}\end{Bmatrix}_i=\begin{Bmatrix}N_xw_{,x}+N_{xy}w_{,y}\\ N_yw_{,y}+N_{xy}w_{,x}\end{Bmatrix}_i, \tag{74}$$

also

$$[N_i]\{\theta\}=\begin{bmatrix}N_x & N_{xy}\\ N_{xy} & N_y\end{bmatrix}_i\begin{Bmatrix}w_{,x}\\ w_{,y}\end{Bmatrix}=\begin{Bmatrix}N_xw_{,x}+N_{xy}w_{,y}\\ N_yw_{,y}+N_{xy}w_{,x}\end{Bmatrix}_i. \tag{75}$$

Then applying Eq. (8) and Eq. (12), the Eq. (74) and Eq. (75) can be expressed as

$$[\theta]^T\{N_i\}=[N_i]\{\theta\}=[N_i][C_\theta]\{a\}=[N_i][B_\theta]\{w_b\}, \tag{76}$$

where $i = b, m, \theta, \phi$ as the resultant force components shown in Eq. (38). From the above relationship, combining Eq. (56) and Eq. (58), the following expression can be obtained

$$\begin{aligned}
&\int_A \left[\frac{1}{2}\{\delta w_m\}^T[B_m]^T[A][\theta][B_\theta]\{w_b\} + \{\delta w_b\}^T[B_\theta]^T[\theta]^T[A][B_m]\{w_m\}\right] \\
&= \int_A \frac{1}{2}\{\delta w_b\}^T[B_\theta]^T[\theta]^T\Big[[A][B_m]\{w_m\} + [N_m][B_\theta]\{w_b\} \\
&+ \frac{1}{2}\{\delta w_m\}^T[B_m]^T[A][\theta][B_\theta]\{w_b\}\Big]dA \\
&= \frac{1}{2}\left(\{\delta w_b\}^T[n1_{bm}]\{w_m\} + \{\delta w_b\}^T[n1_{Nm}]\{w_b\} + \{\delta w_m\}^T[n1_{mb}]\{w_b\}\right),
\end{aligned} \tag{77}$$

where the first-order nonlinear element incremental stiffness matrices are expressed as

$$[n1_{bm}] = \int_A [B_\theta]^T[\theta]^T[A][B_m]dA \tag{78}$$

$$[n1_{Nm}] = \int_A [B_\theta]^T[N_m][B_\theta]dA \tag{79}$$

$$[n1_{mb}] = \int_A [B_m]^T[A][\theta][B_\theta]dA. \tag{80}$$

Then Eq. (60) can be expressed in the following form

$$\begin{aligned}
&\int_A \{\delta w_b\}^T[B_\theta]^T[\theta]^T[P_N][B_\phi]\{w_\phi\}dA \\
&= \frac{1}{2}\{\delta w_b\}^T \int_A [B_\theta]^T \left[[\theta]^T[P_N][B_\phi]\{w_\phi\} - [N_\phi][B_\theta]\{w_b\}\right] dA \\
&= \frac{1}{2}(\{\delta w_b\}^T[n1_{b\phi}]\{w_\phi\} + \{\delta w_b\}^T[n1_{N\phi}]\{w_b\}),
\end{aligned} \tag{81}$$

where

$$[n1_{b\phi}] = \int_A [B_\phi]^T[\theta]^T dA[P_N][B_\phi] \tag{82}$$

$$[n1_{N\phi}] = -\int_A [B_\phi]^T[N_\phi][B_\theta]dA. \tag{83}$$

From Eq. (64), the following expression can be obtained

$$\begin{aligned}\int_A \frac{1}{2}\{\delta w_\phi\}^T[B_\phi]^T[P_N]^T[\theta][B_\theta]\{w_b\}dA \\ = -\frac{1}{2}\{\delta w_\phi\}^T[n1_{\phi b}]\{w_b\},\end{aligned} \tag{84}$$

where

$$[n1_{\phi b}] = [B_\phi]^T[P_N]^T\int_A[\theta][B_\theta]dA = [n1_{b\phi}]^T. \tag{85}$$

In fact, $[n1_{b\phi}], [n1_{N\phi}]$ and $[n1_{\phi b}]$ are the first-order nonlinear incremental stiffness matrices due to electromechanical coupling. Finally, the second-order nonlinear incremental stiffness matrix can be determined from Eq. (59)

$$\begin{aligned}\int_A \frac{1}{2}\{\delta w_b\}^T[B_\theta]^T[\theta]^T[A][\theta][B_\theta]\{w_b\}dA \\ = \frac{1}{3}\{\delta w_b\}^T[n2_b]\{w_b\},\end{aligned} \tag{86}$$

where

$$[n2_b] = \frac{3}{2}\int_A[B_\theta]^T[\theta]^T[A][\theta][B_\theta]dA. \tag{87}$$

Combining the mass matrices obtained in Eq. (49) and all the above matrices, substituting them in Eq. (47), the element equation of motion can be expressed as

$$\begin{Bmatrix}\delta w_b\\ \delta w_m\\ \delta w_\phi\end{Bmatrix}^T\begin{bmatrix}m_b & 0 & 0\\ 0 & m_m & 0\\ 0 & 0 & 0\end{bmatrix}\begin{Bmatrix}\ddot{w}_b\\ \ddot{w}_m\\ \ddot{w}_\phi\end{Bmatrix} + \begin{Bmatrix}\delta w_b\\ \delta w_m\\ \delta w_\phi\end{Bmatrix}^T\left(\begin{bmatrix}k_b & k_{bm} & k_{b\phi}\\ k_{mb} & k_m & k_{m\phi}\\ k_{\phi b} & k_{\phi m} & k_\phi\end{bmatrix} - \frac{1}{2}\begin{bmatrix}n1_{N\phi} & 0 & 0\\ 0 & 0 & 0\\ 0 & 0 & 0\end{bmatrix}\right.$$
$$\left. + \frac{1}{2}\begin{bmatrix}n1_{Nm}+n1_{NB} & n1_{bm} & n1_{b\phi}\\ n1_{mb} & 0 & 0\\ n1_{\phi b} & 0 & 0\end{bmatrix} + \frac{1}{3}\begin{bmatrix}n2_b & 0 & 0\\ 0 & 0 & 0\\ 0 & 0 & 0\end{bmatrix}\right)\begin{Bmatrix}w_b\\ w_m\\ w_\phi\end{Bmatrix} = 0. \tag{88}$$

And cancelling the displacement variation, the final element equation of motion can be expressed

$$\begin{bmatrix} m_b & 0 & 0 \\ 0 & m_m & 0 \\ 0 & 0 & 0 \end{bmatrix} \begin{Bmatrix} \ddot{w}_b \\ \ddot{w}_m \\ \ddot{w}_\phi \end{Bmatrix} + \left(\begin{bmatrix} k_b & k_{bm} & k_{b\phi} \\ k_{mb} & k_m & k_{m\phi} \\ k_{\phi b} & k_{\phi m} & k_\phi \end{bmatrix} - \frac{1}{2} \begin{bmatrix} n1_{N\phi} & 0 & 0 \\ 0 & 0 & 0 \\ 0 & 0 & 0 \end{bmatrix} \right.$$
$$\left. + \frac{1}{2} \begin{bmatrix} n1_{Nm} + n1_{NB} & n1_{bm} & n1_{b\phi} \\ n1_{mb} & 0 & 0 \\ n1_{\phi b} & 0 & 0 \end{bmatrix} + \frac{1}{3} \begin{bmatrix} n2_b & 0 & 0 \\ 0 & 0 & 0 \\ 0 & 0 & 0 \end{bmatrix} \right) \begin{Bmatrix} w_b \\ w_m \\ w_\phi \end{Bmatrix} = 0. \tag{89}$$

II.7.2 System Equation of Motion

To obtain the system matrices, an assembly procedure is needed to be applied on the element equation of motion. In the process, electrical and structural boundary conditions are used [83]. Then the system equation of motion for free vibration of isotropic beams and symmetric composite plates can be expressed as

$$\begin{bmatrix} [M_b] & 0 & 0 \\ 0 & [M_m] & 0 \\ 0 & 0 & 0 \end{bmatrix} \begin{Bmatrix} \ddot{W}_b \\ \ddot{W}_m \\ \ddot{W}_\phi \end{Bmatrix} + \left(\begin{bmatrix} [K_b] & [K_{bm}] & [K_{b\phi}] \\ [K_{mb}] & [K_m] & [K_{m\phi}] \\ [K_{\phi b}] & [K_{\phi m}] & [K_\phi] \end{bmatrix} - \begin{bmatrix} [K1_{N\phi}] & 0 & 0 \\ 0 & 0 & 0 \\ 0 & 0 & 0 \end{bmatrix} \right.$$
$$\left. + \begin{bmatrix} [K1_{Nm}] + [K1_{NB}] & [K1_{bm}] & [K1_{b\phi}] \\ [K1_{mb}] & 0 & 0 \\ [K1_{\phi b}] & 0 & 0 \end{bmatrix} + \begin{bmatrix} [K2_b] & 0 & 0 \\ 0 & 0 & 0 \\ 0 & 0 & 0 \end{bmatrix} \right) \begin{Bmatrix} W_b \\ W_m \\ W_\phi \end{Bmatrix} = 0, \tag{90}$$

where the system matrices are

$$[K1_{N\phi}] = \frac{1}{2}[N1_{N\phi}], \tag{91}$$

$$[K1_{Nm}] = \frac{1}{2}[N1_{Nm}], \tag{92}$$

$$[K1_{NB}] = \frac{1}{2}[N1_{NB}], \tag{93}$$

$$[K1_{bm}] = [K1_{mb}^T] = \frac{1}{2}[N1_{bm}], \tag{94}$$

$$[K1_{b\phi}] = [K1_{\phi b}^T] = \frac{1}{2}[N1_{b\phi}], \tag{95}$$

$$[K2_b] = \frac{1}{3}[N2_b]. \tag{96}$$

For a free vibration problem, no applied mechanical and electric loads are at the right-hand side. Notice the isotropic beam or the symmetric composite plate, bending and inplane force coupling terms $[K_{bm}]$ and $[K_{mb}]$ are zeros. Since we knew from previous work that piezoelectric actuators with bending moment are much more efficient than inplane tension for nonlinear vibration suppression, we assume the piezoelectric resultant force, $\{N_\phi\}$ is zero. Then $[K_{m\phi}], [K1_{N\phi}], [K1_{b\phi}]$ are zero matrices. Furthermore, for a thin plate, the in-plane natural frequencies usually are 2 to 3 order higher than the bending ones, so neglecting the in-plane inertia term will not bring significant error. Therefore, the system equations become

$$\begin{bmatrix} [M_b] & 0 & 0 \\ 0 & 0 & 0 \\ 0 & 0 & 0 \end{bmatrix} \begin{Bmatrix} \ddot{W}_b \\ \ddot{W}_m \\ \ddot{W}_\phi \end{Bmatrix} + \left(\begin{bmatrix} [K_b] & 0 & [K_{b\phi}] \\ 0 & [K_m] & 0 \\ [K_{\phi b}] & 0 & [K_\phi] \end{bmatrix} + \begin{bmatrix} [K1_{Nm}] & [K1_{bm}] & 0 \\ [K1_{mb}] & 0 & 0 \\ 0 & 0 & 0 \end{bmatrix} + \begin{bmatrix} [K2_b] & 0 & 0 \\ 0 & 0 & 0 \\ 0 & 0 & 0 \end{bmatrix} \right) \begin{Bmatrix} W_b \\ W_m \\ W_\phi \end{Bmatrix} = 0. \tag{97}$$

II.8 Equations of Motion and Matrices for Panel Flutter

II.8.1 Quasi-Steady First-Order Piston Aerodynamic Theory

To analyze and control the response of panel flutter, quasi-steady first-order piston aerodynamic theory has been applied here. The theory is based on the assumptions [84] that:

1) the local motion of the panel acts as a piston;

2) the air is ideal and it has a constant specific heat; the process of the airflow is isentropic;

3) the local panel motion velocity is much smaller than the airflow velocity;

4) the airflow is parallel to the panel surface;

5) and the effect of any air entrapped below the panel (cavity) is neglected.

The first-order piston theory considering the flow angle is:

$$P_a = -\frac{2q}{\beta}\left[\frac{\partial w}{\partial x}cos\Lambda + \frac{\partial w}{\partial y}sin\Lambda + \frac{M_\infty^2-2}{M_\infty^2-1}\frac{1}{V}\frac{\partial w}{\partial t}\right], \tag{98}$$

where P_a is the aerodynamic pressure, V is the airflow velocity, M_∞ is the Mach number, $q = \frac{1}{2}\rho_a V^2$ is the dynamic pressure, Λ is the flow yaw angle with respect to plate x-direction, ρ_a is the air mass density, $\beta = \sqrt{M_\infty^2 - 1}$, w is the panel bending displacement. In fact, in this thesis, the flow angle is not considered, so $\Lambda = 0$.

The first-order piston theory in non-dimensional parameters can be expressed as

$$P_a = -\left[\lambda\frac{D_{110}}{L^3}\left(\frac{\partial w}{\partial x}cos\Lambda + \frac{\partial w}{\partial y}sin\Lambda\right) + \frac{g_a}{\omega_0}\frac{D_{110}}{L^4}\frac{\partial w}{\partial t}\right], \tag{99}$$

where for beam, D_{110} is the bending stiffness matrix D; for composite plates, D_{110} is the first element in the laminate bending stiffness matrix D calculated when all the fibers of the composite plate are aligned in the x-direction; L is the panel length; λ is

the non-dimensional dynamic pressure (when λ is larger than a particular value, the panel motion becomes unstable and grows exponentially with time, this value is the critical dynamic pressure value λ_{cr}); μ is the mass ratio; g_a is the non-dimensional aerodynamic damping, and C_a is its coefficient; and ω_0 is a reference frequency. The detailed expressions of above parameters are

$$\lambda = \frac{2qL^3}{\beta D_{110}}, \tag{100}$$

$$\mu = \frac{\rho_a a}{\rho h}, \tag{101}$$

$$C_a = \left(\frac{M_\infty^2 - 2^2}{M_\infty^2 - 1} \right) \frac{\mu}{\beta}, \tag{102}$$

$$g_a = \frac{\rho_a V (M_\infty^2 - 2)}{\beta^3 \rho h \omega_0} = \sqrt{\lambda C_a}, \tag{103}$$

$$\omega_0 = \sqrt{\frac{D_{110}}{\rho h L^4}}. \tag{104}$$

II.8.2 Element and System Equations of Motion for Panel Flutter

Including the aerodynamic damping and aerodynamic stiffness terms into the element equation of motion Eq. (89), and since thermal stresses are also considered for panel flutter case, the new element equation of motion for panel flutter can be

obtained

$$\begin{bmatrix} m_b & 0 & 0 \\ 0 & m_m & 0 \\ 0 & 0 & 0 \end{bmatrix} \begin{Bmatrix} \ddot{w}_b \\ \ddot{w}_m \\ \ddot{w}_\phi \end{Bmatrix} + \begin{bmatrix} g(\lambda, C_a) & 0 & 0 \\ 0 & 0 & 0 \\ 0 & 0 & 0 \end{bmatrix} \begin{Bmatrix} \dot{w}_b \\ \dot{w}_m \\ \dot{w}_\phi \end{Bmatrix} + \left(\lambda \begin{bmatrix} a_a & 0 & 0 \\ 0 & 0 & 0 \\ 0 & 0 & 0 \end{bmatrix} \right.$$
$$+ \begin{bmatrix} k_b & k_{bm} & k_{b\phi} \\ k_{mb} & k_m & k_{m\phi} \\ k_{\phi b} & k_{\phi m} & k_\phi \end{bmatrix} - \begin{bmatrix} k_{\Delta Tb} & 0 & 0 \\ 0 & 0 & 0 \\ 0 & 0 & 0 \end{bmatrix} - \frac{1}{2} \begin{bmatrix} n1_{N\phi} & 0 & 0 \\ 0 & 0 & 0 \\ 0 & 0 & 0 \end{bmatrix} \tag{105}$$
$$\left. + \frac{1}{2} \begin{bmatrix} n1_{Nm} + n1_{NB} & n1_{bm} & n1_{b\phi} \\ n1_{mb} & 0 & 0 \\ n1_{\phi b} & 0 & 0 \end{bmatrix} + \frac{1}{3} \begin{bmatrix} n2_b & 0 & 0 \\ 0 & 0 & 0 \\ 0 & 0 & 0 \end{bmatrix} \right) \begin{Bmatrix} w_b \\ w_m \\ w_\phi \end{Bmatrix} = \begin{Bmatrix} p_{\Delta Tb} \\ p_{\Delta Tm} \\ 0 \end{Bmatrix},$$

where

$$[g(\lambda, C_a)] = \frac{g_a}{\omega_0} \frac{D_{110}}{L^4} [T_b]^T \int_A [H_w]^T [H_w] [T_b] dA, \tag{106}$$

$$[a_a(\lambda)] = \frac{D_{110}}{L^3} [T_b]^T \int_A [H_w]^T \left(\frac{\partial}{\partial x} [H_w] cos\Lambda + \frac{\partial}{\partial y} [H_w] sin\Lambda \right) [T_b] dA, \tag{107}$$

and $[k_{\Delta Tb}]$, $\{p_{\Delta Tb}\}$ and $\{p_{\Delta Tm}\}$ are the stiffness and external force terms for thermal effects

$$[k_{\Delta Tb}] = \int_A [B_\theta]^T [N_{\Delta T}] [B_\theta] dA, \tag{108}$$

$$\{p_{\Delta Tb}\} = \int_A [B_b]^T \{M_{\Delta T}\} dA, \tag{109}$$

$$\{p_{\Delta Tm}\} = \int_A [B_m]^T \{N_{\Delta T}\} dA, \tag{110}$$

where $\{N_{\Delta T}\}$ and $\{M_{\Delta T}\}$ are thermal resultant force and moment,

$$(\{N_{\Delta T}\}, \{M_{\Delta T}\}) = \int_{h/2}^{h/2} [\bar{Q}]_k \{\alpha\}_k \Delta T(1, z) dz, \tag{111}$$

where $\{\alpha\}_k$ are the coefficients of thermal expansion and ΔT is the temperature change. And $[N_{\Delta T}]$ is calculated as

$$[\theta_T]^T\{N_{\Delta T}\} = \begin{bmatrix} \frac{\partial w}{\partial x} & 0 \\ 0 & \frac{\partial w}{\partial y} \\ \frac{\partial w}{\partial y} & \frac{\partial w}{\partial x} \end{bmatrix} \begin{Bmatrix} N_{\Delta T_x} \\ N_{\Delta T_y} \\ N_{\Delta T_{xy}} \end{Bmatrix} = [N_{\Delta T}] \begin{Bmatrix} \frac{\partial w}{\partial x} \\ \frac{\partial w}{\partial y} \end{Bmatrix} = [N_{\Delta T}][B_\theta]\{w_b\}. \quad (112)$$

Assembling above element equation of motions, the system equation of motion for panel flutter is

$$\begin{bmatrix} [M_b] & 0 & 0 \\ 0 & [M_m] & 0 \\ 0 & 0 & 0 \end{bmatrix} \begin{Bmatrix} \ddot{W}_b \\ \ddot{W}_m \\ \ddot{W}_\phi \end{Bmatrix} + \begin{bmatrix} [G(\lambda, C_a)] & 0 & 0 \\ 0 & 0 & 0 \\ 0 & 0 & 0 \end{bmatrix} \begin{Bmatrix} \dot{W}_b \\ \dot{W}_m \\ \dot{W}_\phi \end{Bmatrix} + \left(\lambda \begin{bmatrix} A_a & 0 & 0 \\ 0 & 0 & 0 \\ 0 & 0 & 0 \end{bmatrix} \right.$$
$$+ \begin{bmatrix} [K_b] & [K_{bm}] & [K_{b\phi}] \\ [K_{mb}] & [K_m] & [K_{m\phi}] \\ [K_{\phi b}] & [K_{\phi m}] & [K_\phi] \end{bmatrix} - \begin{bmatrix} [K1_{N\phi}] & 0 & 0 \\ 0 & 0 & 0 \\ 0 & 0 & 0 \end{bmatrix} - \begin{bmatrix} [K_{\Delta Tb}] & 0 & 0 \\ 0 & 0 & 0 \\ 0 & 0 & 0 \end{bmatrix}$$
$$\left. + \begin{bmatrix} [K1_{Nm}] + [K1_{NB}] & [K1_{bm}] & [K1_{b\phi}] \\ [K1_{mb}] & 0 & 0 \\ [K1_{\phi b}] & 0 & 0 \end{bmatrix} + \begin{bmatrix} [K2_b] & 0 & 0 \\ 0 & 0 & 0 \\ 0 & 0 & 0 \end{bmatrix} \right) \begin{Bmatrix} W_b \\ W_m \\ W_\phi \end{Bmatrix} = \begin{Bmatrix} P_{\Delta Tb} \\ P_{\Delta Tm} \\ 0 \end{Bmatrix}. \quad (113)$$

Reduce the system equation like above, the final version is

$$\begin{bmatrix} [M_b] & 0 & 0 \\ 0 & 0 & 0 \\ 0 & 0 & 0 \end{bmatrix} \begin{Bmatrix} \ddot{W}_b \\ \ddot{W}_m \\ \ddot{W}_\phi \end{Bmatrix} + \begin{bmatrix} [G(\lambda, C_a)] & 0 & 0 \\ 0 & 0 & 0 \\ 0 & 0 & 0 \end{bmatrix} \begin{Bmatrix} \dot{W}_b \\ \dot{W}_m \\ \dot{W}_\phi \end{Bmatrix} + \left(\lambda \begin{bmatrix} A_a & 0 & 0 \\ 0 & 0 & 0 \\ 0 & 0 & 0 \end{bmatrix} \right.$$
$$+ \begin{bmatrix} [K_b] & 0 & [K_{b\phi}] \\ 0 & [K_m] & 0 \\ [K_{\phi b}] & 0 & [K_\phi] \end{bmatrix} - \begin{bmatrix} [K_{\Delta Tb}] & 0 & 0 \\ 0 & 0 & 0 \\ 0 & 0 & 0 \end{bmatrix} + \begin{bmatrix} [K1_{Nm}] & [K1_{bm}] & 0 \\ [K1_{mb}] & 0 & 0 \\ 0 & 0 & 0 \end{bmatrix} \tag{114}$$
$$\left. + \begin{bmatrix} [K2_b] & 0 & 0 \\ 0 & 0 & 0 \\ 0 & 0 & 0 \end{bmatrix} \right) \begin{Bmatrix} W_b \\ W_m \\ W_\phi \end{Bmatrix} = \begin{Bmatrix} 0 \\ P_{\Delta Tm} \\ 0 \end{Bmatrix},$$

where $\{P_{\Delta Tb}\} = 0$ because it includes term $\{M_{\Delta T}\}$, and from Eq. (111), it's obvious that this term is equal to zero for isotropic beams and symmetric composite plates. Then collect W_b and W_m together as W, the simplified equation is

$$\begin{bmatrix} [M] & 0 \\ 0 & 0 \end{bmatrix} \begin{Bmatrix} \ddot{W} \\ \ddot{W}_\phi \end{Bmatrix} + \begin{bmatrix} [G] & 0 \\ 0 & 0 \end{bmatrix} \begin{Bmatrix} \dot{W} \\ \dot{W}_\phi \end{Bmatrix} + \left(\lambda \begin{bmatrix} A & 0 \\ 0 & 0 \end{bmatrix} \right.$$
$$+ \begin{bmatrix} [K] & [K_{w\phi}] \\ [K_{\phi w}] & [K_\phi] \end{bmatrix} - \begin{bmatrix} [K_{\Delta T}] & 0 \\ 0 & 0 \end{bmatrix} + \begin{bmatrix} [K_1] & 0 \\ 0 & 0 \end{bmatrix} \tag{115}$$
$$\left. + \begin{bmatrix} [K_2] & 0 \\ 0 & 0 \end{bmatrix} \right) \begin{Bmatrix} W \\ W_\phi \end{Bmatrix} = \begin{Bmatrix} P_{\Delta T} \\ 0 \end{Bmatrix},$$

where

$$[M] = \begin{bmatrix} [M_b] & 0 \\ 0 & 0 \end{bmatrix} \tag{116}$$

$$[G] = \begin{bmatrix} [G(\lambda, C_a)] & 0 \\ 0 & 0 \end{bmatrix} \tag{117}$$

$$[A] = \begin{bmatrix} [A_a] & 0 \\ 0 & 0 \end{bmatrix} \tag{118}$$

$$[K] = \begin{bmatrix} [K_b] & 0 \\ 0 & [K_m] \end{bmatrix} \tag{119}$$

$$[K_{\Delta T}] = \begin{bmatrix} [K_{\Delta Tb}] & 0 \\ 0 & 0 \end{bmatrix} \tag{120}$$

$$[K_{w\phi}] = \begin{bmatrix} [K_{b\phi}] \\ 0 \end{bmatrix} = [K_{\phi w}]^T \tag{121}$$

$$[K_1] = \begin{bmatrix} [K1_{Nm}] & [K1_{bm}] \\ [K1_{mb}] & 0 \end{bmatrix} \tag{122}$$

$$[K_2] = \begin{bmatrix} [K2_b] & 0 \\ 0 & 0 \end{bmatrix} \tag{123}$$

$$\{P_{\Delta T}\} = \begin{Bmatrix} 0 \\ P_{\Delta Tm} \end{Bmatrix}. \tag{124}$$

From the above equation, it's easy to find that free vibration of isotropic beams or symmetric composite plates is the special case of panel flutter when aerodynamic damping, aerodynamic stiffness matrices, thermal stiffness and thermal external force matrices equal to zero. So in derivation of the actuators, modal equations, etc., expressions for panel flutter will be used as a general case.

II.9 Critical Dynamic Temperature

The critical dynamic temperature of a panel is the temperature at which the panel starts to buckle. Since before or at the point of the buckling, the panel motion is linear, this is a static linear eigenvalue problem. Dynamic terms $[M_b]$ and $[G(\lambda, C_a)]$ will not be considered in the static problem. From Eq. (114), when only structure DOF is considered, the equation can be derived as:

$$\left(\lambda\begin{bmatrix} A_a & 0 \\ 0 & 0 \end{bmatrix} + \begin{bmatrix} [K_b] & 0 \\ 0 & [K_m] \end{bmatrix} - \begin{bmatrix} [K_{\Delta Tb}] & 0 \\ 0 & 0 \end{bmatrix} + \begin{bmatrix} [K1_{Nm}] & [K1_{bm}] \\ [K1_{mb}] & 0 \end{bmatrix} + \begin{bmatrix} [K2_b] & 0 \\ 0 & 0 \end{bmatrix}\right)\begin{Bmatrix} W_b \\ W_m \end{Bmatrix} = \begin{Bmatrix} 0 \\ P_{\Delta Tm} \end{Bmatrix}, \tag{125}$$

Let

$$\{\Psi(W)\} = ([K] + [K_{w1}] + [K_{w2}])\{W\} - \{P\} = 0, \tag{126}$$

where

$$\begin{aligned} [K] &= \begin{bmatrix} [K_b] - [K_{\Delta Tb}] & 0 \\ 0 & [K_m] \end{bmatrix}, \\ [K_{w1}] &= \begin{bmatrix} [K1_{Nm}] & [K1_{bm}] \\ [K1_{mb}] & 0 \end{bmatrix}, \\ [K_{w2}] &= \begin{bmatrix} [K2_b] & 0 \\ 0 & 0 \end{bmatrix}, \\ \{P\} &= \begin{Bmatrix} 0 \\ P_{\Delta Tm} \end{Bmatrix}. \end{aligned} \tag{127}$$

Then differentiating Eq. (126) by $\{W\}$, the incremental form of Eq. (126) is obtained:

$$[\frac{d\Psi(W)}{dW}]\{W\} = ([K] + 2[K_{w1}] + 3[K_{w2}])\{\Delta W\} = 0. \tag{128}$$

When only considering linear temperature effect, aerodynamic term and nonlinear terms in above equations are neglected. Incremental form of the thermal equations are

$$\begin{bmatrix} [K_b] - [K_{\Delta Tb}] + [K1_m(\{W_m\}_0)] & 0 \\ 0 & [K_m] \end{bmatrix} \begin{Bmatrix} \Delta W_b \\ \Delta W_m \end{Bmatrix} = 0, \tag{129}$$

where

$$\{W_m\}_0 = [K_m]^{-1}\{P_{m\Delta T}\}. \tag{130}$$

Obviously, temperature does not have relationship with inplane displacement $\{W_m\}$, but does have with bending displacement $\{W_b\}$. And from Eq. (??)-Eq. (111) and Eq. (130), $[K_{\Delta Tb}]$ and $[K1_m]$ are proportional to ΔT. Suppose λ_T is a random scalar, the thermal bending equation in an eigenvalue form is

$$[K_b]\{\phi\} = \lambda_T([K_{\Delta Tb}] - [K1_m(\{W_m\}_0)])\{\phi\}. \tag{131}$$

So the critical buckling temperature is determined by the minimum value of λ_T,

$$\Delta T_{cr} = \lambda_{Tmin}\Delta T. \tag{132}$$

II.10 Piezoelectric Actuators and Sensors

II.10.1 Separate Piezoelectric Actuators and Sensors

For a separate case, a piezoelectric material patch is applied as an actuator or as a sensor. So the electrical DOF are partitioned into sensor DOF and actuator DOF,

so the $\{W_\phi\}$ can be expressed as

$$\{W_\phi\} = \begin{Bmatrix} W_\phi^a \\ W_\phi^s \end{Bmatrix}. \tag{133}$$

Then other matrices also need to be wrote as

$$\begin{aligned} [K_{\phi w}] &= \begin{bmatrix} [K_{\phi w}^a] \\ [K_{\phi w}^s] \end{bmatrix} \\ [K_\phi] &= \begin{bmatrix} [K_\phi^a] & 0 \\ 0 & [K_\phi^s] \end{bmatrix}. \end{aligned} \tag{134}$$

From Eq. (115), two equations can be obtained:

$$[M]\{\ddot{W}\} + [G]\{\dot{W}\} + ([K_{lin}] + [K_1] + [K_2])\{W\} = \{P_{\Delta T}\} - [K_{w\phi}]\{W_\phi\}, \tag{135}$$

$$[K_{\phi w}]\{W\} = -[K_\phi]\{W_\phi\}, \tag{136}$$

where $[K_{lin}]$ can be expressed as

$$[K_{lin}] = [K] + [A] - [K_{\Delta T}]. \tag{137}$$

First, Eq. (136) is considered. The sensor equation from it is

$$\{q^s\} = [K_\phi^s]\{W_\phi^s\} = -[K_{\phi w}^s]\{W\}. \tag{138}$$

Since $\{W_\phi^s\}$ is the sensor voltage and $[K_\phi^s]$ is regarded as a capacitance here, the $\{q^s\}$ means the electric charge. So the output of the system is given by the charge sensor. Also the actuator equation can be derived from it,

$$\{q^a\} = [K_\phi^a]\{W_\phi^a\} = -[K_{\phi w}^a]\{W\}. \tag{139}$$

Similarly $\{q^a\}$ means actuator charge, which is not of interest, so Eq. (139) is ignored. Then, Eq. (135) is considered. It gives the relationship between the actuator voltage, sensor voltage and the deflection.

$$[M]\{\ddot{W}\} + [G]\{\dot{W}\} + ([K_{lin}] + [K_1] + [K_2])\{W\} = \{P_{\Delta T}\} - [K^a_{w\phi}]\{W^a_\phi\} - [K^s_{w\phi}]\{W^s_\phi\}. \tag{140}$$

And since the actuator voltage is much larger than the sensor voltage, the Eq. (140) can be reduced as

$$[M]\{\ddot{W}\} + [G]\{\dot{W}\} + ([K_{lin}] + [K_1] + [K_2])\{W\} = \{P_{\Delta T}\} - [K^a_{w\phi}]\{W^a_\phi\}. \tag{141}$$

From Eq. (116) and Eq. (118) – Eq. (120), the actuator and sensor equations are

$$[M_b]\{\ddot{W}_b\} + [G(\lambda, C_a)]\{\dot{W}_b\} + ([K] + [K2])\{W_b\} = -[K^a_{b\phi}]\{W^a_\phi\} \tag{142}$$

$$\{q^s\} = -[K^s_{\phi b}]\{W_b\}, \tag{143}$$

where the $[K]$ and $[K2]$ can be expressed like

$$\begin{aligned} [K] &= [K_b] + \lambda[A_a] + [K_{\Delta Tb}] + [K_{Nm}(\{W_m\}_0)] \\ [K2] &= [K2_b] - [K1_{bm}][K_m]^{-1}[K1_{mb}] - [K1_{Nm}(\{W_m\}_2)], \end{aligned} \tag{144}$$

and

$$\{W_m\}_0 = -[K_m]^{-1}\{P_{m\Delta T}\} \tag{145}$$

$$\{W_m\}_2 = -[K_m]^{-1}[K1_{mb}]\{W_b\}. \tag{146}$$

II.10.2 Self-sensing Actuators

For self-sensing actuators, they are simultaneously actuators and sensors. So $\{W_\phi\}$, $[K_{w\phi}]$, $[K_{\phi w}]$ and $[K_\phi]$ are not separated into two parts [61]. Then the equations for self-sensing actuators are

$$[M_b]\{\ddot{W}_b\} + [G(\lambda, C_a)]\{\dot{W}_b\} + ([K] + [K2])\{W_b\} = -[K_{b\phi}]\{W_\phi\} \tag{147}$$

$$\{q^s\} = -[K_{\phi b}]\{W_b\}. \tag{148}$$

II.11 Modal Equation

II.11.1 General Modal Equation for Beam, Plate and Panel Flutter

Since for a set of modal equations, there is no need to assemble and update the nonlinear stiffness matrices at each time integration step and the number of modal equations is much smaller than the number of equations of structure DOF [61]. We apply modal transformation to obtain the system modal equation of motion.

The bending displacements of the system as a linear combination of some known function

$$\{W_b\} = \sum_{r=1}^{n} q_r(t)\{\phi_r\} = [\Phi]\{q\}. \tag{149}$$

The linear frequencies and the corresponding natural modes are obtained from the linear vibration of the system

$$\omega_r^2[M_b]\{\phi_r\} = [K_b]\{\phi_r\}. \tag{150}$$

Since the element nonlinear stiffness matrices can be expressed by the element displacements $\{w_b\}$ and $\{w_m\}$, in turn, they can be expressed by the linear modes $\{\phi_r\}$.

So that the actuating equations of motion in modal coordinates become

$$[\bar{M}_b]\{\ddot{q}\} + [\bar{G}]\{\dot{q}\} + \left([\bar{K}] + [\bar{K}_{qq}]\right)\{q\} = -[\bar{K}^a_{b\phi}]\{W^a_\phi\}, \tag{151}$$

for self-sensing actuators, $\{W^a_\phi\}$ and $[\bar{K}^s_{\phi b}]$ are substituted by $\{W_\phi\}$ and $[\bar{K}_{\phi b}]$. And the sensing equation is

$$\{q^s\} = -[\bar{K}^s_{\phi b}]\{q\}, \tag{152}$$

for self-sensing actuators, $[\bar{K}^s_{\phi b}]$ is substituted by $[\bar{K}_{\phi b}]$. Then in above equation, the modal mass, linear stiffness and aerodynamic damping matrices are

$$\left([\bar{M}_b], [\bar{K}], [\bar{G}]\right) = [\Phi]^T \left([M_b], [K], [G(\lambda, C_a)]\right)[\Phi]. \tag{153}$$

The second order nonlinear modal stiffness matrix is

$$[\bar{K}_{qq}] = [\Phi]^T \sum_{r=1}^{n}\sum_{s=1}^{n} q_r q_s \left([K2_b]^{rs} - [K1_{Nm}(\{W_m\}_2)]^{rs} - [K1_{bm}]^r [K_m]^{-1} [K1_{mb}]^s\right)[\Phi]. \tag{154}$$

The modal piezoelectric control force is

$$[\bar{K}_{b\phi}] = \begin{bmatrix} [\bar{K}^a_{b\phi}] \\ [\bar{K}^s_{b\phi}] \end{bmatrix} = [\Phi]^T \begin{bmatrix} [K^a_{b\phi}] \\ [K^s_{b\phi}] \end{bmatrix} = [\Phi]^T [K_{b\phi}] = [\bar{K}_{\phi b}]^T. \tag{155}$$

II.11.2 Modal Participation

About the modes that will be included in the response analysis, they can be determined from the modal participation values [24, 61, 84],

$$Par_{r-th} = \frac{max|q_r|}{\sum_{s=1}^{n} max|q_s|}. \tag{156}$$

CHAPTER III

CONTROLLER DESIGN

III.1 State Space of the System

Based on the modal equations of motion Eq. (151), a standard state space for control design and simulation can be formed. $\mathbf{X}$ is the system state vector, which consists of the modal amplitudes and velocities:

$$\mathbf{X} = \begin{Bmatrix} q \\ \dot{q} \end{Bmatrix}. \tag{157}$$

$\mathbf{U}$ is the control input and $\mathbf{Y}$ is the sensor output:

$$\mathbf{U} = \{W_\phi^a\} \tag{158}$$

$$\mathbf{Y} = \{q^s\}, \tag{159}$$

for self-sensing actuators, $\{W_\phi^a\}$ is replaced by $\{W_\phi\}$. Then the state space form for the modal equations of motion is

$$\begin{aligned} \dot{\mathbf{X}} &= \bar{\mathbf{A}}(\mathbf{X}, \mathbf{t}) \cdot \mathbf{X} + \mathbf{B}\mathbf{U} \\ \mathbf{Y} &= \mathbf{C}\mathbf{X} + \mathbf{D}\mathbf{U}, \end{aligned} \tag{160}$$

where the system matrices are

$$\bar{\mathbf{A}} = \begin{bmatrix} 0 & I \\ -[\bar{M}_b]^{-1}[\bar{K}] & -[\bar{M}_b]^{-1}[\bar{G}] \end{bmatrix} + \begin{bmatrix} 0 & 0 \\ -[\bar{M}_b]^{-1}[\bar{K}_{qq}(\mathbf{X},\mathbf{t})] & 0 \end{bmatrix}$$

$$\mathbf{B} = \begin{bmatrix} 0 \\ -[\bar{M}_b]^{-1}[\bar{K}^a_{b\phi}] \end{bmatrix} \tag{161}$$

$$\mathbf{C} = \begin{bmatrix} -[\bar{K}^s_{\phi b}] & 0 \end{bmatrix}$$

$$\mathbf{D} = 0,$$

where $\bar{\mathbf{A}}$ is a real system state matrix. $[\bar{K}^a_{\phi b}]$ and $[\bar{K}^s_{\phi b}]$ are both $[\bar{K}_{\phi b}]$ for self-sensing actuators. In designing a controller for the system, we use its linearization form by applying Taylor series approach. In fact, the linearized result $\mathbf{A}$ matrix is the first part of $\bar{\mathbf{A}}$

$$\mathbf{A} = \begin{bmatrix} 0 & I \\ -[\bar{M}_b]^{-1}[\bar{K}] & -[\bar{M}_b]^{-1}[\bar{G}] \end{bmatrix}. \tag{162}$$

It is noted that the active control of nonlinear free vibrations is a special case of the general case of control of nonlinear panel flutter by settling $\lambda[A_a]$, $[G(\lambda, C_a)]$, $[K_{\Delta Tb}]$ and $\{P_{\Delta Tm}\}$ to zeros.

III.2 Linear Quadratic Regulator Control

Here a linear quadratic regulator (LQR) is used for the system. This method seeks a solution for the linear full state feedback problem defined as:

$$\mathbf{U} = -\mathbf{K}\mathbf{X}, \tag{163}$$

which minimizes a quadratic performance index, $\mathbf{J}$, that is a function of system states and control effort

$$\mathbf{J} = \int_0^\infty \left[\mathbf{X^T Q X} + \mathbf{U^T R U}\right] \mathbf{dt}, \tag{164}$$

where $\mathbf{Q}$ is a symmetric positive semi-definite state weighting and $\mathbf{R}$ is a symmetric positive definite control effort weighting. Minimizing Eq. (164), the controller gain is

$$\mathbf{K} = \mathbf{R^{-1} B^T P}, \tag{165}$$

where $\mathbf{P}$ is a positive definit symmetric matrix determined from the solution of the algebraic Riccati equation

$$\mathbf{A^T P + P A - P B R^{-1} B^T P + Q = 0}. \tag{166}$$

III.3 Extended Kalman Filter

To apply the LQR control, we have to know all the states of the system. In fact, it's difficult for sensor to give the accurate information of every state. So state estimator needs to be used like the linear Kalman Filter. It uses the linearized system equations and the nonlinear effects are not considered during the process. This may deteriorate the state estimation performance for large amplitude limit cycle amplitudes [61]. Therefore, the extended Kalman Filter (EKF) [85] is employed. It replaces the nominal trajectory based on the linearized system by the estimated trajectory, then evaluats the Taylor series about the estimated trajectory. Thus, if the system is sufficiently observable, the estimated trajectory is close to actual trajectory

sufficiently, and makes the estimation valid. The nonlinear state estimation is

$$\dot{\hat{\mathbf{X}}} = \bar{\mathbf{A}}\left(\hat{\mathbf{X}}, \mathbf{t}\right)\hat{\mathbf{X}} + \mathbf{BU} + \mathbf{K_e(t)}\left(\mathbf{Y} - \mathbf{C}\hat{\mathbf{X}}\right), \tag{167}$$

and the nonlinear measurement estimation is

$$\hat{\mathbf{Y}} = \mathbf{C}\hat{\mathbf{X}}. \tag{168}$$

The EKF contains the nonlinearity for the system dynamics, which is linearized in traditional Kalman Filter. That's one of the reasons why the extended Kalman Filter can have better robustness. The EKF uses linear approximation over very small range of the state space, then solves the Riccati equation to obtain the EFK gains. In fact, in our system, the linear approximation is for every step of the iteration for the nonlinear system. That linearization's range is much smaller than the linearization of the traditional Kalman Filter (which is the same as the linearization for LQR). And that is also a reason why the EKF can have better estimation.

The linear approximation matrix:

$$\mathbf{F(t)} \approx \left.\frac{\partial \mathbf{f}\left(\mathbf{X}, \mathbf{t}\right)}{\partial \mathbf{X}}\right|_{\mathbf{X}=\hat{\mathbf{X}}(\mathbf{t})} = \left[\begin{array}{ccccc} \frac{\partial \mathbf{f_1}}{\partial \mathbf{x_1}} & \frac{\partial \mathbf{f_1}}{\partial \mathbf{x_2}} & \frac{\partial \mathbf{f_1}}{\partial \mathbf{x_3}} & \cdots & \frac{\partial \mathbf{f_1}}{\partial \mathbf{x_n}} \\ \frac{\partial \mathbf{f_2}}{\partial \mathbf{x_1}} & \frac{\partial \mathbf{f_2}}{\partial \mathbf{x_2}} & \frac{\partial \mathbf{f_2}}{\partial \mathbf{x_3}} & \cdots & \frac{\partial \mathbf{f_2}}{\partial \mathbf{x_n}} \\ \frac{\partial \mathbf{f_3}}{\partial \mathbf{x_1}} & \frac{\partial \mathbf{f_3}}{\partial \mathbf{x_2}} & \frac{\partial \mathbf{f_3}}{\partial \mathbf{x_3}} & \cdots & \frac{\partial \mathbf{f_3}}{\partial \mathbf{x_n}} \\ \vdots & \vdots & \vdots & \ddots & \vdots \\ \frac{\partial \mathbf{f_n}}{\partial \mathbf{x_1}} & \frac{\partial \mathbf{f_n}}{\partial \mathbf{x_2}} & \frac{\partial \mathbf{f_n}}{\partial \mathbf{x_3}} & \cdots & \frac{\partial \mathbf{f_n}}{\partial \mathbf{x_n}} \end{array}\right]\Bigg|_{\mathbf{X}=\hat{\mathbf{X}}(\mathbf{t})}, \tag{169}$$

where

$$\mathbf{f(X, t)} = \dot{\mathbf{X}} = \bar{\mathbf{A}}(\mathbf{X}, \mathbf{t}) \cdot \mathbf{X} + \mathbf{BU}, \tag{170}$$

$$\{\mathbf{X}\} = [\mathbf{x_1}, \mathbf{x_2}, \mathbf{x_3}, \mathbf{x_4}, \mathbf{x_5}, \mathbf{x_6}, \mathbf{x_7}, \mathbf{x_8}]^{\mathbf{T}}. \tag{171}$$

Then

$$\left.\frac{\partial \mathbf{f}(\mathbf{X},\mathbf{t})}{\partial \mathbf{X}}\right|_{\mathbf{X}=\hat{\mathbf{X}}(\mathbf{t})} = \left.\frac{\partial(\bar{\mathbf{A}}(\mathbf{X},\mathbf{t})\cdot\mathbf{X}+\mathbf{B}\mathbf{U})}{\partial \mathbf{X}}\right|_{\mathbf{X}=\hat{\mathbf{X}}(\mathbf{t})}, \tag{172}$$

where $\mathbf{B}$ and $\mathbf{U}$ are not function of $\mathbf{X}$, so

$$\left.\frac{\partial \mathbf{f}(\mathbf{X},\mathbf{t})}{\partial \mathbf{X}}\right|_{\mathbf{X}=\hat{\mathbf{X}}(\mathbf{t})} = \left.\frac{\partial(\bar{\mathbf{A}}(\mathbf{X},\mathbf{t})\cdot\mathbf{X})}{\partial \mathbf{X}}\right|_{\mathbf{X}=\hat{\mathbf{X}}(\mathbf{t})} = \left.\frac{\partial(\mathbf{A}\mathbf{X}+\tilde{\mathbf{A}}(\mathbf{X},\mathbf{t})\cdot\mathbf{X})}{\partial \mathbf{X}}\right|_{\mathbf{X}=\hat{\mathbf{X}}(\mathbf{t})}, \tag{173}$$

and from Eq. (161),

$$\mathbf{A} = \begin{bmatrix} 0 & I \\ -[\bar{M}_b]^{-1}[\bar{K}] & -[\bar{M}_b]^{-1}[\bar{G}] \end{bmatrix}, \tilde{\mathbf{A}} = \begin{bmatrix} 0 & 0 \\ -[\bar{M}_b]^{-1}[\bar{K}_{qq}(\mathbf{X},\mathbf{t})] & 0 \end{bmatrix}. \tag{174}$$

So

$$\left.\frac{\partial \mathbf{f}(\mathbf{X},\mathbf{t})}{\partial \mathbf{X}}\right|_{\mathbf{X}=\hat{\mathbf{X}}(\mathbf{t})} = \mathbf{A} + \left.\frac{\partial(\tilde{\mathbf{A}}(\mathbf{X},\mathbf{t})\cdot\mathbf{X})}{\partial \mathbf{X}}\right|_{\mathbf{X}=\hat{\mathbf{X}}(\mathbf{t})} = \mathbf{A} + \left.\left(\tilde{\mathbf{A}}(\mathbf{X},\mathbf{t}) + \frac{\partial \tilde{\mathbf{A}}(\mathbf{X},\mathbf{t})}{\partial \mathbf{X}}\mathbf{X}\right)\right|_{\mathbf{X}=\hat{\mathbf{X}}(\mathbf{t})}, \tag{175}$$

and then

$$\mathbf{F}(\mathbf{t}) \approx \mathbf{A} + \left.\left(\tilde{\mathbf{A}}(\mathbf{X},\mathbf{t}) + \frac{\partial \tilde{\mathbf{A}}(\mathbf{X},\mathbf{t})}{\partial \mathbf{X}}\mathbf{X}\right)\right|_{\mathbf{X}=\hat{\mathbf{X}}(\mathbf{t})}. \tag{176}$$

In the program, $\frac{\partial(\tilde{\mathbf{A}}(\mathbf{X},\mathbf{t})\cdot\mathbf{X})}{\partial \mathbf{X}}$ is calculated by MATLAB function "Jacobian".

The Riccati equation for EKF:

$$\dot{\mathbf{P}}_\mathbf{e}(\mathbf{t}) = \mathbf{F}(\mathbf{t})\mathbf{P}_\mathbf{e}(\mathbf{t}) + \mathbf{P}_\mathbf{e}(\mathbf{t})\mathbf{F}(\mathbf{t})^\mathbf{T} - \mathbf{P}_\mathbf{e}(\mathbf{t})\mathbf{C}^\mathbf{T}\mathbf{R}_\mathbf{e}^{-1}\mathbf{C}\mathbf{P}_\mathbf{e}(\mathbf{t}) + \mathbf{Q}_\mathbf{e}. \tag{177}$$

The EKF gain:

$$\mathbf{K}_\mathbf{e}(\mathbf{t}) = \mathbf{P}_\mathbf{e}(\mathbf{t})\mathbf{C}^\mathbf{T}\mathbf{R}_\mathbf{e}^{-1}. \tag{178}$$

It is indicated from above equations that the EKF gain is evaluated on-line.

III.4 System Identification

In this paper, the parameters identification [86, 87] with a linear structure is proposed to identify the frequency of LCO. A commonly used linear model is the auto regressive exogenous (ARX) model with

$$\begin{aligned} y(k) = {} & \alpha_1 y(k-1) + \alpha_2 y(k-2) + \cdots + \alpha_p y(k-p) \\ & + \beta_0 u(k) + \beta_1 u(k-1) + \beta_2 u(k-2) + \cdots + \beta_p u(k-p) \end{aligned} . \tag{179}$$

It has 1 output and 1 control input, y and u can be selected from measured output and input. The coefficients α_i and β_i called observer Markov parameters with $i = 0, 1, 2, \ldots, p$ must be identified during operation. The parameter p is the order for the linear structure. Considering the simplification and accuracy of the frequency identification, the ARX model in this paper is represented with a second order equation involving only y ($\beta_i = 0$)

$$y(k) = -\alpha_1 y(k-1) - \alpha_2 y(k-2) . \tag{180}$$

System parameters or Markov parameters α_i, β_i can be found by using the recursive least squares method. Eq. (179) can be written in a vector form

$$y(k) = \bar{\mathbf{Y}} \mathbf{v_p} (k-1) , \tag{181}$$

where

$$\bar{\mathbf{Y}} = \begin{bmatrix} \alpha_1 & \alpha_2 & \cdots & \alpha_p & \beta_0 & \beta_1 & \beta_2 & \cdots & \beta_p \end{bmatrix} , \tag{182}$$

$$\mathbf{v_p}\,(k-1) = \begin{bmatrix} y(k-1) \\ \vdots \\ y(k-p) \\ u(k) \\ \vdots \\ u(k-p) \end{bmatrix}. \tag{183}$$

For different value of k, Eq. (181) can be written as

$$y = \bar{\mathbf{Y}}\mathbf{V_p}, \tag{184}$$

where

$$\begin{aligned} y &= \begin{bmatrix} y(k) & y(k+1) & \cdots & y(k+N-p-1), \end{bmatrix} \\ \mathbf{V_p} &= \begin{bmatrix} \mathbf{v_p}(k-1) & \mathbf{v_p}(k) & \cdots & \mathbf{v_p}(k+N-p-2), \end{bmatrix} \\ k &= p+1, p+2, \ldots. \end{aligned} \tag{185}$$

The integer N is the number of samples processed in the system identification. The system parameters, at time $(k+N-p-2)+1$, can be identified by using the least squares method

$$\bar{\mathbf{Y}} = y\mathbf{V_p}^T \left[\mathbf{V_p}\mathbf{V_p^T}\right]^+. \tag{186}$$

The symbol $^+$ represents pseudo inverse of matrix. Equation. (184) can be also used to formulate the batch system identification described in the next section. Then for our system

$$y = [y\,(2)\,y\,(3)\ \cdots y\,(k)] = [-\alpha_1 - \alpha_2] \begin{bmatrix} y\,(1) & y\,(2) & \cdots & y\,(k-1) \\ y\,(0) & y\,(3) & \cdots & y\,(k-2) \end{bmatrix}. \tag{187}$$

If transferred to z domain, the corresponding characteristic equation to Eq. (180) is

$$z^2 + \alpha_1 z + \alpha_2 = 0. \tag{188}$$

This characteristic equation can be used to identify the LCO frequency. First step is to find the roots of characteristic equation. Then free vibration natural frequency is calculated by using the relationship between Z-domain and S-domain for the poles

$$z = e^{sT}, \tag{189}$$

where T is the sampling time. One of the roots of the characteristic equation is the discrete system pole

$$z = z_0 + jz_1. \tag{190}$$

It can be represented by

$$z = \sqrt{z_0^2 + z_1^2}\,(z_0' + jz_1') = e^{s_1 T} e^{js_2 T}, \tag{191}$$

with

$$\sqrt{z_0^2 + z_1^2} = e^{s_1 T}, \tag{192}$$

and

$$z_0' + jz_1' = e^{js_2 T}, \tag{193}$$

where

$$z_0' = \frac{z_0}{\sqrt{z_0^2 + z_1^2}}, \tag{194}$$

and

$$z_1' = \frac{z_1}{\sqrt{z_0^2 + z_1^2}}. \tag{195}$$

For the discrete pole location z, one can calculate s_1 and s_2, then obtain the system pole $s_1 + js_2$ in the S-domain.

$$\begin{aligned} s_1 &= \frac{1}{T} \ln \sqrt{z_0^2 + z_1^2}, \\ s_2 &= \tan^{-1}\left(\frac{z_1'}{z_2'}\right). \end{aligned} \tag{196}$$

The free vibration natural frequency is

$$\omega_n = \sqrt{s_1^2 + s_2^2}. \tag{197}$$

And the LCO period becomes

$$\mathbf{T_p} = \frac{2\pi}{\omega_n} \quad \text{sec.} \tag{198}$$

III.5 Control Method with System Identification

For the nonlinear system in our case, if using EKF without an accurate initial estimation of states at the time when control begins, it's hard to provide a good estimation of the states, which will affect the control results very much. The system is periodic, so for a certain frequency, the states values at different time point within the period are distinct. Then before implementing the controller, several frequency-state value relationships can be obtained. During the control stage, the sensors will give us the information about the displacement, from which the nonlinear frequency of the free vibration can be calculated. Then through interpolation, certain state values can be derived from the relationship between the frequency and state values at a particular time point. Thus, even if the system changes its frequency suddenly for some reason, the frequency can still be detected and a good initial states estimation can be obtained for EKF.

To obtain the frequency-state value relationship, two steps are needed. First, based on material properties of the objects, the relationship between nonlinear frequency and vibration amplitude can be known. Curves expressing such relationships will be shown in next chapter. From such relationships and the frequency identified, the amplitude of the system can be obtained. Second, if the amplitude is known, state values of a particular time point can be calculated by a numerical method – shooting method [88].

CHAPTER IV

ACTUATOR AND SENSOR PLACEMENT

Placement of sensors and actuators is another important factor in suppression of the large amplitude vibration and flutter response of the system. Optimal locations for the sensors and actuators would make the control very effective. On the contrary, bad locations of them may degrade the control results and even produce spillover of the system. Here, the NFCG, H_2 and NKFEG methods are used to choose the optimal locations for the actuators and sensors.

For the NFCG norm method [1,2], the sum of the square of every element of the LQR gain can be calculated when an actuator is placed at each element of the object.

$$\text{NFCG} = \sqrt{\sum_{j=1}^{2n} k_{ij}^2}, \quad (i = 1, 2, ...N), \tag{199}$$

where k_{ij} is the element of the feedback gain $\mathbf{K}$ from Eq. (165). If the value for the location is higher, the more control authority it has for the location. Since each NFCG norm is calculated for each location, locations with higher NFCG norm are chosen to be the optimal locations for the actuators. Similarly, the optimal sensor location can be chosen by the Kalman Filter feedback estimation gain (NKFEG) [61]:

$$\text{NKFEG} = \sqrt{\sum_{j=1}^{2n} ke_{ij}^2}, \quad (i = 1, 2, ...N), \tag{200}$$

where ke_{ij} is the element of the feedback gain $\mathbf{K_e}$ from Eq. (178). If the value for the location is higher, the more sensing ability it has for the location. Since each NKFEG norm is calculated for each location, locations with higher NKFEG norm are chosen to be the optimal locations for the sensors.

For the H_2 norm method, H_2 norm of the transfer function can be used to obtain the response characteristic at the location where the actuator is placed.

$$\|G_i\|_2^2 = \frac{1}{2\pi}\int_{-\infty}^{\infty}\{G_i(j\omega, x_1, y_1) * G_i(j\omega, x_1, y_1)\}, \quad (i = 1, 2, ...N), \tag{201}$$

where G_i is the transfer function of the largest deflection point (x_1, y_1). A higher H_2 norm represent a higher controllability. Locations with higher H_2 norm are chosen to be the optimal locations for the actuators.

After the locations of actuators and sensors are determined, combine both together, and they are the optimal locations for self-sensing actuators.

CHAPTER V

FREE VIBRATIONS CONTROL RESULTS

V.1 Material Properties

The system equations of motion of the beam and the composite plate are transferred into modal equations. The time domain numerical method is employed to obtain the limit cycle oscillation (LCO). The fourth order Runge-Kutta method is used [89]. The properties of the isotropic beam, composite plate, the PZT5A and MFC are shown in table 1.

Table 1 The Material Properties for the Isotropic Beam, Composite Plate, PZT5A and MFC.

Materials	Aluminum	Graphite-epoxy	PZT5A	MFC
Young's Modulus (psi) (N/m^2)	$E = 8.85e6$ $(6.10e10)$	$E_1 = 22.50e6$ $(15.5e10)$ $E_2 = 1.17e6$ $(8.07e9)$	$E_p = 9.00e6$ $(6.21e10)$	$E_{p1} = 5.29e6$ $(6.51e10)$ $E_{p2} = 1.10e6$ $(7.58e9)$
Shear Modulus (psi) (N/m^2)	$G = 3.38e6$ $(2.33e10)$	$G_{12} = 0.66e6$ $(4.55e9)$	$G_p = 3.46e6$ $(2.39e10)$	$G_{p12} = 2.12e6$ $(1.46e10)$ $G_{p23} = 1.06e6$ $(7.31e9)$
Poisson's Ratio	$\nu = 0.31$	$\nu_1 = 0.22$ $\nu_2 = 0.011$	$\nu_p = 0.30$	$\nu_{p1} = 0.25$ $\nu_{p2} = 0.05$
Density (lb-$sec^2/inch^4$) (kg/m^3)	$\rho = 2.54e-4$ (2702)	$\rho = 1.458e-4$ (1550)	$\rho_p = 7.10e-4$ (7582)	$\rho_p = 7.07e-4$ (7552)
Thickness (inch) (m)	$h = 0.054$ $(1.37e-3)$	$h = 0.054$ $(1.37e-3)$	$h = 0.009$ $(2.3e-4)$	$h = 0.009$ $(2.3e-4)$
Charge Constant (inch/V) (m/V)			$d_{31} = -7.51e-9$ $(1.91e-10)$	$d_{11} = 2.09e-8$ $(5.31e-10)$ $d_{12} = -8.27e-9$ $(-2.10ee-10)$
Electrode Space (inch) (m)			$h_k = 0.009$ $(2.3e-4)$	$h_k = 0.042$ $(1.07e-3)$
Maximum Voltage (V)			$Vmax = 820$	$Vmax = 2000$

V.2 Adaptive Beam Vibration Control

V.2.1 Dimensions of the Beam

To suppress the large amplitude nonlinear free vibration, a clamped beam is first considered. The dimension of the aluminum beam is of $102.87 \times 5.715 \times 0.1372$ cm^3 ($40.5 \times 2.25 \times 0.054$ in.^{3}), and the finite element mesh has been chosen as 24×1 for the whole beam model. Three methods are used to decide the optimal locations of the self-sensing piezoelectric actuators.

V.2.2 Placement of Self-sensing Actuators

The NFCG method is used to find the optimal locations for the actuators. The result is shown in Fig. V.1(a). One can apply the NKFEG method to find the optimal locations for the sensors by calculating the norm of Kalman Filter estimation gain. The result is shown in Fig. V.2(b). Then one can place the self-sensing actuators at the optimal locations of both actuators and sensors as shown in Fig. V.1(c). The self-sensing actuators are bonded on the top and bottom of the beam using NFCG norm > 84 and NKFEG norm > 1.35. Based on the optimal locations, four control inputs/ouputs are used.

One can repeat the whole process by using the H_2 norm method for optimal actuator locations. About this method, self-sensing actuators are placed at the locations where H_2 norm > 75 and NKFEG norm > 1.35. The result is shown in Fig. 2. Based on the optimal locations, three control inputs/ouputs are used.

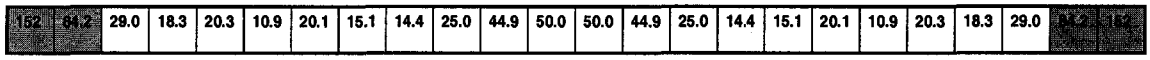

(a) NFCG norm of every element of the whole beam

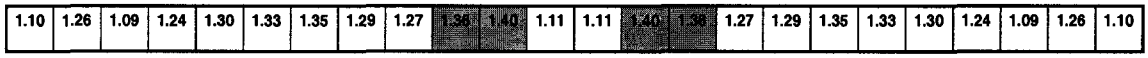

(b) NKFEG norm of every element of the whole beam

(c) The optimal locations based on the two norms for the whole beam

Figure 1 Actuators' and sensors' locations on the beam based on NFCG and NKFEG norms.

(a) H_2 norm of every element of the whole beam

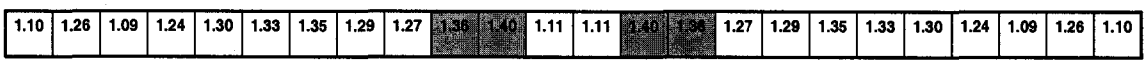

(b) NKFEG norm of every element of the whole beam

(c) The optimal locations based on the two norms for the whole beam

Figure 2 Actuators' locations on the beam based on H_2 and NKFEG norms.

V.2.3 Free Vibration of the Beam

Results for free vibration of the beam are shown in the following. First, the relationship of the frequency ratio and W_{max}/h is shown in Fig. V.3(a). The time history, the phase plot and the power spectrum density plot of the free vibration of the beam are shown in Fig. V.3(b)– V.3(d). The time histories of the first four symmetric modes, $q_1(t), q_3(t), q_5(t)$ and $q_7(t)$, are shown in Fig. 4. Obviously, it is a limit cycle oscillation.

V.2.4 Adaptive Beam Vibration Control with NFCG Norm and PZT5A

The control of the beam vibration is shown in Fig. 5. The control inputs shown in all the figures are obtained through dividing the original control inputs by the maximum control inputs shown in table 1. It is hard for the controller to suppress the free vibration.

So the adaptive control is used to solve the problem. The relationship between system frequency ratio and the amplitude shown in Fig. V.3(a) is used. Before the controller is implemented, five or six frequency ratios and corresponding amplitudes W_{max}/h are chosen. Then corresponding to each known frequency ratio or amplitude W_{max}/h, all the states at the initial or some other time can be obtained by shooting method. So the relationship between frequency ratio and state values can be obtained. The system identification algorithm is implemented right before the controller is activated so that accurate estimated states can be used for EKF. For NFCG method case, the LQR/EKF is turned on at t = 0.45 sec and t = 0.826 sec, so the system ID is turned on during the period of t = 0.4 sec to t = 0.45 sec, and

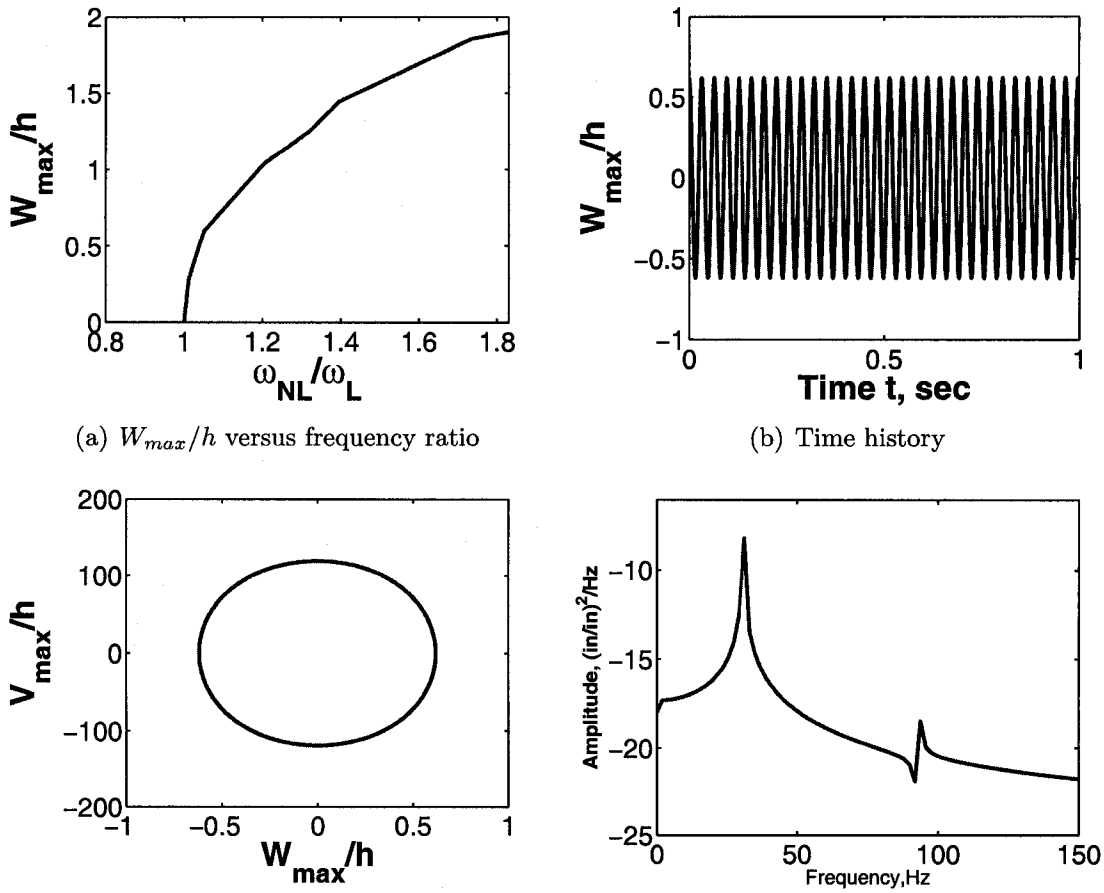

(a) W_{max}/h versus frequency ratio

(b) Time history

(c) Phase plot

(d) Power spectrum density

Figure 3 Free vibration response of the clamped beam using 4 symmetric modes.

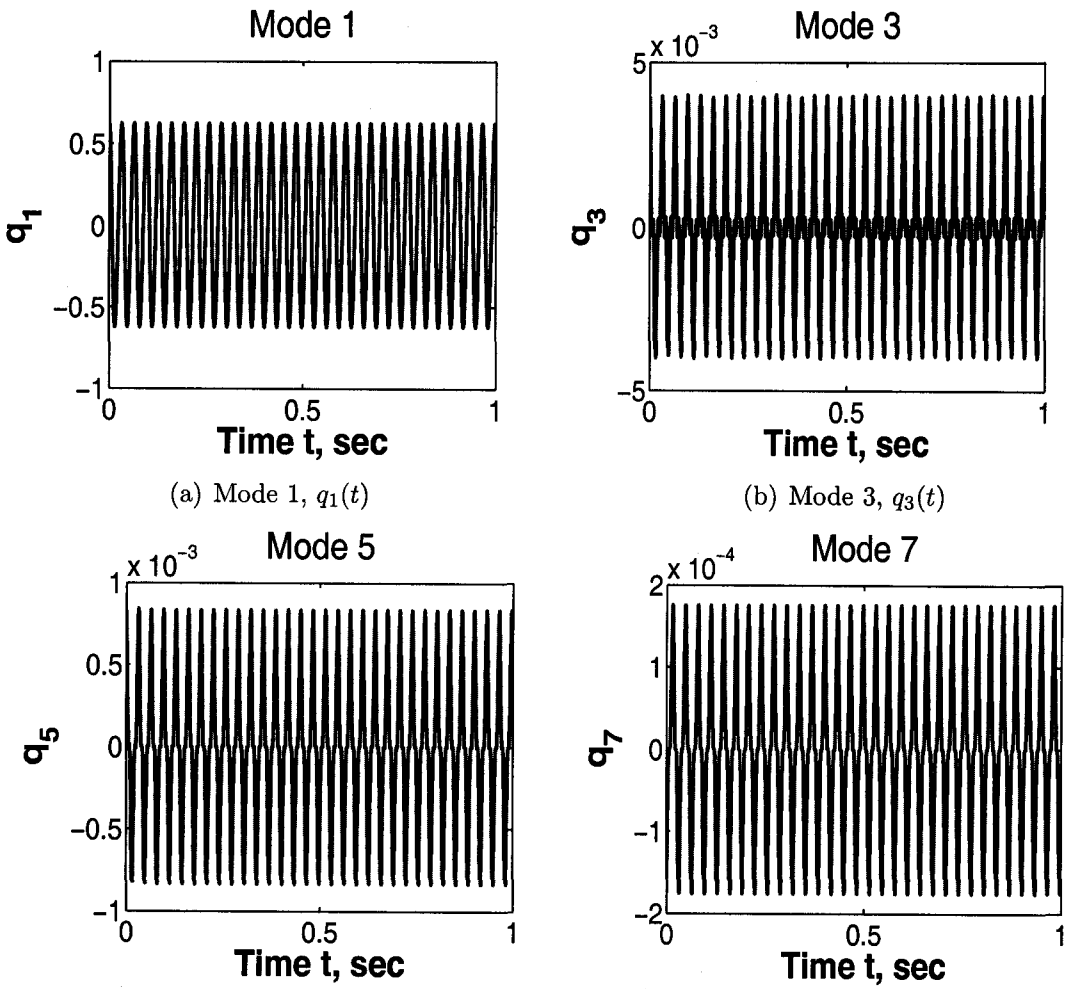

(a) Mode 1, $q_1(t)$

(b) Mode 3, $q_3(t)$

(c) Mode 5, $q_5(t)$

(d) Mode 7, $q_7(t)$

Figure 4 Time histories of the 4 symmetric modes for the free vibration of a clamped beam.

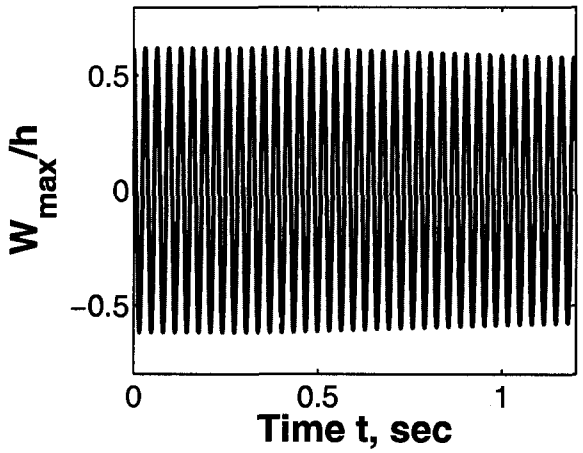

(a) Controlled vibration

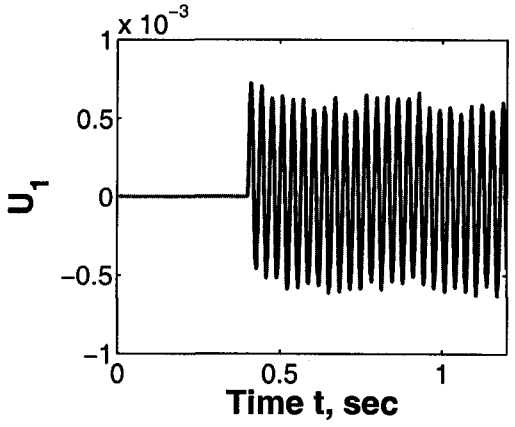

(b) Control input 1

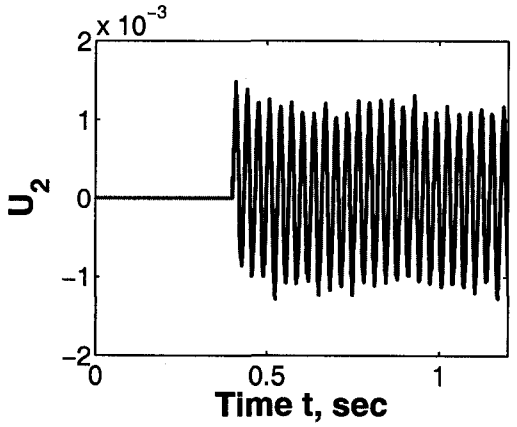

(c) Control input 2

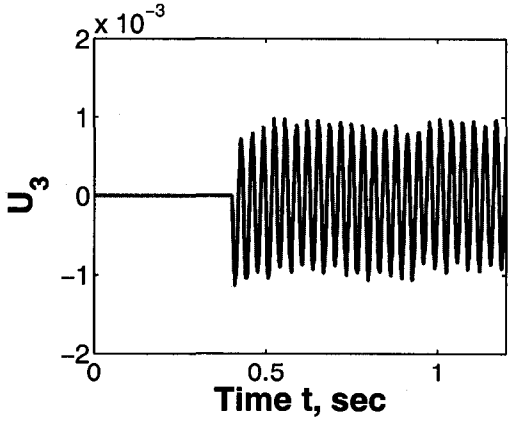

(d) Control input 3

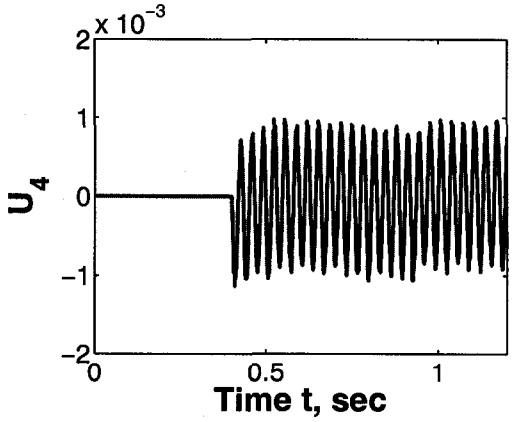

(e) Control input 4

Figure 5 The displacement and control input for the 4-mode beam control using LQR/EKF with NFCG norm and PZT5A.

t = 0.8 sec to t = 0.826 sec. Figure. 7 shows the time period when system ID is working. Figure 6 shows that the adaptive control efficiently suppress the vibration even its amplitude changes suddenly at t = 0.8 sec.

From the sensors, the displacement information is known, and the nonlinear frequency ratio of the system can be calculated. Although multiple outputs exist, only the dominant one is used for frequency identification. So only the output 1, which is from the sensors at the maximum deflection is used for both NFCG and H_2 method. For each frequency ratio, the state values can be obtained through interpolation. So when the limit cycle motion suddenly changes for some unknown causes, the new frequency ratio can be detected by the modal frequency identification algorithm. After that, some state values for the vibration are determined. And these values can be used as the updated initial state estimation for the extended Kalman Filter. Then, controlling for the system can be realized based on the updated initial state estimation. Figures. 6–8 show that the system amplitude W_{max}/h changes suddenly from 0.6 to 1.2, and the adaptive control suppresses the vibration successfully.

V.2.5 Adaptive Beam Vibration Control with H_2 norm and PZT5A

Another actuator placement method, H_2 norm method is considered. The results for adaptive control for these cases are shown in Figs. 8. From the control results, the overshooting and settling time of the condition of H_2 norm are almost the same as the NFCG norm method. When the control results are comparable, the actuators can be connected together as 3 pieces using H_2 norms instead of 4 pieces using NFCG norms (see Figs. 1 and 2). When the number of inputs/outputs is larger, the connection of wires will be more complicated and the corresponding method is

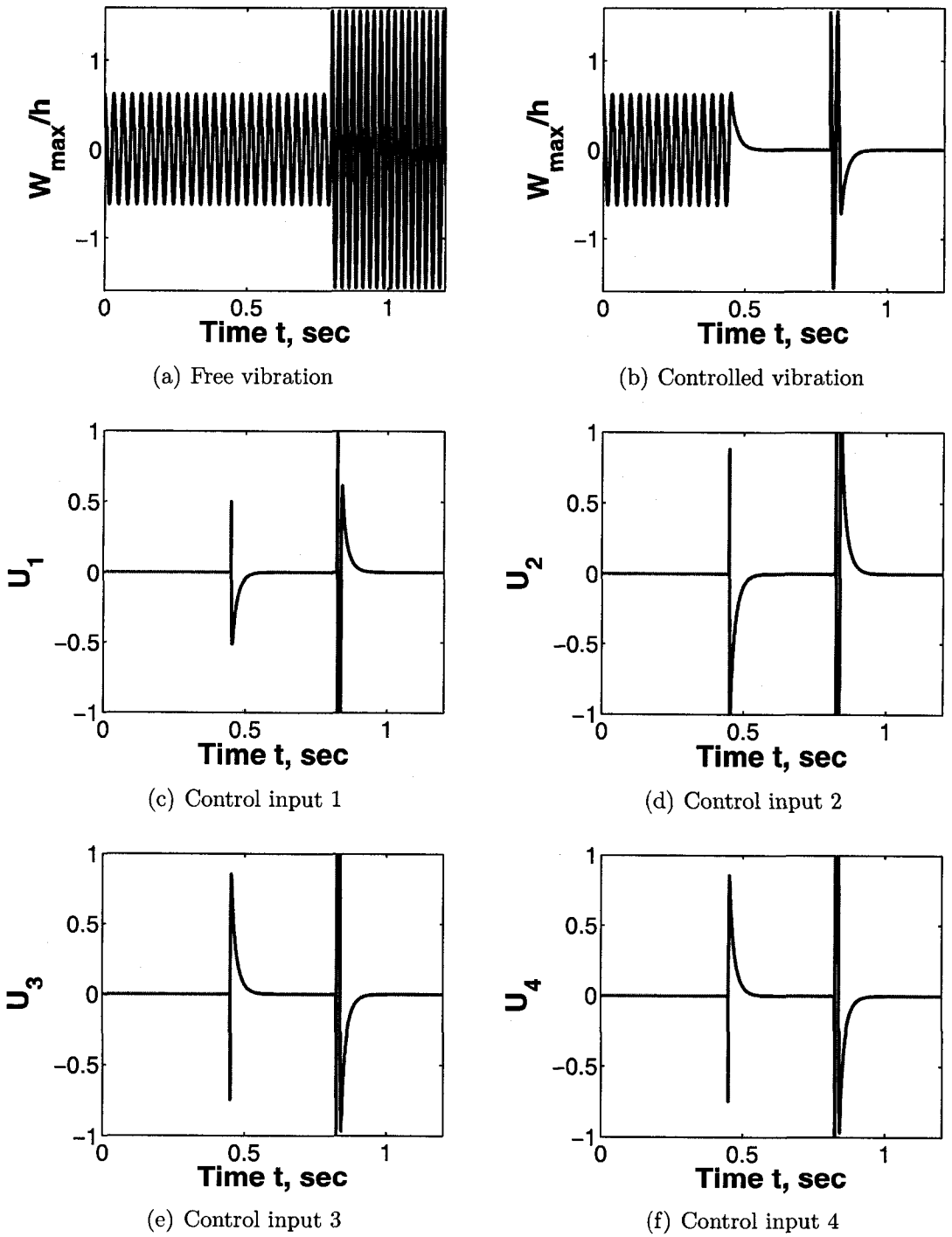

(a) Free vibration

(b) Controlled vibration

(c) Control input 1

(d) Control input 2

(e) Control input 3

(f) Control input 4

Figure 6 A changed free vibration and adaptive control for the 4-mode clamped beam by using NFCG norm and PZT5A.

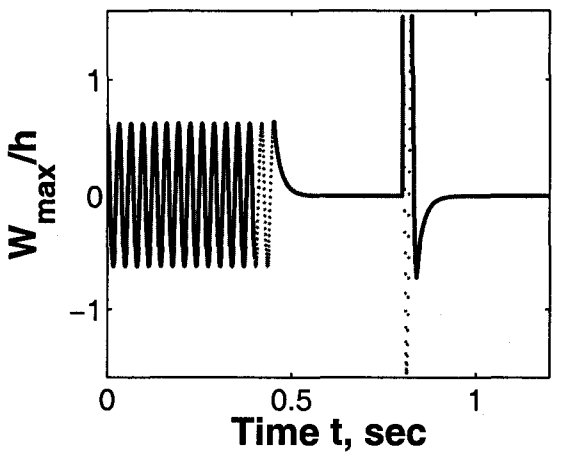

(a) Controlled vibration with system identification

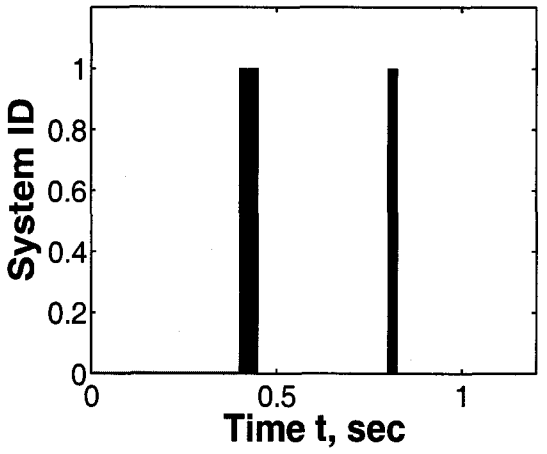

(b) System identification working period

Figure 7 System identification working period corresponding to controlled vibration.

more difficult to realize in practice. So the H_2 norm method for optimal actuator locations is preferred here.

V.3 Adaptive Composite Plate Vibration Control

The methods for the beam control and optimal location of self-sensing actuators can be applied to a clamped 6-layer $[0/60°/-60°]_s$ rectangular composite plate. The composite plate is of $85.725 \times 57.15 \times 0.1372$ cm^3 ($33.75 \times 22.5 \times 0.054$ in.^{3}), and the mesh is 16×16 or 256 BFS elements for the full plate model.

V.3.1 Placement of Self-sensing Actuators

NFCG, H_2 and NKFEG norms are applied here. The three types of norms for the whole composite plate and the locations of the self-sensing actuators for a whole plate are shown in Figs. 9 and 11, respectively. First, the NFCG norm > 71 and $NKFEG$ norm > 8.2 are applied to embed the PZT5A on the top and bottom of the composite plate. About another method, self-sensing actuators are placed at the locations where H_2 norm > 0.12 and NKFEG norm > 8.2.

V.3.2 Free Vibration of the Composite Plate

The results of the frequency ratio versus W_{max}/h, time history of the free vibration, phase plot and power spectrum density are shown in Fig. 13. It is clearly a limit cycle oscillation. Figure. 14 shows the time history of the amplitudes of the 4 lowest symmetric modes: $q_{11}(t), q_{31}(t), q_{13}(t)$ and $q_{33}(t)$.

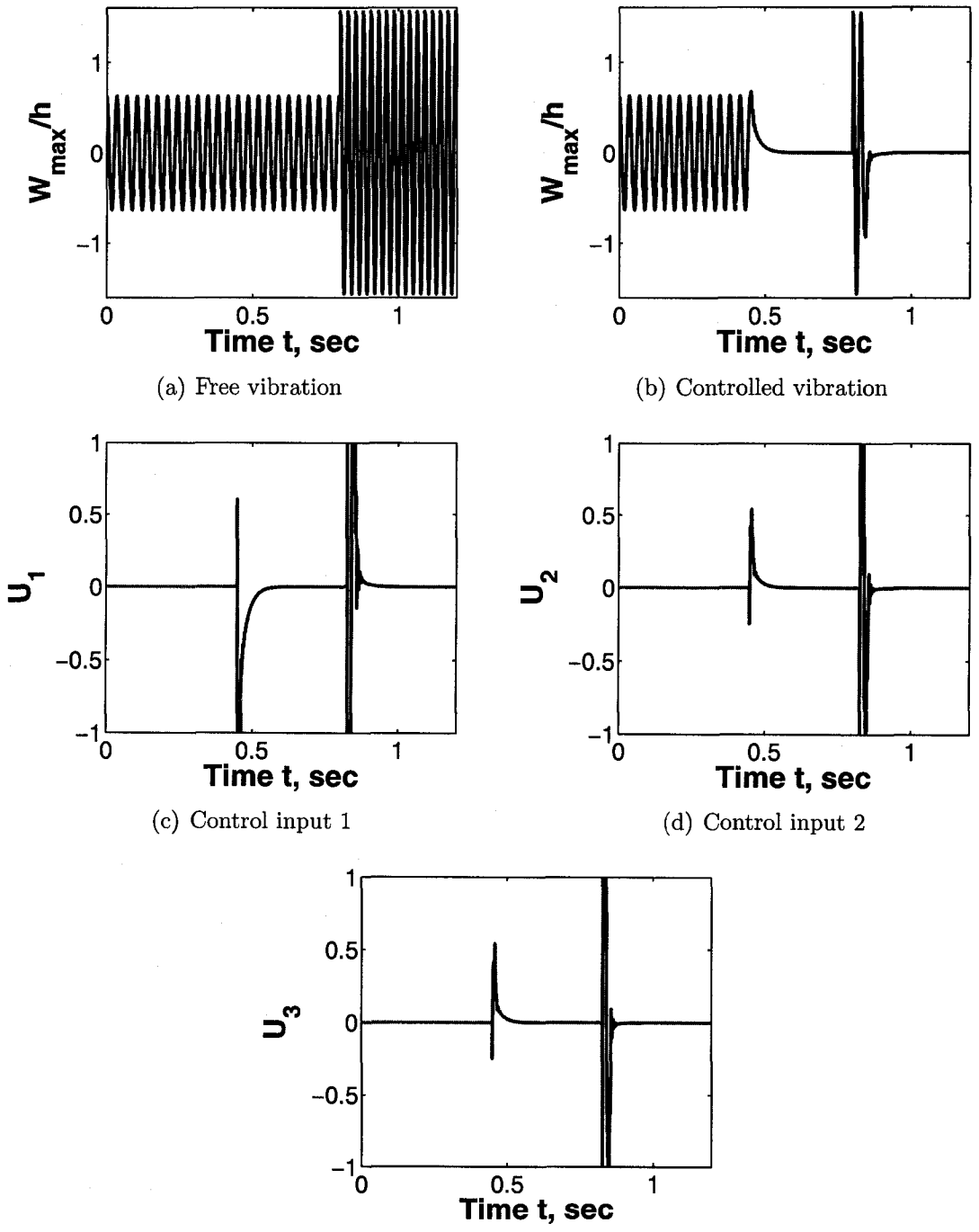

(a) Free vibration

(b) Controlled vibration

(c) Control input 1

(d) Control input 2

(e) Control input 3

Figure 8 A changed free vibration and adaptive control for the 4-mode clamped beam by using H_2 norm and PZT5A.

1.48	6.74	19.6	30.9	36.4	22.9	34.5	44.8	46.6	33.5	10.3	5.91	5.52	2.91	1.52	1.03
2.73	1.5	1.36	1.74	2.87	3.92	4.3	4.6	4.79	5.3	3.37	2.14	1.39	1.24	1.4	1.22
7.97	1.4	10.1	20.5	19.8	21.5	34.3	34	20.5	10.7	10.7	20.7	20.7	4.03	1.23	2.04
17.5	2.28	19.4	39.5	33.9	26.3	51	61.5	44.2	20.4	17.3	50.4	51.9	24.7	1.26	4.36
32.1	4.83	22.6	42.3	33.8	14.3	32.4	64.3	48.3	17.3	7.28	32.9	56.4	34.7	1.55	9.21
38.4	3.39	20.5	46.2	39.2	8.9	19.4	64.8	57.5	20.9	2.31	13.9	16	9.68	2.35	18.6
41.8	3.45	23	45.5	49.7	12.1	21.4	61	74.8	31.5	5.51	19.6	24.8	14.7	4.14	34.4
40	3.69	22.9	45.5	47.7	19	32.1	65.1	71.6	39.6	16.1	34.3	33.3	17.3	4.36	35.8
35.8	4.36	17.3	33.3	34.3	16.1	39.6	71.6	65.1	32.1	19	47.7	45.5	22.9	3.69	40
34.4	4.14	14.7	24.8	19.6	5.51	31.5	74.8	61	21.4	12.1	49.7	45.5	23	3.45	41.8
18.6	2.35	9.68	16	13.9	2.31	20.9	57.5	64.8	19.4	8.9	39.2	46.2	20.5	3.39	38.4
9.21	1.55	34.7	56.4	32.9	7.28	17.3	48.3	64.3	32.4	14.3	33.8	42.3	22.6	4.83	32.1
4.36	1.26	24.7	51.9	50.4	17.3	20.4	44.2	61.5	51	26.3	33.9	39.5	19.4	2.28	17.5
2.04	1.23	4.03	20.7	20.7	10.7	10.7	20.5	34	34.3	21.5	19.8	20.5	10.1	1.4	7.97
1.22	1.4	1.24	1.39	2.14	3.37	5.3	4.79	4.6	4.3	3.92	2.87	1.74	1.36	1.5	2.73
1.03	1.52	2.91	5.52	5.91	10.3	33.5	46.6	44.8	34.5	22.9	36.4	30.9	19.6	6.74	1.48

(a) NFCG norm of every element of the composite plate

4	4	4	4	4	5.62	5.33	5.64	6.67	5.69	4.5	4	4.39	4	4	4
4	4.01	4	4	4.06	4.06	4.04	4.02	4.01	4.01	4.01	4	4.06	4.03	4	4
4	4	4	4	4	6.28	6.39	6	5.38	4.96	3.98	4	4	4	4.04	4
4	4	5.24	4	4	4	8.21	8.22	6.81	5.78	5.06	4	4.01	4	4	4
4	4.05	5.72	5.97	4	4	6.4	7.53	6.36	4.97	4.84	4	4.01	4.01	4	4
4.47	4.1	4.01	4	4	4.86	4.17	6.27	5.33	5.16	4.56	4.26	4	4.98	4.01	4
6.03	4.13	4.22	8.13	6.76	5.3	4.04	5.85	5.96	5.8	5.01	5.72	6.49	5.73	4.01	5.06
6.08	4.1	4.24	8.57	7.66	6.64	4.05	7.36	7.3	4.05	6.2	7.21	7.87	4.18	4.05	5.82
5.82	4.05	4.18	7.87	7.21	6.2	4.05	7.3	7.36	4.05	6.64	7.66	8.57	4.24	4.1	6.08
5.06	4.01	5.73	6.49	5.72	5.01	5.8	5.96	5.85	4.04	5.3	6.76	8.13	4.22	4.13	6.03
4	4.01	4.98	4	4.26	4.55	5.16	5.33	6.27	4.17	4.86	4	4	4.01	4.1	4.47
4	4	4.01	4.01	4	4.84	4.97	6.36	7.53	6.4	4	4	5.97	5.72	4.04	4
4	4	4	4.01	4.01	5.06	5.78	6.81	8.22	8.21	4	4	4	5.24	4	4
4	4.04	4	4	4	4.05	4.96	5.38	6	6.39	6.28	4	4	4	4	4
4	4	4.03	4.06	4	4.01	4.01	4.01	4.02	4.04	4.06	4.06	4	4	4.01	4
4	4	4	4.39	4	4.5	5.69	6.67	5.64	5.33	5.62	4	4	4	4	4

(b) NKFEG norm of every element of the composite plate

Figure 9 NFCG and NKFEG norms for the composite plate.

V.3.3 Adaptive Composite Plate Vibration Control with NFCG and H_2 norms, PZT5A

The results for vibration control of the composite plate are shown in Figs. 15–16. The control performance of both NFCG and H_2 norm is good. The optimal location of the self-sensing actuators based on the NFCG norm method is easier to implement because the number of inputs or outputs is 5 when using NFCG norm but 8 using H_2 norm. The NFCG norm method for optimal actuator locations is preferred here for the simplicity.

From all the results above, it is obvious that LQR/EKF with system identification is a good method for the free vibration control. Especially when there is a sudden change in the amplitude/frequency, the system identification algorithm can supply an accurate initial state values for the EKF in a very short time. With the good initial state estimation, EKF can give a very good estimation to LQR, and LQR can supply an efficient control performance. So the system ID works as a key part in the control. It decides the operation efficiency of EKF and then decides the whole performance of the controller.

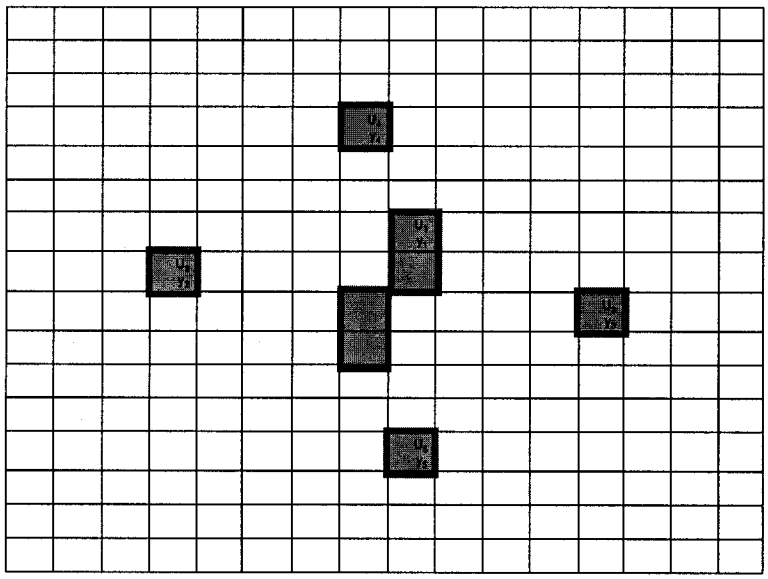

Figure 10 The optimal locations of actuators and sensors based on the two norms for the composite plate.

0.028	0.048	0.06	0.067	0.057	0.064	0.063	0.072	0.075	0.052	0.058	0.066	0.065	0.059	0.047	0.025
0.034	0.022	0.033	0.032	0.024	0.034	0.04	0.04	0.031	0.018	0.037	0.045	0.042	0.031	0.026	0.038
0.045	0.034	0.063	0.067	0.064	0.068	0.078	0.082	0.076	0.057	0.095	0.078	0.083	0.066	0.034	0.05
0.049	0.035	0.084	0.078	0.073	0.074	0.087	0.093	0.092	0.077	0.057	0.103	0.109	0.086	0.047	0.056
0.043	0.021	0.136	0.083	0.072	0.075	0.107	0.081	0.088	0.085	0.062	0.068	0.144	0.092	0.051	0.057
0.054	0.052	0.114	0.087	0.061	0.085	0.097	0.058	0.067	0.1	0.094	0.045	0.065	0.09	0.049	0.052
0.062	0.057	0.115	0.086	0.057	0.088	0.106	0.084	0.074	0.107	0.097	0.071	0.08	0.115	0.043	0.041
0.064	0.057	0.116	0.094	0.079	0.102	0.107	0.1	0.097	0.106	0.098	0.084	0.094	0.107	0.052	0.059
0.059	0.052	0.107	0.094	0.084	0.098	0.106	0.097	0.1	0.107	0.102	0.079	0.094	0.116	0.057	0.064
0.041	0.043	0.115	0.08	0.071	0.097	0.107	0.074	0.084	0.106	0.088	0.057	0.086	0.115	0.057	0.062
0.052	0.049	0.09	0.065	0.045	0.094	0.1	0.067	0.058	0.097	0.085	0.061	0.087	0.114	0.052	0.054
0.057	0.051	0.092	0.144	0.068	0.062	0.085	0.088	0.081	0.107	0.075	0.072	0.083	0.119	0.021	0.043
0.056	0.047	0.086	0.109	0.103	0.057	0.077	0.092	0.093	0.087	0.074	0.073	0.078	0.084	0.035	0.049
0.05	0.034	0.066	0.083	0.078	0.095	0.057	0.076	0.082	0.078	0.068	0.064	0.067	0.063	0.034	0.045
0.038	0.026	0.031	0.042	0.045	0.037	0.018	0.031	0.04	0.04	0.034	0.024	0.032	0.033	0.022	0.034
0.025	0.047	0.059	0.065	0.066	0.058	0.052	0.075	0.072	0.063	0.064	0.057	0.067	0.06	0.048	0.028

(a) H_2 norm of every element of the composite plate

4	4	4	4	4	5.62	5.33	5.64	6.67	5.69	4.5	4	4.39	4	4	4
4	4.01	4	4	4.06	4.06	4.04	4.02	4.01	4.01	4.01	4	4.06	4.03	4	4
4	4	4	4	4	6.28	6.39	6	5.38	4.96	3.98	4	4	4	4.04	4
4	4	5.24	4	4	4	8.21	8.22	6.81	5.78	5.06	4	4.01	4	4	4
4	4.05	5.72	5.97	4	4	6.4	7.53	6.36	4.97	4.84	4	4.01	4.01	4	4
4.47	4.1	4.01	4	4	4.86	4.17	6.27	5.33	5.16	4.56	4.26	4	4.98	4.01	4
6.03	4.13	4.22	8.13	6.76	5.3	4.04	5.85	5.96	5.8	5.01	5.72	6.49	5.73	4.01	5.06
6.08	4.1	4.24	8.57	7.66	6.64	4.05	7.36	7.3	4.05	6.2	7.21	7.87	4.18	4.05	5.82
5.82	4.05	4.18	7.87	7.21	6.2	4.05	7.3	7.36	4.05	6.64	7.66	8.57	4.24	4.1	6.08
5.06	4.01	5.73	6.49	5.72	5.01	5.8	5.96	5.85	4.04	5.3	6.76	8.13	4.22	4.13	6.03
4	4.01	4.98	4	4.26	4.55	5.16	5.33	6.27	4.17	4.86	4	4	4.01	4.1	4.47
4	4	4.01	4.01	4	4.84	4.97	6.36	7.53	6.4	4	4	5.97	5.72	4.04	4
4	4	4	4.01	4.01	5.06	5.78	6.81	8.22	8.21	4	4	4	5.24	4	4
4	4.04	4	4	4	4.05	4.96	5.38	6	6.39	6.28	4	4	4	4	4
4	4	4.03	4.06	4	4.01	4.01	4.01	4.02	4.04	4.06	4.06	4	4	4.01	4
4	4	4	4.39	4	4.5	5.69	6.67	5.64	5.33	5.62	4	4	4	4	4

(b) NKFEG norm of every element of the composite plate

Figure 11 H_2 and NKFEG norms for the composite plate.

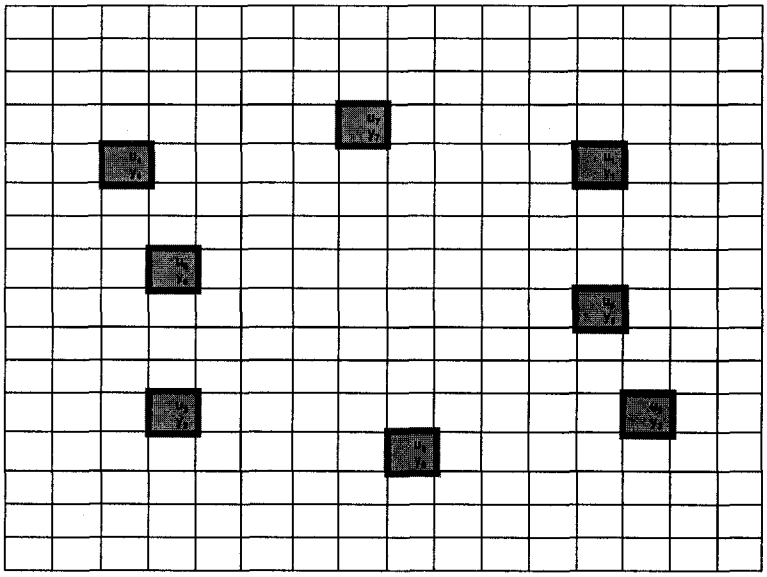

Figure 12 The optimal locations of actuators and sensors based on the two norms for the composite plate.

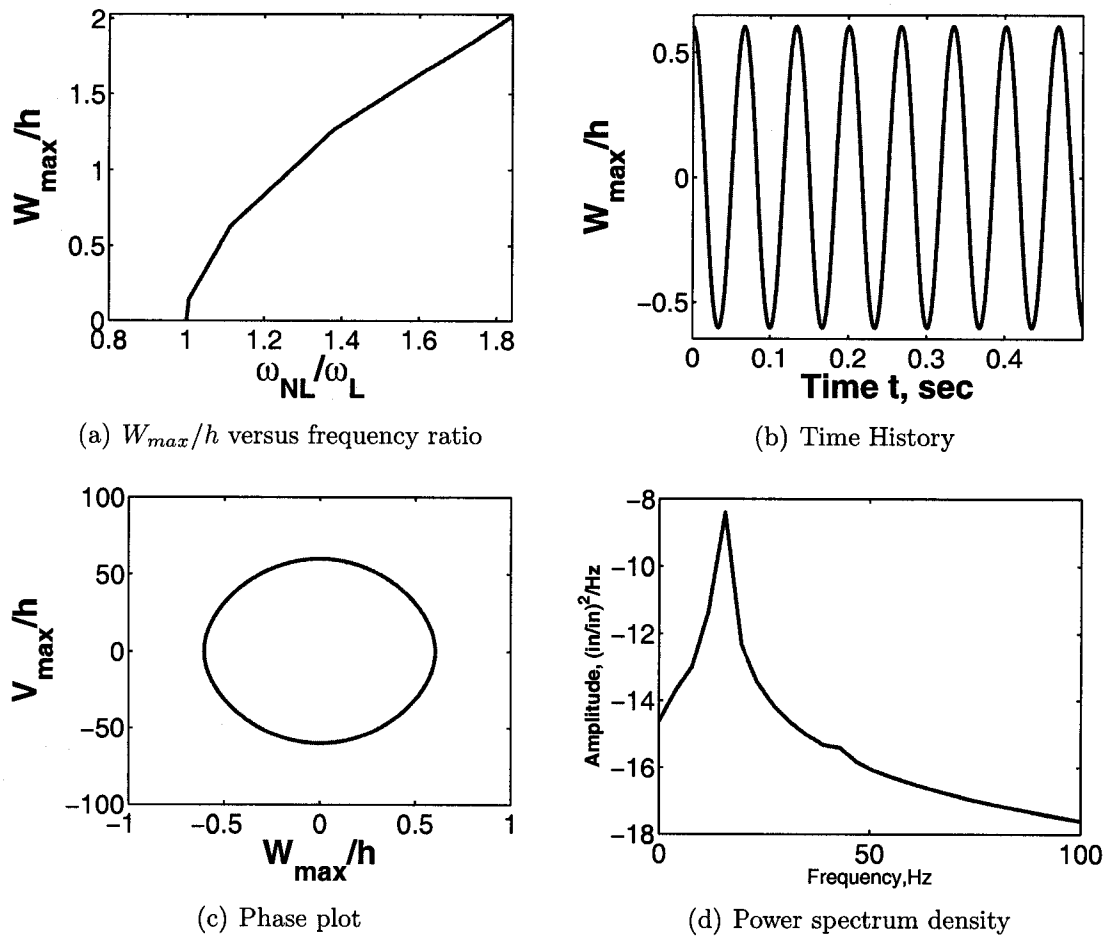

(a) W_{max}/h versus frequency ratio

(b) Time History

(c) Phase plot

(d) Power spectrum density

Figure 13 Free vibration response of the clamped composite plate using 4 lowest modes.

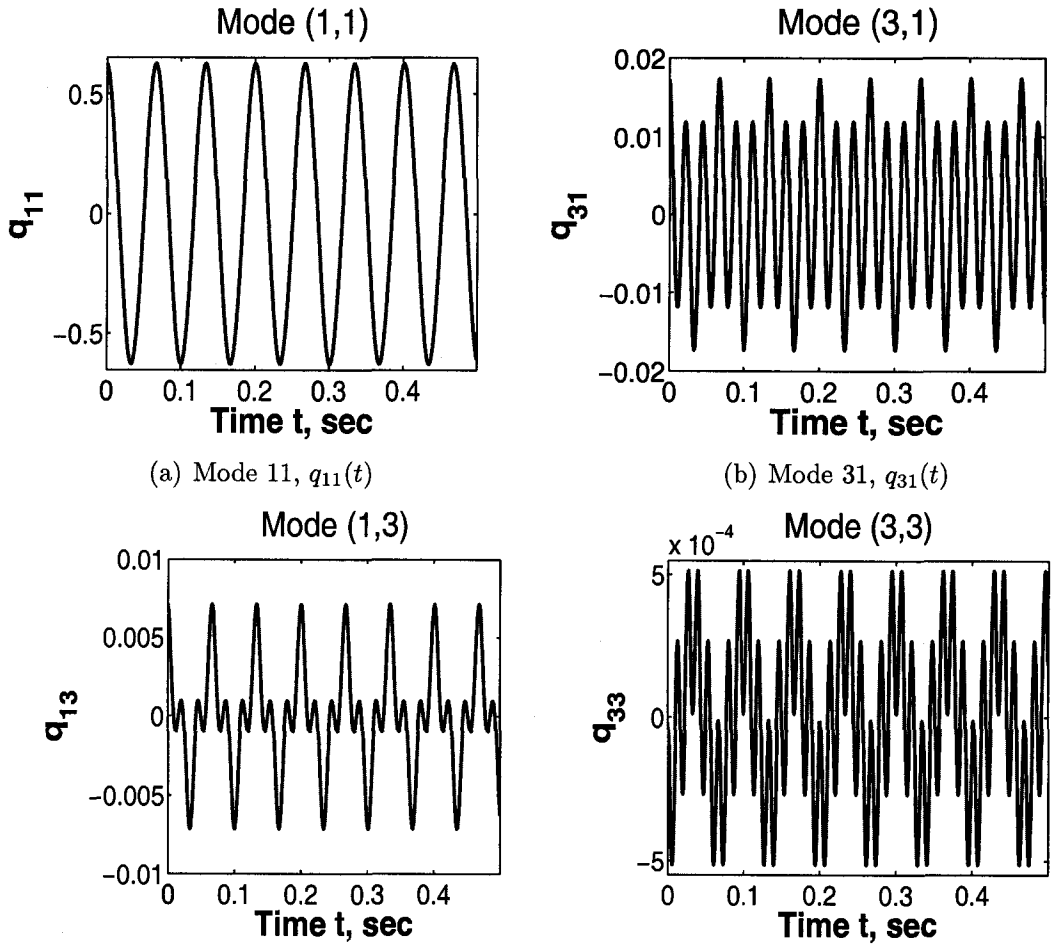

(a) Mode 11, $q_{11}(t)$

(b) Mode 31, $q_{31}(t)$

(c) Mode 13, $q_{13}(t)$

(d) Mode 33, $q_{33}(t)$

Figure 14 Time histories of the 4 lowest modes for the free vibration of a clamped composite plate.

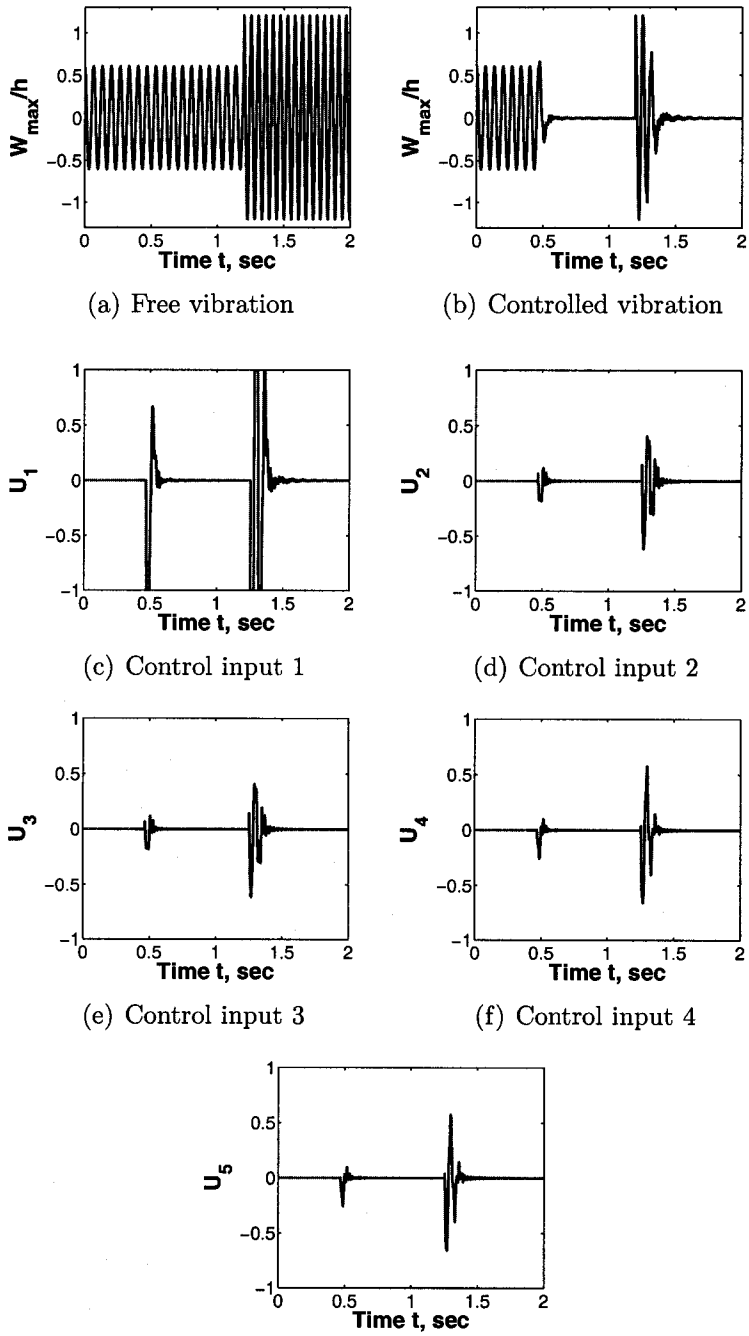

(a) Free vibration (b) Controlled vibration

(c) Control input 1 (d) Control input 2

(e) Control input 3 (f) Control input 4

(g) Control input 5

Figure 15 A changed free vibration and adaptive control for the 4-mode clamped composite plate by using NFCG norm and PZT5A.

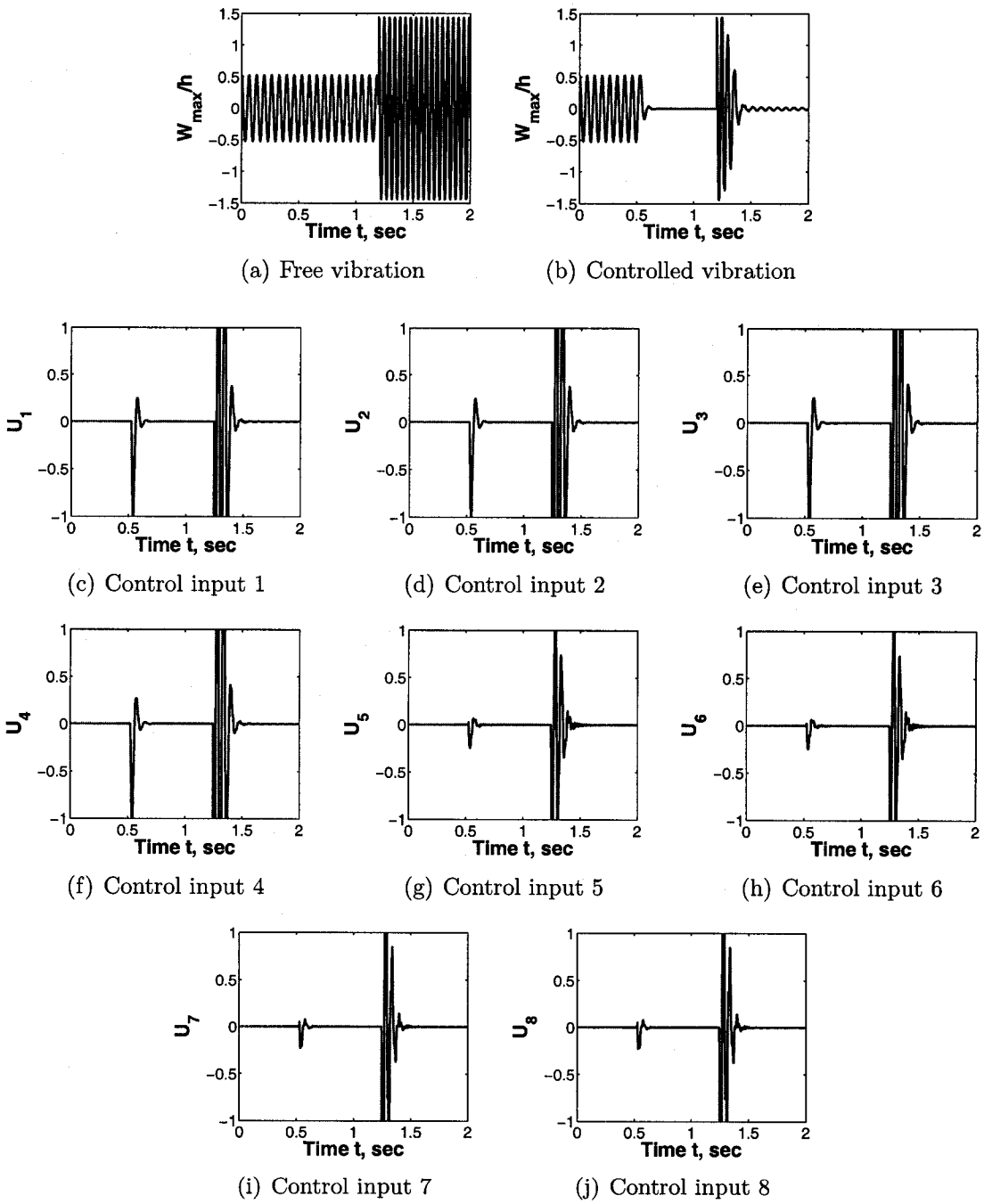

(a) Free vibration (b) Controlled vibration

(c) Control input 1 (d) Control input 2 (e) Control input 3

(f) Control input 4 (g) Control input 5 (h) Control input 6

(i) Control input 7 (j) Control input 8

Figure 16 A changed free vibration and adaptive control for the 4-mode clamped composite plate by using H_2 norm and PZT5A.

CHAPTER VI

PANEL FLUTTER CONTROL RESULTS

The properties of the 2-D and 3-D panels are the same as the isotropic beam and the composite plate shown in table 1.

VI.1 LCO Control

When there is no thermal loads, the panel flutter produces limit cycle oscillation (LCO). Control of 2-D and 3-D LCO panel flutter is discussed in this section.

VI.1.1 2-D Panel Flutter Control

The dimensions of the 2-D panel is $171.45 \times 5.715 \times 0.1372$ cm^3 ($67.5 \times 2.25 \times 0.054$ in.^{3}), and the finite element mesh have been chosen as 20×1 for the whole model.

Placement of Self-sensing Actuators

From the results of last chapter, control performance obtained by using NFCG norm method is similar to H_2 norm method in choosing actuators' locations. In this part, only NFCG method will be implemented. NKFEG method is used for optimal sensor location. After calculation of NFCG and NKFEG norms, self-sensing actuators will be placed at both the optimal locations for actuators and sensors. For LCO case, NFCG and NKFEG norms of PZT5A actuators and sensors are shown in Fig. 17. Another piezoelectric material, MFC, is also implemented as actuators and sensors here. Since MFC's stress constant is twice larger than that of PZT5A ($d_{11} > 2d_{31}$), MFC can provide more control force than PZT5A. So theoretically,

MFC can supply better control performance than PZT5A. The results later will show that less actuators or sensors are needed in flutter suppression when using MFC. NFCG and NKFEG norms of MFC actuators and sensors are shown in Fig. 18.

2-D Panel Flutter Analysis

For a no thermal stresses case, when the actuators and sensors are placed on the 2-D panel using NFCG and NKFEG norms, the relationship of the dynamic pressure and W_{max}/h is shown in Fig. VI.19(a). And the time history, the phase plot and power spectrum density plot of the free vibration of the beam are shown in Fig. VI.19(b) – VI.19(d). The time histories of the first four lowest modes, $q_1(t), q_2(t), q_3(t)$ and $q_4(t)$, are shown in Fig. 20. Obviously, it is a limit cycle oscillation.

2-D Panel Flutter Suppression with PZT5A and MFC

Theoretically, MFC is more efficient than PZT5A in vibration control. To prove this point, a small number of MFC will be applied than PZT5A when both provide good control performance. In Fig. 21 and Fig. 22, both PZT5A and MFC suppressed panel flutter successfully; 2 MFC's are used but 3 PZT5A's are used to achieve the same results (Dynamic pressure $\lambda = 900$). Actuators and sensors have been optimally applied in both cases; less actuators or sensors may produce unstable results. The results in Figs. 21–22 show the advantage of MFC. By the way, only LQR/EFK can provide good control performance even the initial state estimation is not so accurate. That is because, aerodynamic damping exist in the supersonic panel flutter, and the damping will make the panel flutter converge to a particular motions no matter what

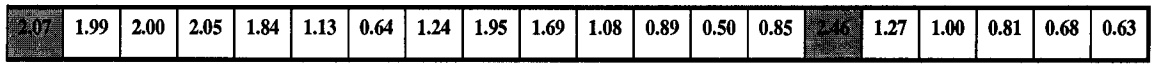

(a) NFCG norm of every element of the whole 2-D panel

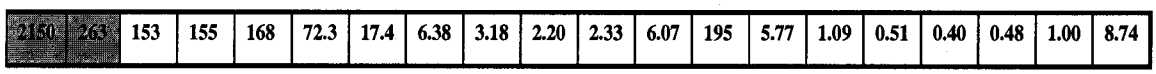

(b) NKFEG norm of every element of the whole 2-D panel

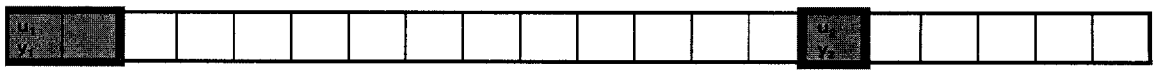

(c) optimal locations of actuators and sensors of the whole 2-D panel

Figure 17 NFCG, NKFEG norms and actuators' and sensors' locations on the 2-D panel for PZT5A and LCO case.

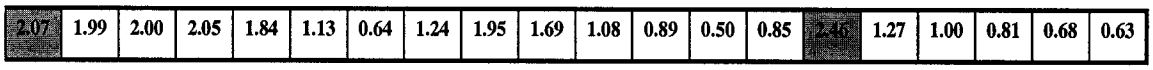

(a) NFCG norm of every element of the whole 2-D panel

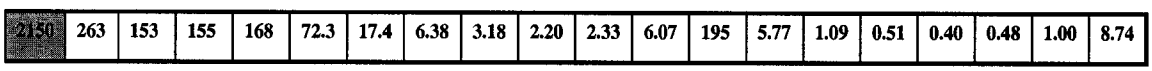

(b) NKFEG norm of every element of the whole 2-D panel

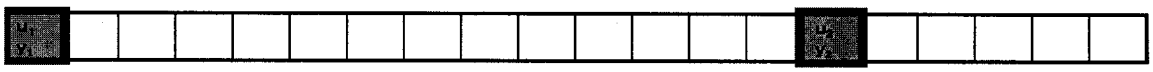

(c) optimal locations of actuators and sensors of the whole 2-D panel

Figure 18 NFCG, NKFEG norms and actuators' and sensors' locations on the 2-D panel for MFC and LCO case.

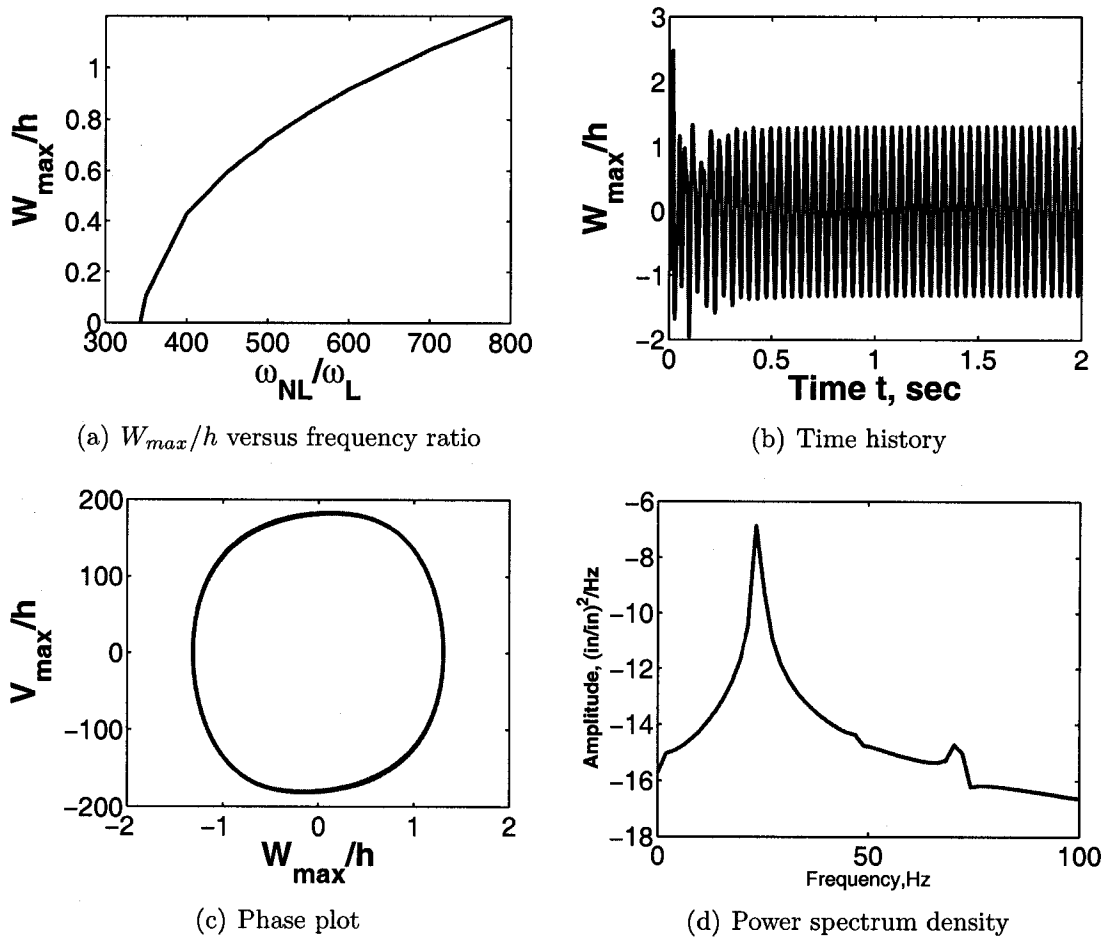

(a) W_{max}/h versus frequency ratio

(b) Time history

(c) Phase plot

(d) Power spectrum density

Figure 19 LCO response of the 2-D panel flutter at $\lambda = 900$ using 4 lowest modes.

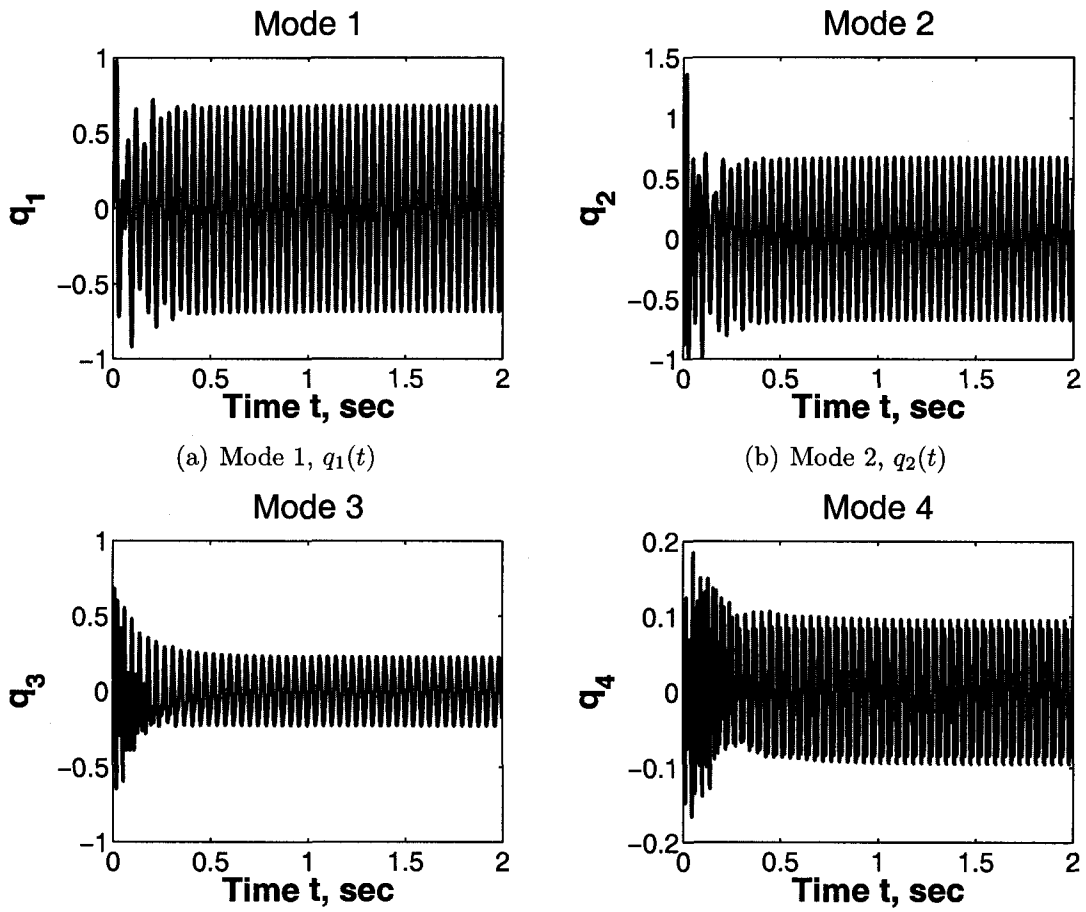

(a) Mode 1, $q_1(t)$

(b) Mode 2, $q_2(t)$

(c) Mode 3, $q_3(t)$

(d) Mode 4, $q_4(t)$

Figure 20 Time histories of the 4 lowest modes for the 2-D LCO panel flutter at $\lambda = 900$.

kind of initial states the system has. With this aerodynamic damping, the estimated states from EKF can converge to real states much faster than free vibration. So LQR/EKF can give good control performance in the suppression of panel flutter of all cases (LCO, static deflections and chaotic motions).

VI.1.2 3-D Panel Flutter Control

The dimensions of the 3-D panel is $102.87 \times 68.58 \times 0.1372$ cm^3 ($40.5 \times 27 \times 0.054$ in.^{3}), and the finite element mesh have been chosen as 12×12 for the whole model.

Placement of Self-sensing Actuators

Similar to 2-D case, suppression of 3-D panel flutter also applied separated actuators and sensors. NFCG and NKFEG norms of PZT5A and MFC actuators and sensors are shown in Fig. 23 – Fig. 26. Also, the number of MFC is less than that of PZT5A when both of them suppressed the 3-D panel flutter successfully.

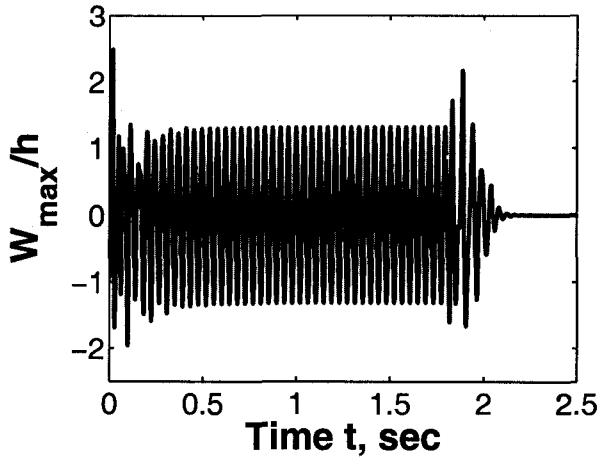

(a) Controlled panel flutter

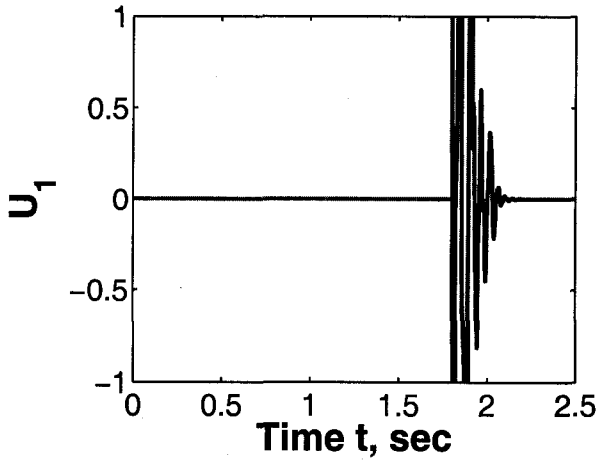

(b) Control input 1

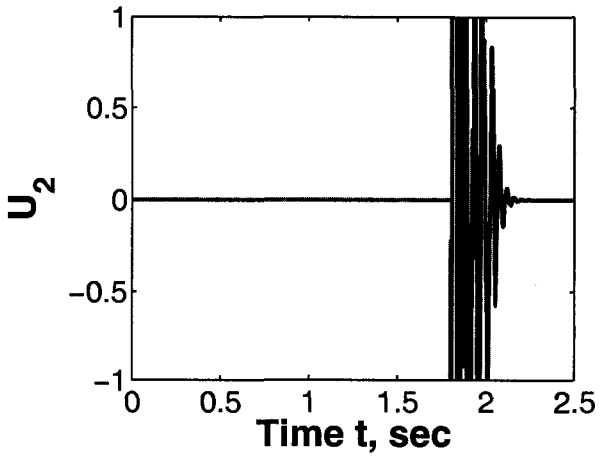

(c) Control input 2

Figure 21 2-D panel flutter ($\lambda = 900$) suppression for the 4-mode LCO model using PZT5A.

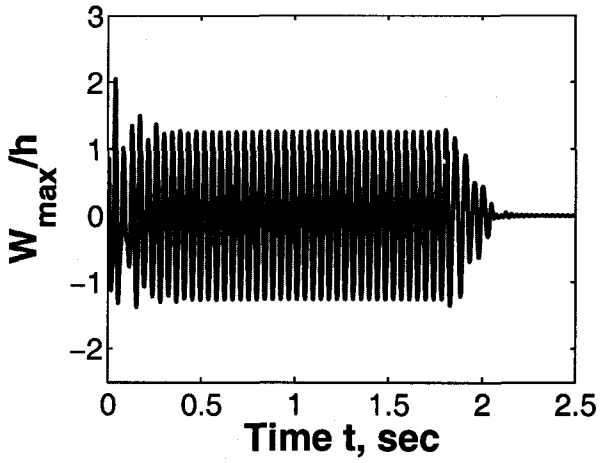

(a) Controlled panel flutter

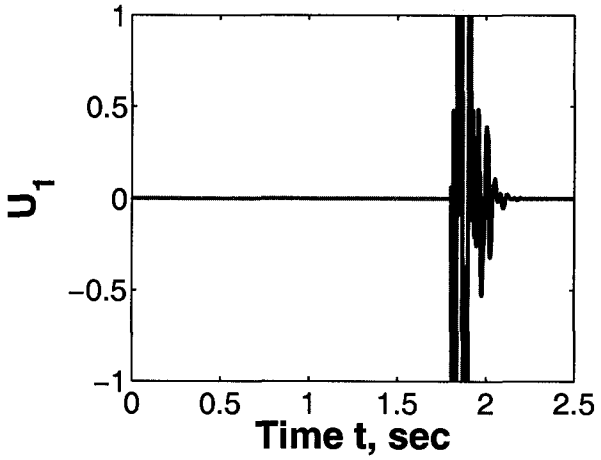

(b) Control input 1

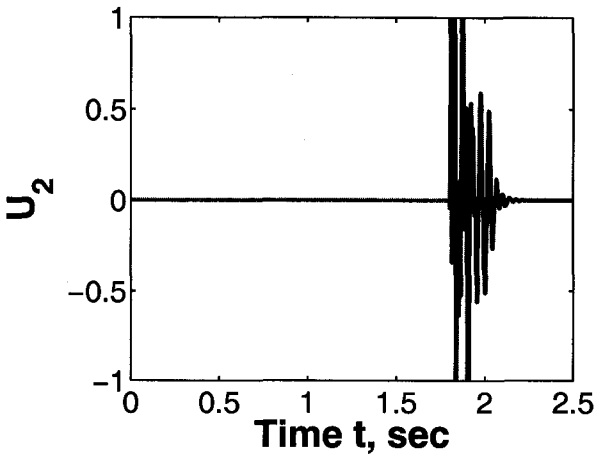

(c) Control input 2

Figure 22 2-D panel flutter ($\lambda = 900$) suppression for the 4-mode LCO model using MFC.

11.1	11.4	13.3	3.07	27.4	11.7	3.72	2.51	5.68	5.97	38.3	8.74
10.6	10.7	11.9	3.91	16.4	10.6	5.22	2.32	6.58	4.34	23.3	29.8
10.4	10.2	11.5	4.96	16.5	10.2	5.54	2.97	6.34	4.61	24.5	16.8
10.2	9.45	11.4	5.43	4.71	10.2	5.7	3.85	5.87	4.41	12.7	5.96
10.1	9.72	10.9	5.25	4.75	10.1	5.68	4.24	5.88	4.18	3.29	2.61
9.98	9.99	10.4	5.05	4.61	10.2	5.86	4.45	6.3	5.27	11.4	2.63
9.69	9.89	10.8	5.27	4.25	10.4	6.03	4.09	7.61	8.18	54	3.75
9.99	10	11	5.25	4.52	10.8	6.35	4.2	8.25	8.96	28.3	4.52
9.95	10.3	10.8	4.66	4.84	11	6.5	3.83	8.95	7.31	20.8	3.49
9.72	10.6	10.9	4.77	4.83	11.8	6.76	3.97	14.2	18.9	37.5	3.96
9.46	10.7	11.8	4.91	4.97	13.6	6.61	4.86	29.9	43.3	42.7	9.87
6.02	9.96	12.1	3.75	5.37	24.8	6.7	7.77	42.9	22.4	25.9	8.63

(a) NFCG norm of every element of the whole 3-D panel

1.52	1.6	1.06	5.65	1.25	4.6	1.97	1.16	0.705	3.72	6.76	2.5
0.021	0.676	0.672	1.1	0.16	0.33	0.144	0.141	0.065	0.322	0.474	0.07
0.0041	0.229	0.09	0.125	0.07	0.131	0.047	0.038	0.029	0.129	0.154	0.011
0.0025	0.002	0.01	0.029	0.005	0.091	0.02	0.018	0.018	0.08	0.083	0.005
0.0045	0.004	0.012	0.019	0.002	0.038	0.009	0.014	0.013	0.059	0.056	0.003
0.003	0.033	0.009	0.014	0.002	0.025	0.008	0.013	0.011	0.046	0.041	0.002
0.0014	0.06	0.003	0.008	0.001	0.021	0.006	0.019	0.011	0.036	0.034	0.002
0.0022	0.004	0.002	0.007	0.001	0.02	0.004	0.025	0.011	0.032	0.029	0.002
0.013	0.08	0.003	0.009	0.002	0.017	0.003	0.088	0.014	0.039	0.027	0.002
0.0367	0.12	0.011	0.015	0.004	0.024	0.004	0.217	0.028	0.063	0.051	0.003
0.0681	0.302	0.045	0.043	0.015	0.061	0.008	0.178	0.099	0.177	0.131	0.005
0.0333	1.76	0.305	0.577	0.205	0.932	0.103	1.99	1.44	2.36	1.63	0.039

(b) NKFEG norm of every element of the whole 3-D panel

Figure 23 NFCG, NKFEG norms of the 3-D panel for PZT5A and LCO case.

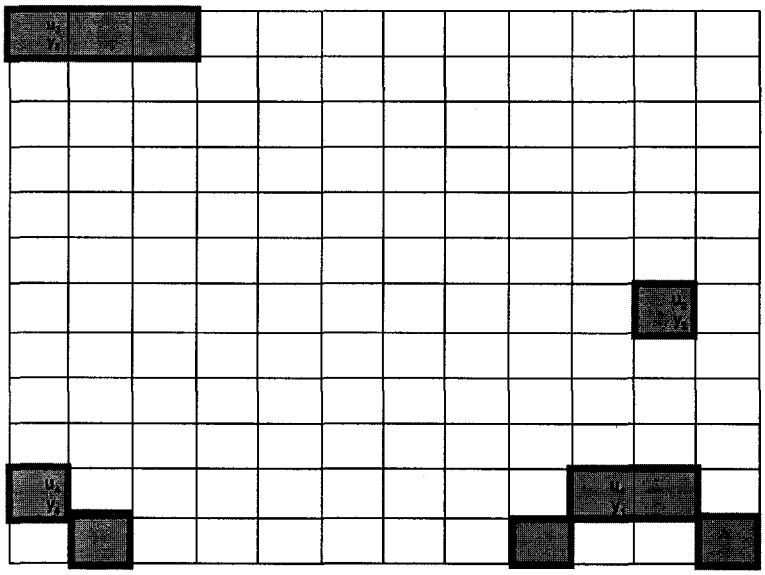

Figure 24 Optimal locations of actuators and sensors of the whole 3-D panel for PZT5A and LCO case.

11.1	11.4	13.3	3.07	27.4	11.7	3.72	2.51	5.68	5.97	38.3	8.74
10.6	10.7	11.9	3.91	16.4	10.6	5.22	2.32	6.58	4.34	23.3	29.8
10.4	10.2	11.5	4.96	16.5	10.2	5.54	2.97	6.34	4.61	24.5	16.8
10.2	9.45	11.4	5.43	4.71	10.2	5.7	3.85	5.87	4.41	12.7	5.96
10.1	9.72	10.9	5.25	4.75	10.1	5.68	4.24	5.88	4.18	3.29	2.61
9.98	9.99	10.4	5.05	4.61	10.2	5.86	4.45	6.3	5.27	11.4	2.63
9.69	9.89	10.8	5.27	4.25	10.4	6.03	4.09	7.61	8.18	[illegible]	3.75
9.99	10	11	5.25	4.52	10.8	6.35	4.2	8.25	8.96	28.3	4.52
9.95	10.3	10.8	4.66	4.84	11	6.5	3.83	8.95	7.31	20.8	3.49
9.72	10.6	10.9	4.77	4.83	11.8	6.76	3.97	14.2	18.9	37.5	3.96
9.46	10.7	11.8	4.91	4.97	13.6	6.61	4.86	29.9	[illegible]	42.7	9.87
6.02	9.96	12.1	3.75	5.37	24.8	6.7	7.77	[illegible]	22.4	25.9	[illegible]

(a) NFCG norm of every element of the whole 3-D panel

1.52	1.5	1.06	5.65	1.25	4.6	1.97	1.16	0.705	3.72	6.76	2.5
0.021	0.676	0.672	1.1	0.16	0.33	0.144	0.141	0.065	0.322	0.474	0.07
0.0041	0.229	0.09	0.125	0.07	0.131	0.047	0.038	0.029	0.129	0.154	0.011
0.0025	0.002	0.01	0.029	0.005	0.091	0.02	0.018	0.018	0.08	0.083	0.005
0.0045	0.004	0.012	0.019	0.002	0.038	0.009	0.014	0.013	0.059	0.056	0.003
0.003	0.033	0.009	0.014	0.002	0.025	0.008	0.013	0.011	0.046	0.041	0.002
0.0014	0.06	0.003	0.008	0.001	0.021	0.006	0.019	0.011	0.036	0.034	0.002
0.0022	0.004	0.002	0.007	0.001	0.02	0.004	0.025	0.011	0.032	0.029	0.002
0.013	0.08	0.003	0.009	0.002	0.017	0.003	0.088	0.014	0.039	0.027	0.002
0.0367	0.12	0.011	0.015	0.004	0.024	0.004	0.217	0.028	0.063	0.051	0.003
0.0681	0.302	0.045	0.043	0.015	0.061	0.008	0.178	0.099	0.177	0.131	0.005
0.0333	1.76	0.305	0.577	0.205	0.932	0.103	1.99	1.44	2.36	1.63	0.039

(b) NKFEG norm of every element of the whole 3-D panel

Figure 25 NFCG, NKFEG norms of the 3-D panel for MFC and LCO case.

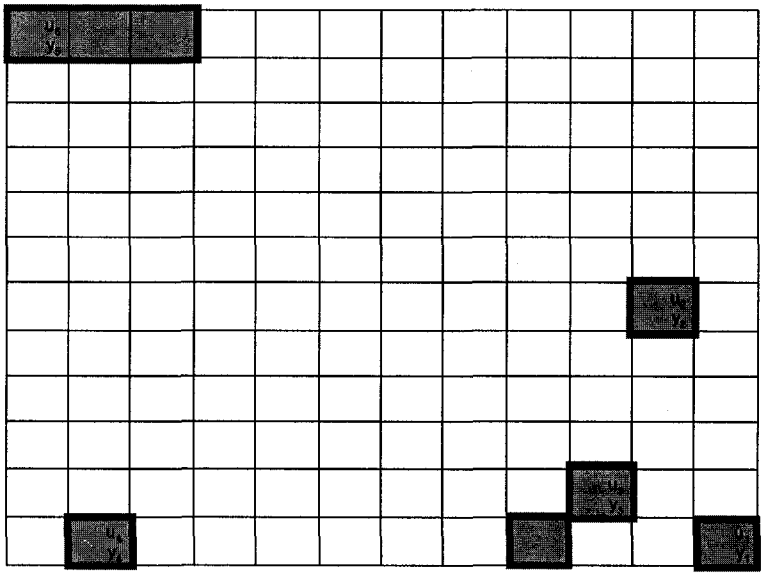

Figure 26 Optimal locations of actuators and sensors of the whole 3-D panel for MFC and LCO case.

3-D Panel Flutter Analysis

The analysis results for 3-D panel flutter are shown in Fig. VI.19(a) – Fig. VI.27(d) like those in 2-D case. Also the four lowest modes: mode (1,1), (2,1), (3,1), (4,1) are used here. Mode shapes are shown in Fig. 28.

3-D Panel Flutter Suppression with PZT5A and MFC

Similar to 2-D case, MFC is more efficient than PZT5A in 3-D panel flutter suppression. When aerodynamic pressure λ equals to 700, two more PZT5A's than MFC's are needed to suppress the flutter. Fig. 29 and Fig. 30 show control results for PZT5A and MFC cases.

VI.2 Static Thermal Post-buckling Deflection Control

When considering thermal stresses, panel flutter produces LCO (including periodic motions), static thermal post-buckling deflections and chaotic motions. Most literatures discussed control of LCO (including periodic motions), but they did not consider or not achieve flutter suppression of the latter two cases. In this research, both static deflection and chaotic motions are suppressed successfully. The dimensions of the 2-D and 3-D panels are the same as those in LCO control part.

Since considering thermal loads, the panels become stiffer, the critical dynamic pressure λ_{cr} is smaller than that in LCO case. That means under a lower dynamic pressure, even lower than λ_{cr} for LCO case, ($\lambda_{cr} = 343$ for 2-D isotropic panel and 512 for 3-D isotropic panel) and some thermal loads, the panel can present large amplitude responses, which is also called thermal post-buckling. Sometimes panels

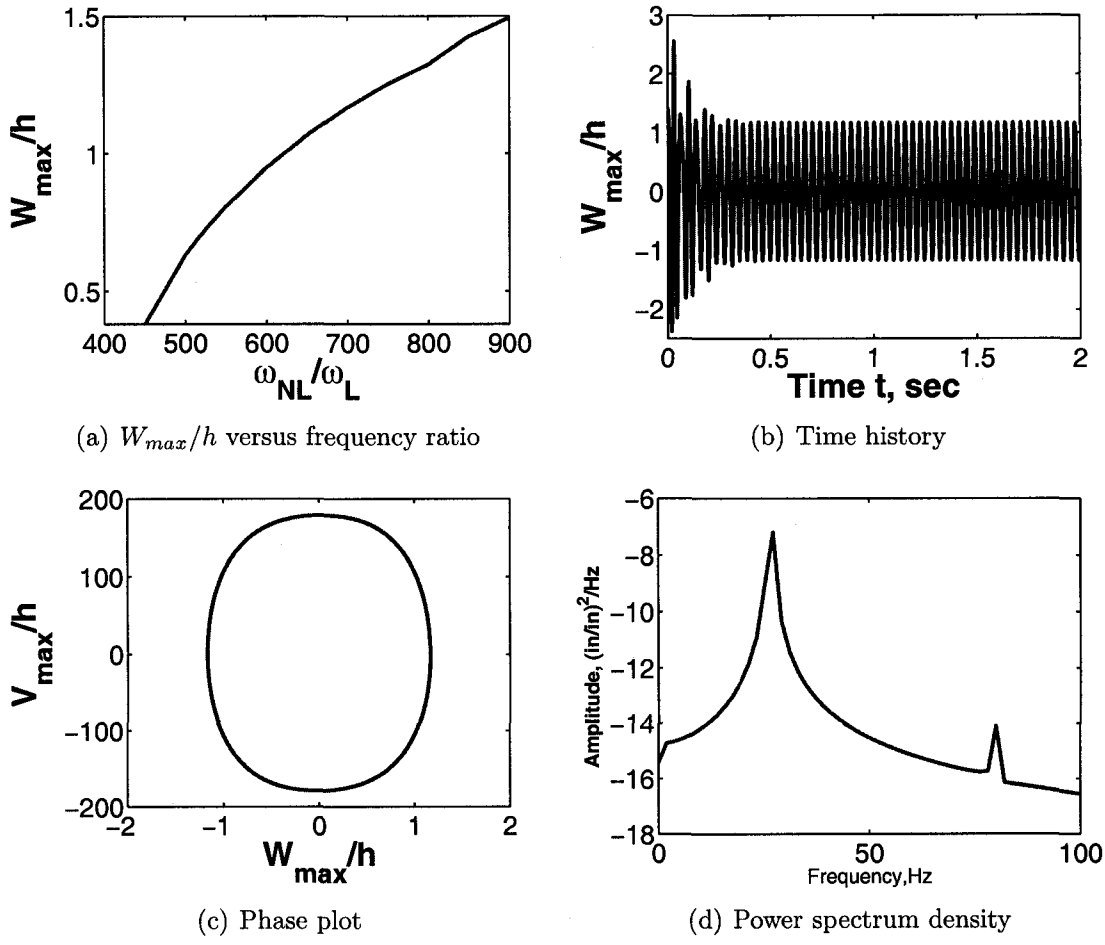

(a) W_{max}/h versus frequency ratio

(b) Time history

(c) Phase plot

(d) Power spectrum density

Figure 27 LCO response of the 3-D panel flutter at $\lambda = 700$ using 4 lowest modes.

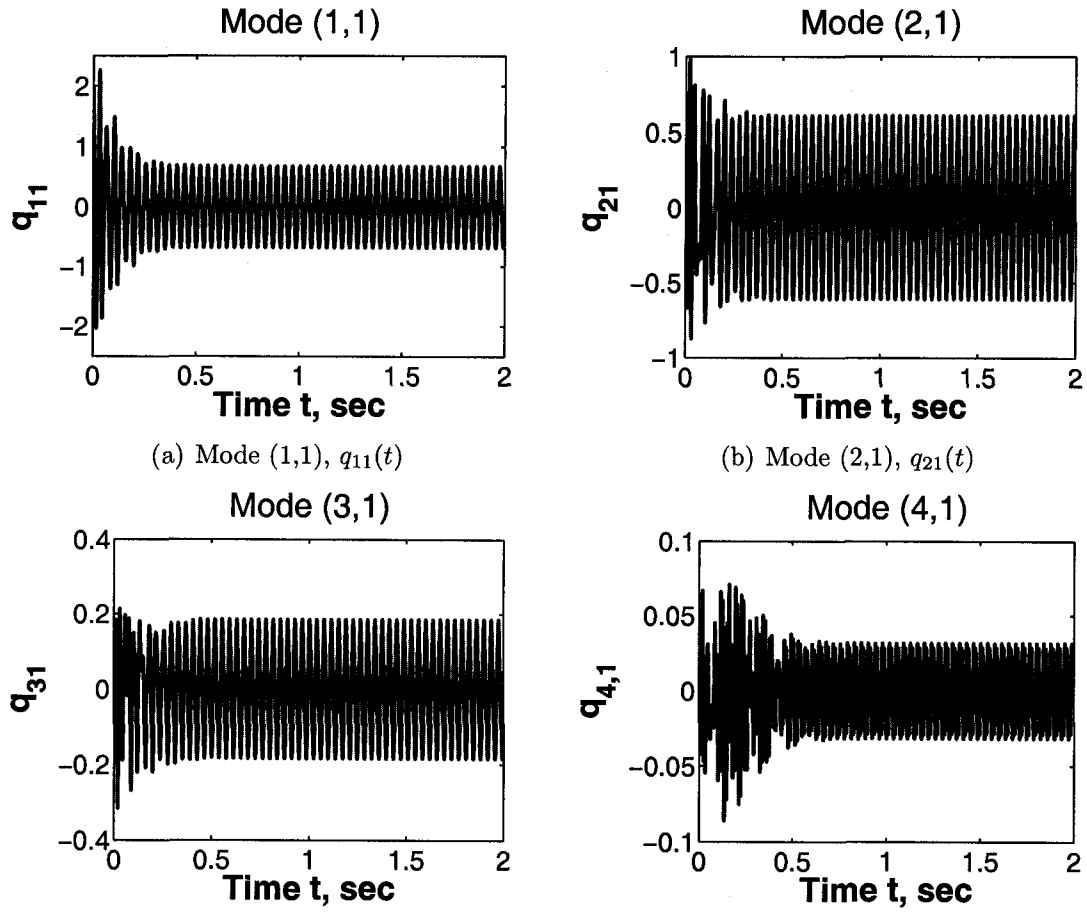

(a) Mode (1,1), $q_{11}(t)$

(b) Mode (2,1), $q_{21}(t)$

(c) Mode (3,1), $q_{31}(t)$

(d) Mode (4,1), $q_{41}(t)$

Figure 28 Time histories of the 4 modes for the 3-D LCO panel flutter at $\lambda = 700$.

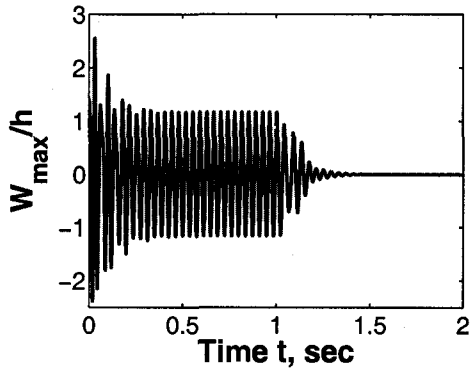

(a) Controlled panel flutter

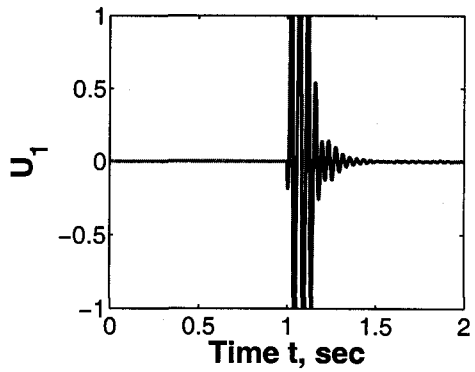

(b) Control input 1

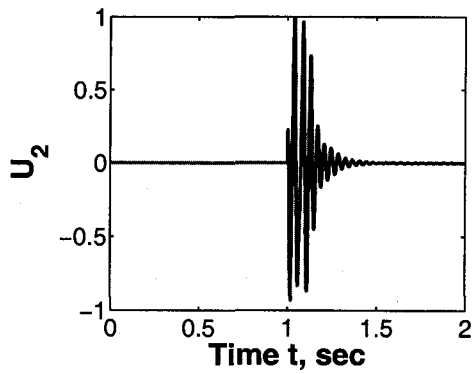

(c) Control input 2

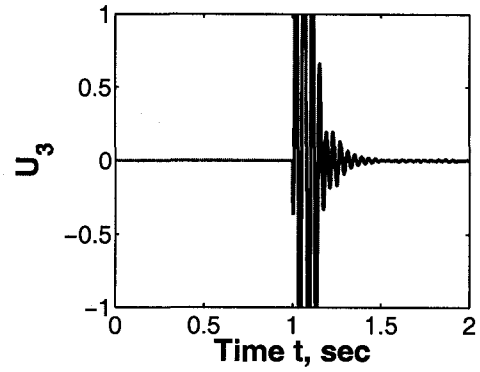

(d) Control input 3

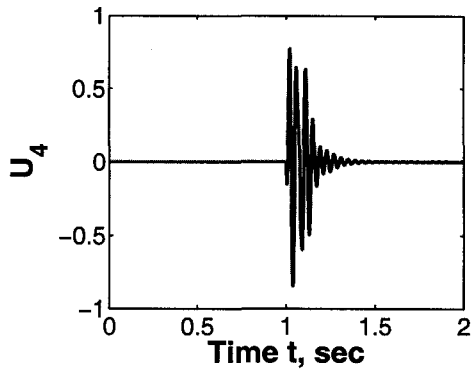

(e) Control input 4

Figure 29 3-D panel flutter ($\lambda = 700$) suppression for the 4-mode LCO model using PZT5A.

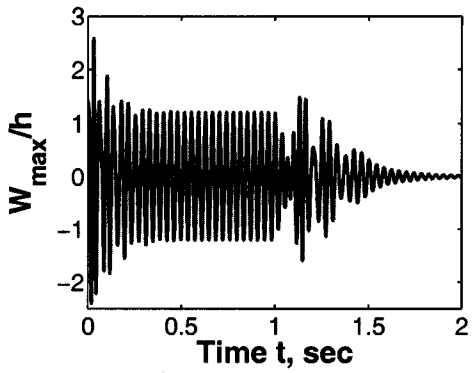

(a) Controlled panel flutter

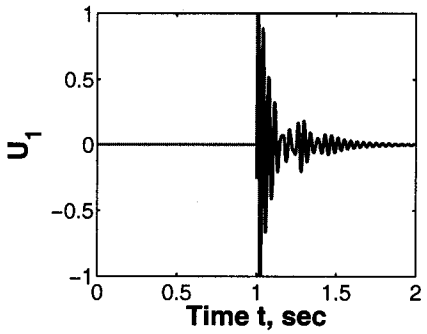

(b) Control input 1

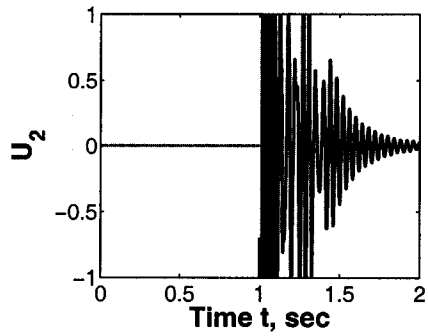

(c) Control input 2

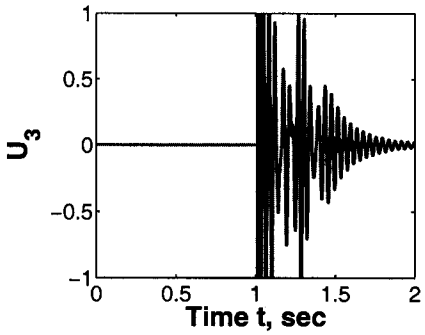

(d) Control input 3

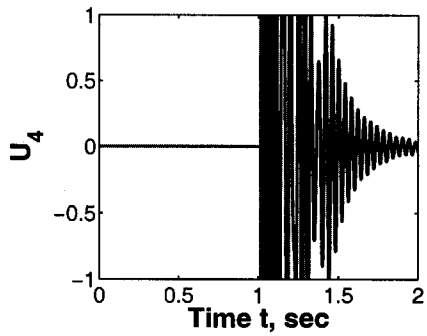

(e) Control input 4

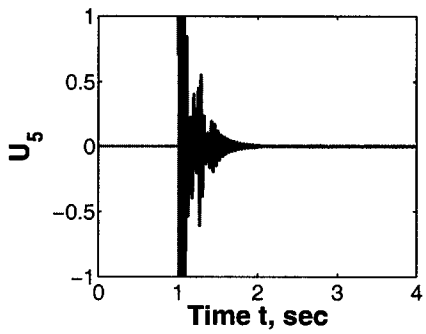

(f) Control input 5

Figure 30 3-D panel flutter ($\lambda = 700$) suppression for the 4-mode LCO model using MFC.

with very small dynamic pressure and certain thermal loads can produce much larger amplitude response than LCO case with a larger dynamic pressure. After some trials, larger number of PZT5A or MFC than LCO case are needed to suppress such static deflections and also the chaotic motions later. One thing should be noticed, estimator is a very important part in the control. Sometimes, such as in 2-D control case, few actuators are enough to achieve the suppression, but a lot more sensors are needed to supply the estimation information for the output feedback control. So additional sensors may be needed beside the self-sensing actuators.

VI.2.1 2-D Panel Flutter Control

Placement of Self-sensing Actuators

The placement method of actuators and sensors in this section is still NFCG and NKFEG norms as in LCO case. More control forces are needed to suppress the static deflection, so more actuators are needed. Similar with the LCO control case, small number of MFC is used than that of PZT5A when both of them provide good control performance. The locations of PZT5A and MFC actuators and sensors are shown in Fig. 31 and Fig. 32. Combination of locations of actuators and sensors, locations of self-sensing actuators are decided.

2-D Panel Flutter Analysis

For the 2-D panel flutter, when using Eqs. (125)–(132), the critical temperature can be obtained ($T_{cr} = 0.1286F°$). The thermal loads of this 2-D panel is 8 times of the critical temperature. The dynamic pressure $\lambda = 130$, which is less than the critical dynamic pressure in LCO case. But from the free vibration history, the panel

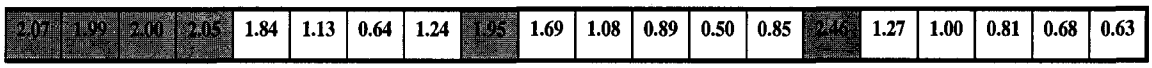

(a) NFCG norm of every element of the whole 2-D panel

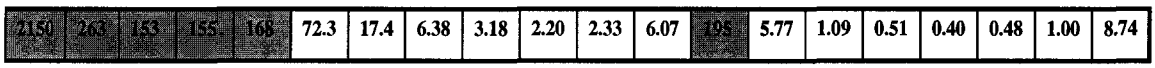

(b) NKFEG norm of every element of the whole 2-D panel

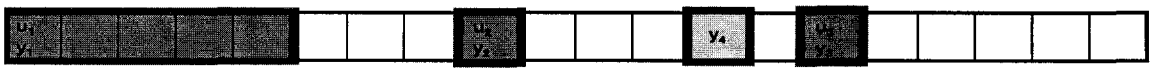

(c) optimal locations of actuators and sensors of the whole 2-D panel

Figure 31 NFCG, NKFEG norms and actuators' and sensors' locations on the 2-D panel for PZT5A: static thermal post-buckling and chaos.

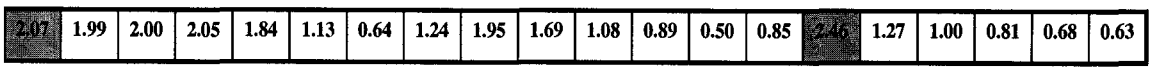

(a) NFCG norm of every element of the whole 2-D panel

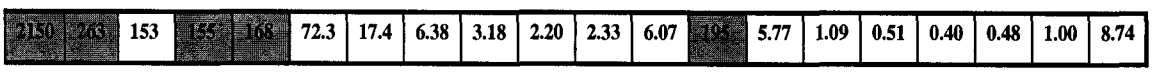

(b) NKFEG norm of every element of the whole 2-D panel

(c) optimal locations of actuators and sensors of the whole 2-D panel

Figure 32 NFCG, NKFEG norms and actuators' and sensors' locations on the 2-D panel for MFC: static thermal post-buckling and chaos.

still produces large amplitude static deflections.

Various analysis results for 2-D static panel flutter under thermal loads are shown in Fig. 33 and Fig. 34.

2-D Panel Flutter Suppression with PZT5A and MFC

Static flutter suppression results are shown in Figs. 35–36. More self-sensing actuators are applied than LCO case because of the thermal loads. Sensing is a very important part in suppression of static responses under thermal loads. One more sensor is used in the control besides all the self-sensing actuators in the PZT5A case. Successful suppression can not be obtained if using another self-sensing actuator or just an actuator to replace the sensor. The additional sensor is so important because it's more difficult for EKF to give estimation under thermal loads. Without good estimation, even the control force is large, it's still hard to suppress the panel flutter under thermal environment. So more sensors are needed in the panel flutter control considering temperatures. Under most conditions, both sensors and actuators are combined as self-sensing actuators. But sometime, additional sensors are still needed as the control of static responses using PZT5A. In all, 2 more PZT5A's than MFC's are needed in suppression of the static responses. Control results are shown in Figs. 35–36.

VI.2.2 3-D Panel Flutter Control

Placement of Self-sensing Actuators

The thermal loads of this 3-D panel is 8 times of the critical temperature ($0.2203F°$). The dynamic pressure $\lambda = 430$, which is less than the critical dynamic pressure in LCO case. But from the free vibration history, the panel still produces large amplitude static thermal post-buckling responses. Similar to 2-D static thermal post-buckling deflection case, in 3-D case, using NFCG and NKFEG norm method, the optimal locations for PZT5A and MFC actuators and sensors are shown in Figs. 37–40.

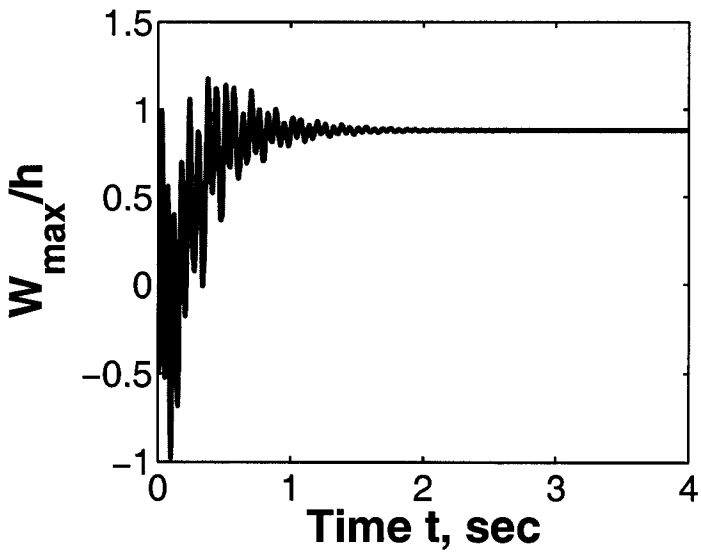

Figure 33 Response of the 2-D panel flutter at $\lambda = 130$ and $\Delta T/\Delta T_{cr} = 8$ using 4 lowest modes.

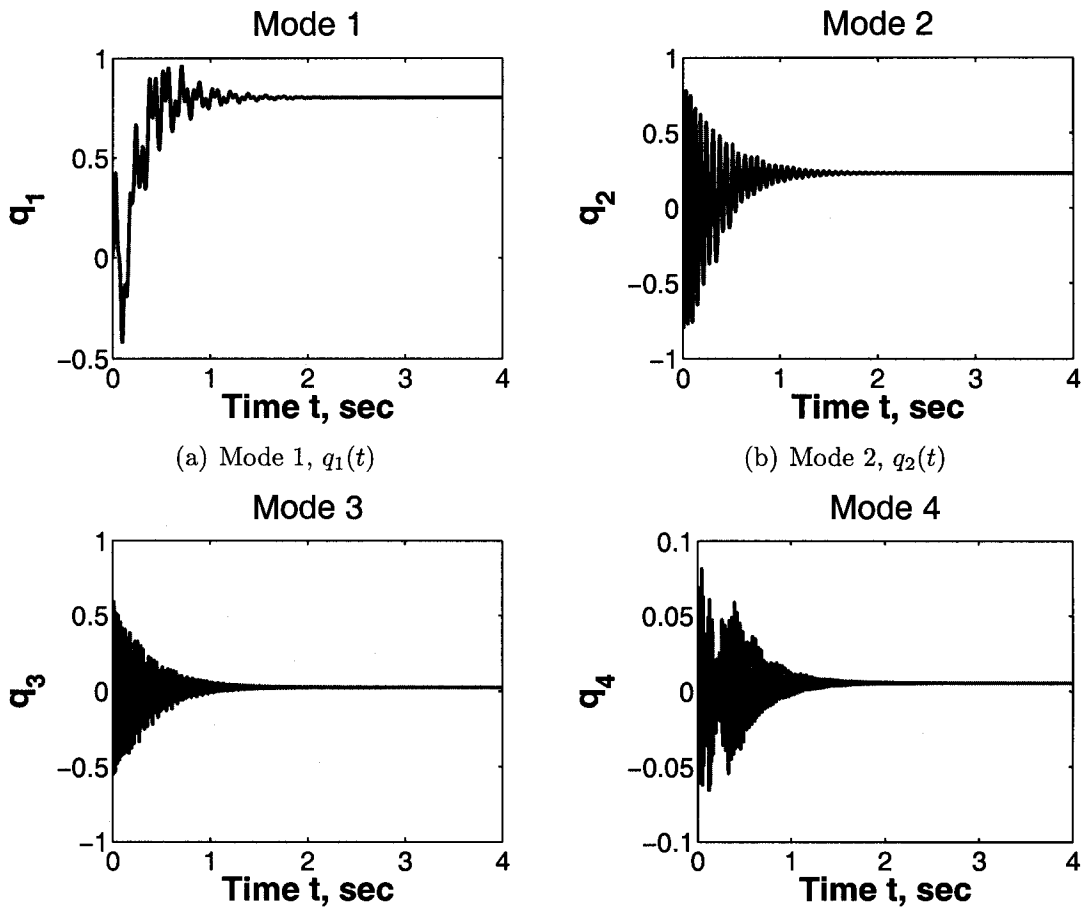

(a) Mode 1, $q_1(t)$

(b) Mode 2, $q_2(t)$

(c) Mode 3, $q_3(t)$

(d) Mode 4, $q_4(t)$

Figure 34 Time histories of the 4 lowest modes for the 2-D panel flutter at $\lambda = 130$ and $\Delta T/\Delta T_{cr} = 8$.

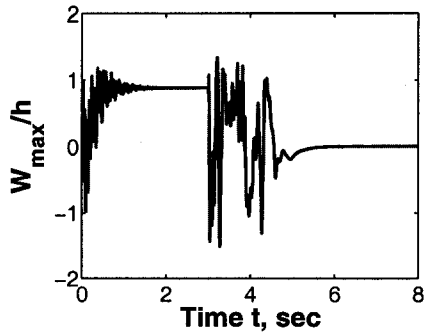

(a) Controlled panel flutter

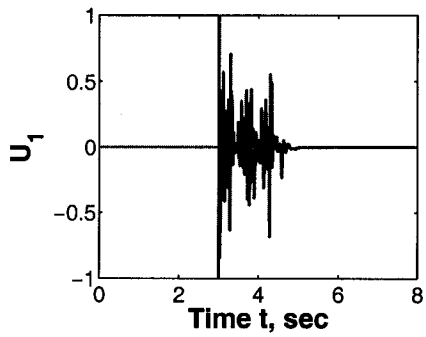

(b) Control input 1

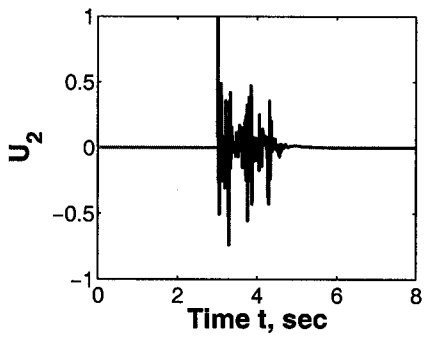

(c) Control input 2

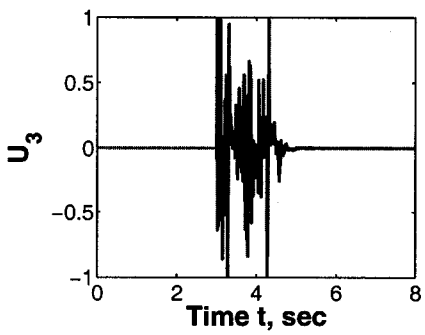

(d) Control input 3

Figure 35 2-D panel flutter ($\lambda = 130$, $\Delta T/\Delta T_{cr} = 8$) suppression for the 4-mode model using PZT5A.

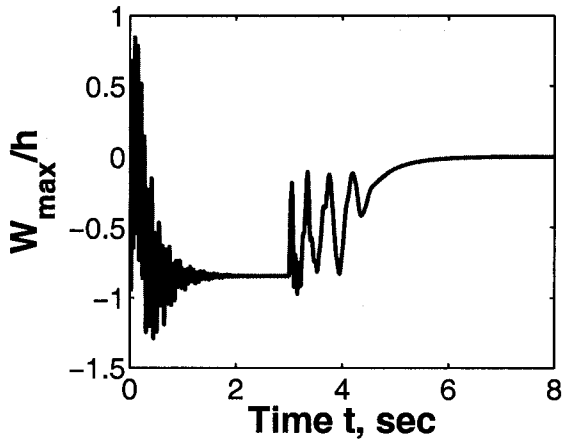

(a) Controlled panel flutter

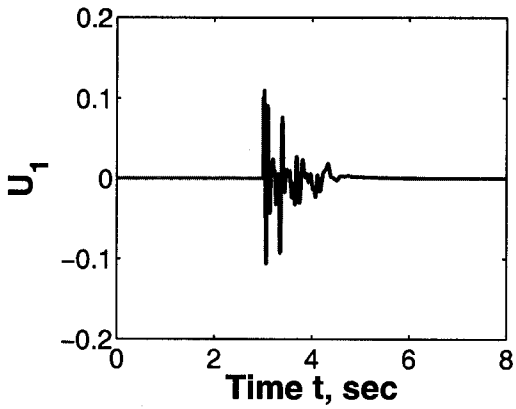

(b) Control input 1

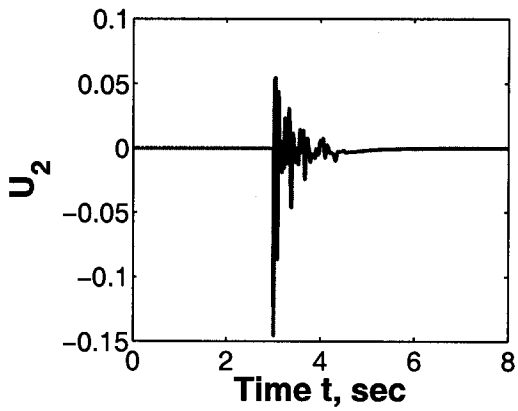

(c) Control input 2

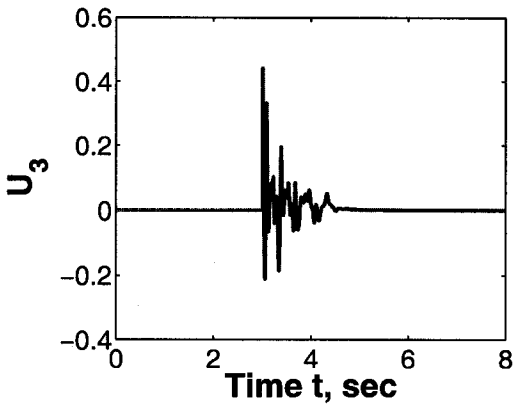

(d) Control input 3

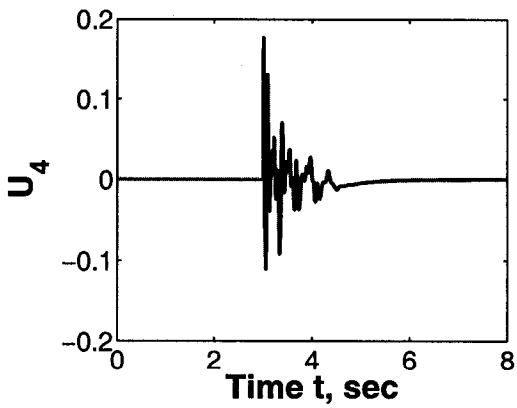

(e) Control input 4

Figure 36 2-D panel flutter ($\lambda = 130$, $\Delta T/\Delta T_{cr} = 8$) suppression for the 4-mode model using MFC.

11.1	11.4	13.3	3.07	27.4	11.7	3.72	2.51	5.68	5.97	35.3	8.74
10.6	10.7	11.9	3.91	16.4	10.6	5.22	2.32	6.58	4.34	23.1	29.6
10.4	10.2	11.5	4.96	16.5	10.2	5.54	2.97	6.34	4.61	24.5	16.6
10.2	9.45	11.4	5.43	4.71	10.2	5.7	3.85	5.87	4.41	12.7	5.96
10.1	9.72	10.9	5.25	4.75	10.1	5.68	4.24	5.88	4.18	3.29	2.61
9.98	9.99	10.4	5.05	4.61	10.2	5.86	4.45	6.3	5.27	11.4	2.63
9.69	9.89	10.8	5.27	4.25	10.4	6.03	4.09	7.61	8.18	24	3.75
9.99	10	11	5.25	4.52	10.8	6.35	4.2	8.25	8.96	28.3	4.52
9.95	10.3	10.8	4.66	4.84	11	6.5	3.83	8.95	7.31	20.8	3.49
9.72	10.6	10.9	4.77	4.83	11.8	6.76	3.97	14.2	18.9	37.5	3.96
9.46	10.7	11.8	4.91	4.97	13.6	6.61	4.86	29.9	43.3	42.7	9.87
6.02	9.96	12.1	3.75	5.37	24.8	6.7	7.77	42.9	22.4	24.9	865

(a) NFCG norm of every element of the whole 3-D panel

1.52	1.5	1.06	5.65	1.25	4.6	1.97	1.16	0.705	3.72	6.76	2.5
0.021	0.075	0.072	1.1	0.16	0.33	0.144	0.141	0.065	0.322	0.474	0.07
0.0041	0.229	0.09	0.125	0.07	0.131	0.047	0.038	0.029	0.129	0.154	0.011
0.0025	0.002	0.01	0.029	0.005	0.091	0.02	0.018	0.018	0.08	0.083	0.005
0.0045	0.004	0.012	0.019	0.002	0.038	0.009	0.014	0.013	0.059	0.056	0.003
0.003	0.033	0.009	0.014	0.002	0.025	0.008	0.013	0.011	0.046	0.041	0.002
0.0014	0.06	0.003	0.008	0.001	0.021	0.006	0.019	0.011	0.036	0.034	0.002
0.0022	0.004	0.002	0.007	0.001	0.02	0.004	0.025	0.011	0.032	0.029	0.002
0.013	0.08	0.003	0.009	0.002	0.017	0.003	0.088	0.014	0.039	0.027	0.002
0.0367	0.12	0.011	0.015	0.004	0.024	0.004	0.217	0.028	0.063	0.051	0.003
0.0651	0.302	0.045	0.043	0.015	0.061	0.008	0.178	0.099	0.177	0.131	0.005
0.0333	1.78	0.305	0.577	0.205	0.932	0.103	1.99	1.44	2.36	1.63	0.039

(b) NKFEG norm of every element of the whole 3-D panel

Figure 37 NFCG, NKFEG norms of the 3-D panel for PZT5A: static thermal post-buckling and chaos.

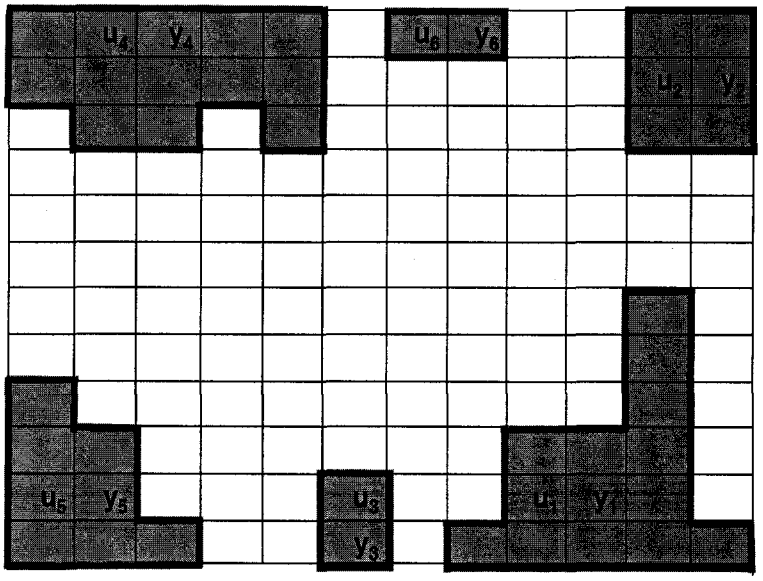

Figure 38 Optimal locations of actuators and sensors of the whole 3-D panel for PZT5A: static thermal post-buckling and chaos.

11.1	11.4	13.3	3.07	27.4	11.7	3.72	2.51	5.68	5.97	36.3	8.74
10.6	10.7	11.9	3.91	16.4	10.6	5.22	2.32	6.58	4.34	23.3	29.8
10.4	10.2	11.5	4.96	16.6	10.2	5.54	2.97	6.34	4.61	24.5	16.6
10.2	9.45	11.4	5.43	4.71	10.2	5.7	3.85	5.87	4.41	12.7	5.96
10.1	9.72	10.9	5.25	4.75	10.1	5.68	4.24	5.88	4.18	3.29	2.61
9.98	9.99	10.4	5.05	4.61	10.2	5.86	4.45	6.3	5.27	11.4	2.63
9.69	9.89	10.8	5.27	4.25	10.4	6.03	4.09	7.61	8.18	14.4	3.75
9.99	10	11	5.25	4.52	10.8	6.35	4.2	8.25	8.96	28.3	4.52
9.95	10.3	10.8	4.66	4.84	11	6.5	3.83	8.95	7.31	20.8	3.49
9.72	10.6	10.9	4.77	4.83	11.8	6.76	3.97	14.2	18.9	97.5	3.96
9.46	10.7	11.8	4.91	4.97	13.6	6.61	4.86	29.9	43.3	42.7	9.87
6.02	9.96	12.1	3.75	5.37	24.8	6.7	7.77	42.9	22.4	25.9	7.865

(a) NFCG norm of every element of the whole 3-D panel

1.52	1.5	1.06	5.65	1.25	4.6	1.97	1.16	0.705	3.72	6.76	2.5
0.021	0.678	0.672	1.1	0.16	0.33	0.144	0.141	0.065	0.322	0.474	0.07
0.0041	0.229	0.09	0.125	0.07	0.131	0.047	0.038	0.029	0.129	0.154	0.011
0.0025	0.002	0.01	0.029	0.005	0.091	0.02	0.018	0.018	0.08	0.083	0.005
0.0045	0.004	0.012	0.019	0.002	0.038	0.009	0.014	0.013	0.059	0.056	0.003
0.003	0.033	0.009	0.014	0.002	0.025	0.008	0.013	0.011	0.046	0.041	0.002
0.0014	0.06	0.003	0.008	0.001	0.021	0.006	0.019	0.011	0.036	0.034	0.002
0.0022	0.004	0.002	0.007	0.001	0.02	0.004	0.025	0.011	0.032	0.029	0.002
0.013	0.08	0.003	0.009	0.002	0.017	0.003	0.088	0.014	0.039	0.027	0.002
0.0367	0.12	0.011	0.015	0.004	0.024	0.004	0.217	0.028	0.063	0.051	0.003
0.0681	0.302	0.045	0.043	0.015	0.061	0.008	0.178	0.099	0.177	0.131	0.005
0.0333	1.78	0.306	0.577	0.205	0.932	0.103	1.99	1.44	2.36	1.63	0.039

(b) NKFEG norm of every element of the whole 3-D panel

Figure 39 NFCG, NKFEG norms of the 3-D panel for MFC: static thermal post-buckling and chaos.

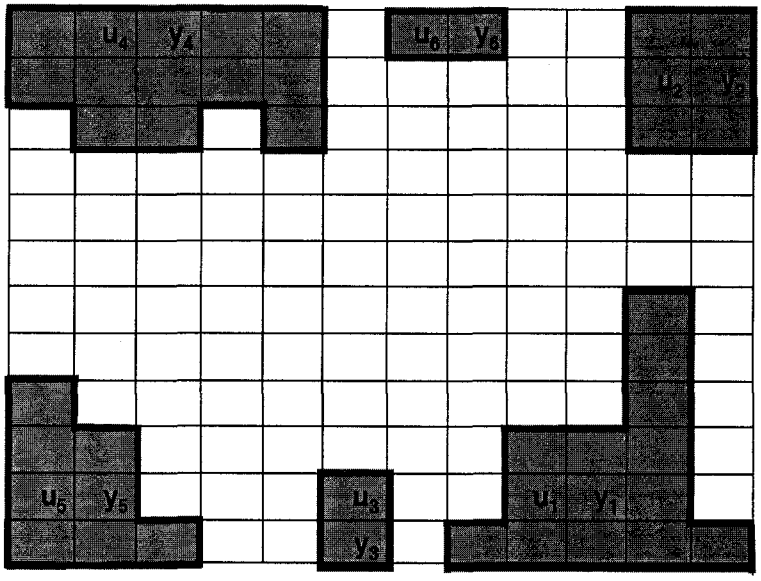

Figure 40 Optimal locations of actuators and sensors of the whole 3-D panel for MFC: static thermal post-buckling and chaos.

3-D Panel Flutter Analysis

All the analysis results for 3-D static thermal post-buckling responses are shown in Figs. 41–42.

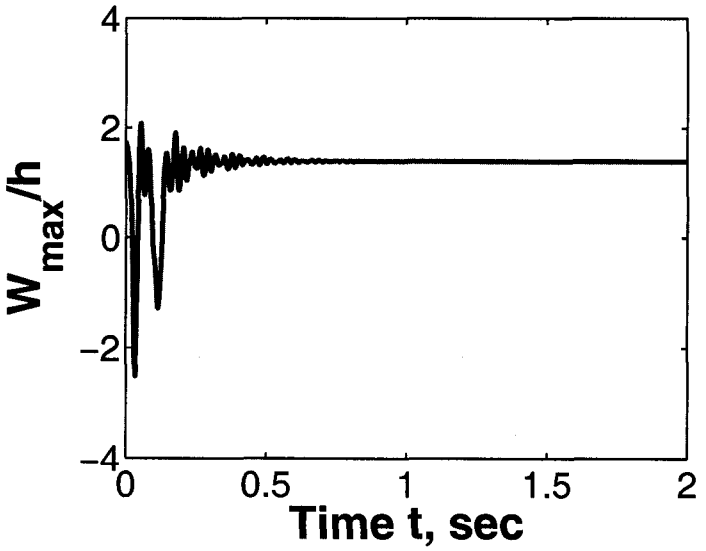

Figure 41 Response of the 3-D panel flutter at $\lambda = 430$ and $\Delta T/\Delta T_{cr} = 8$ using 4 modes.

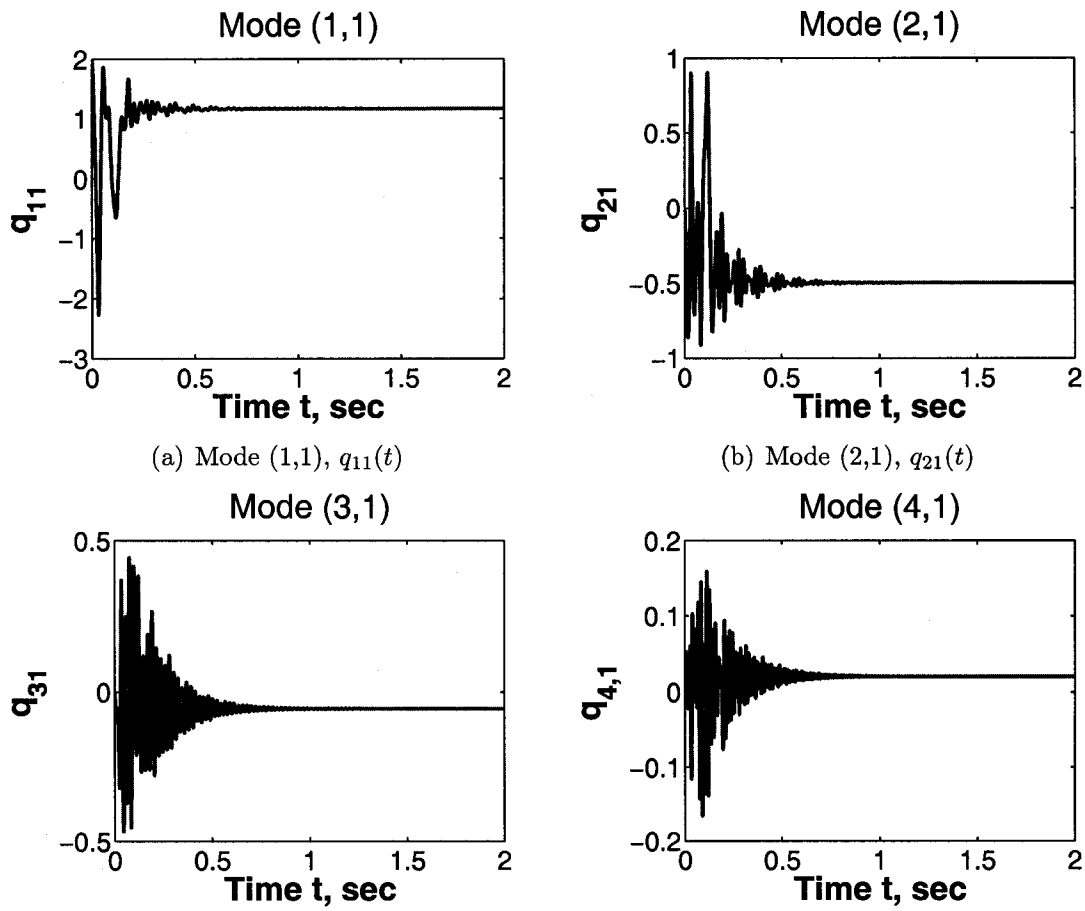

(a) Mode (1,1), $q_{11}(t)$

(b) Mode (2,1), $q_{21}(t)$

(c) Mode (3,1), $q_{31}(t)$

(d) Mode (4,1), $q_{41}(t)$

Figure 42 Time histories of the 4 modes for the 3-D panel flutter at $\lambda = 430$ and $\Delta T/\Delta T_{cr} = 8$.

3-D Panel Flutter Suppression with PZT5A and MFC

The control results are shown in Figs. 44–46. In fact, when both cases suppressed the static responses successfully, the number of MFC is 6 less than that of PZT5A used, which obviously display the efficiency of MFC in vibration suppression.

VI.3 Chaotic Control

In this research, chaotic motion is analyzed and some successful control results are shown. The dimensions of the 2-D and 3-D panels are the same as those in LCO control part. And the locations of chaotic motion control are the same as the static thermal post-buckling response control.

VI.3.1 2-D Panel Flutter Control

2-D Panel Flutter Analysis

The thermal loads of this 2-D panel is 8 times of the critical temperature ($0.1286F°$). The dynamic pressure $\lambda = 270$, which is less than the critical dynamic pressure in LCO case. But from the free vibration history, the panel still produces large amplitude chaotic motion.

Various analysis results for 2-D panel flutter under thermal loads are shown in Fig. 47 and Fig. 48. For chaotic case considered here, no maximum amplitude and dynamic pressure relationship can be shown. That is because the amplitude is not a constant for every certain dynamic pressure for chaotic motion.

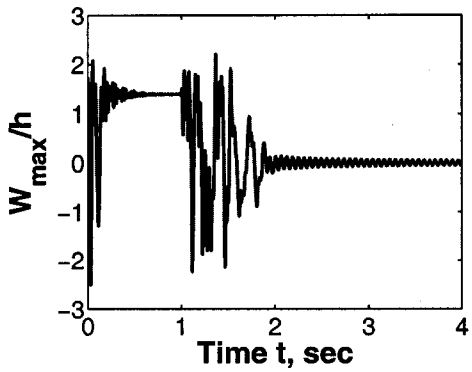

Figure 43 3-D panel flutter ($\lambda = 430$, $\Delta T/\Delta T_{cr} = 8$) suppression for the 4-mode model using PZT5A.

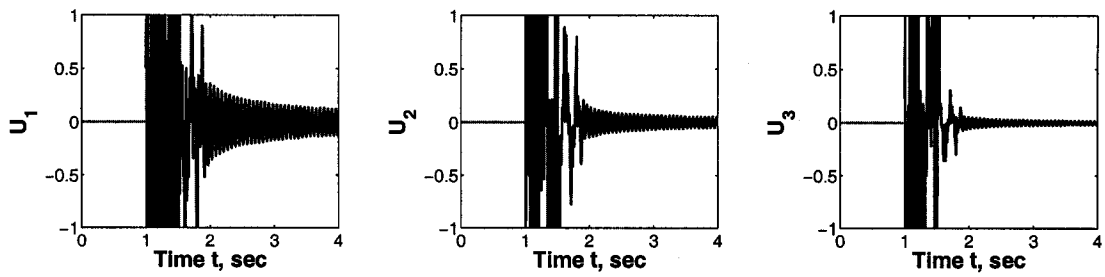

(a) Control input 1 (b) Control input 2 (c) Control input 3

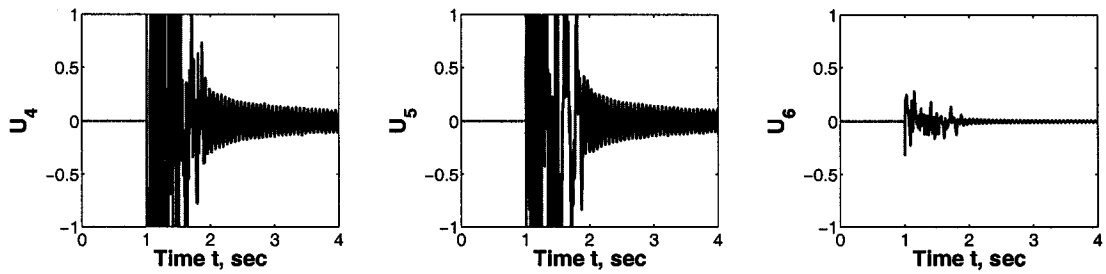

(d) Control input 4 (e) Control input 5 (f) Control input 6

Figure 44 Control Inputs for the 4-mode 3-D panel flutter at $\lambda = 430$ and $\Delta T/\Delta T_{cr} = 8$ using PZT5A.

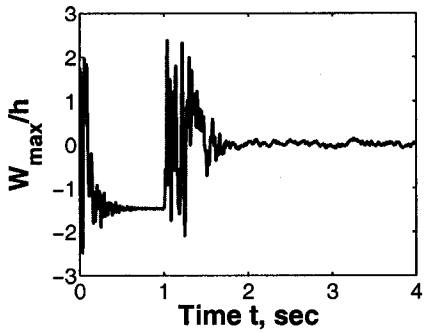

Figure 45 3-D panel flutter ($\lambda = 430$, $\Delta T/\Delta T_{cr} = 8$) suppression for the 4-mode model by using MFC.

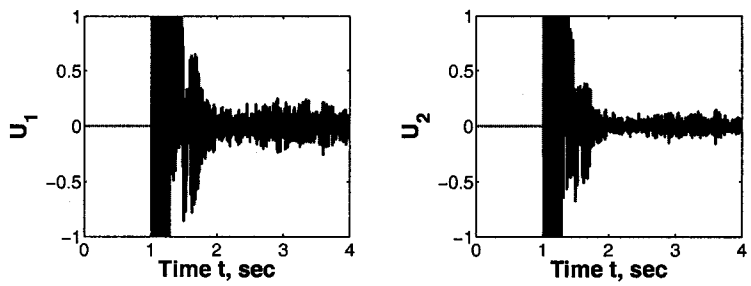

(a) Control input 1

(b) Control input 2

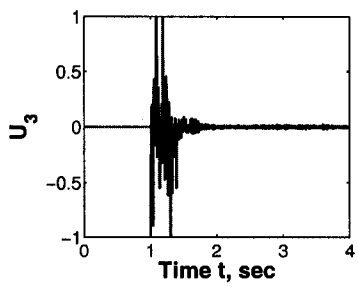

(c) Control input 3

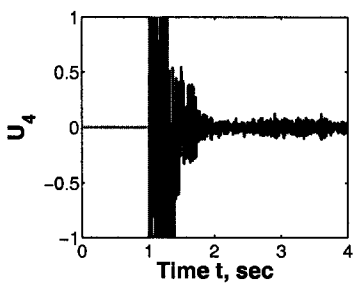

(d) Control input 4

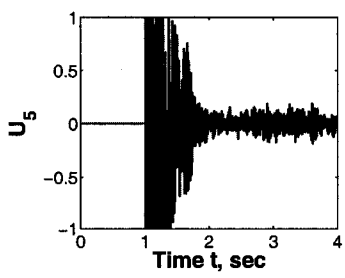

(e) Control input 5

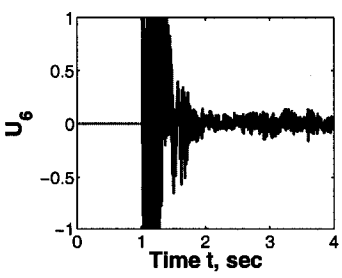

(f) Control input 6

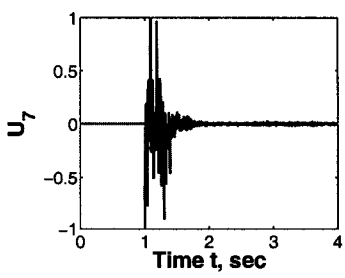

(g) Control input 7

Figure 46 Control Inputs for the 4-mode 3-D panel flutter at $\lambda = 430$ and $\Delta T/\Delta T_{cr} = 8$ using MFC.

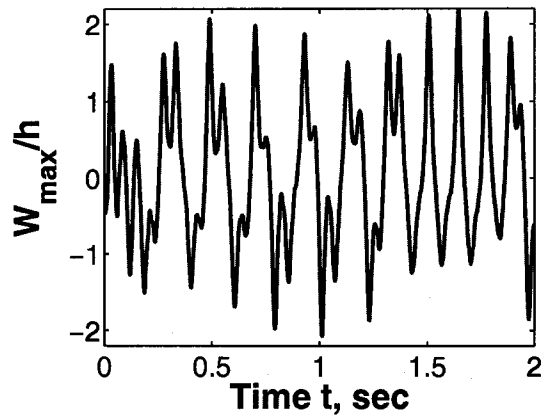

(a) Time history

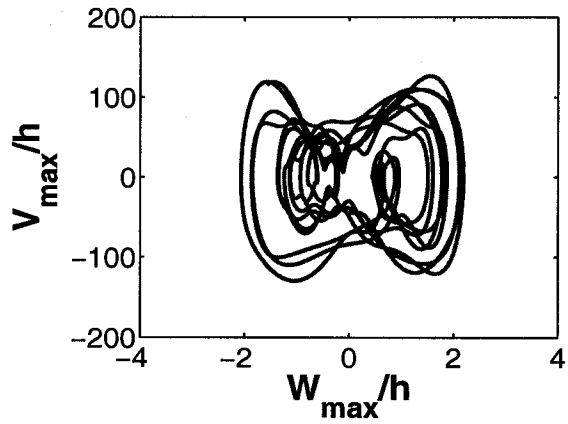

(b) Phase plot

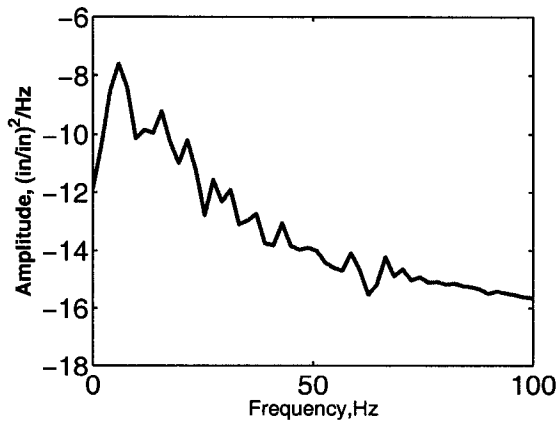

(c) Power spectrum density

Figure 47 Response of the 2-D chaotic panel flutter at $\lambda = 270$ and $\Delta T/\Delta T_{cr} = 8$ using 4 lowest modes.

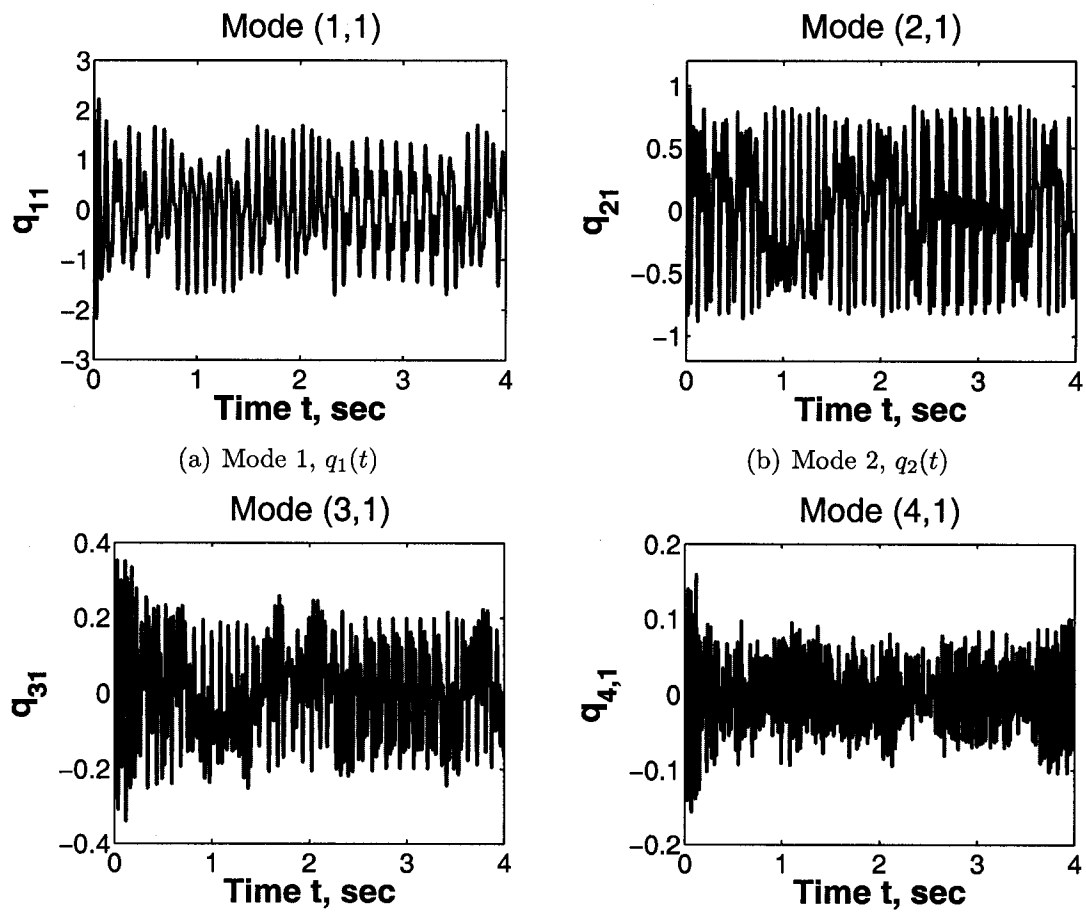

(a) Mode 1, $q_1(t)$

(b) Mode 2, $q_2(t)$

(c) Mode 3, $q_3(t)$

(d) Mode 4, $q_4(t)$

Figure 48 Time histories of the 4 lowest modes for the 2-D chaotic panel flutter at $\lambda = 270$ and $\Delta T/\Delta T_{cr} = 8$.

2-D Panel Flutter Suppression with PZT5A and MFC

Chaotic flutter suppression results are shown in Figs. 49–50.

VI.3.2 3-D Panel Flutter Control

The locations of the self-sensing actuators are the same as the static thermal post-buckling deflection suppression.

3-D Panel Flutter Analysis

The thermal loads of this 3-D panel is 8 times of the critical temperature ($0.2203F°$). The dynamic pressure $\lambda = 440$, which is less than the critical dynamic pressure in LCO case. All the analysis results for 3-D chaotic panel flutter are shown in Figs. 51–52.

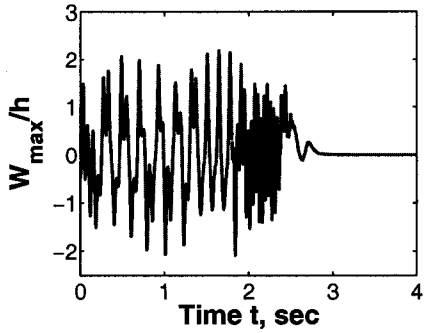

(a) Controlled panel flutter

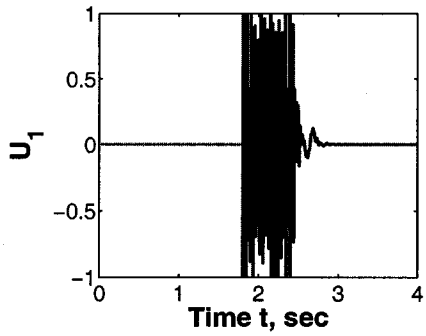

(b) Control input 1

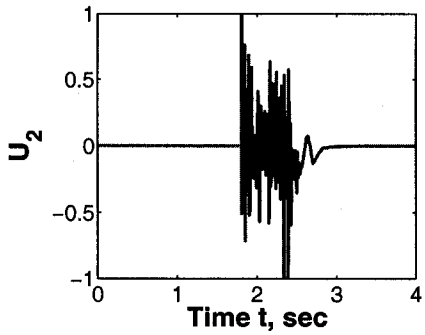

(c) Control input 2

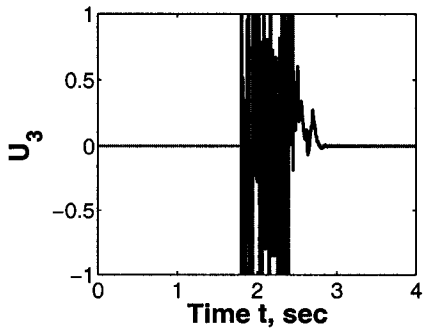

(d) Control input 3

Figure 49 2-D panel flutter ($\lambda = 270$, $\Delta T/\Delta T_{cr} = 8$) suppression for the 4-mode chaotic model using PZT5A.

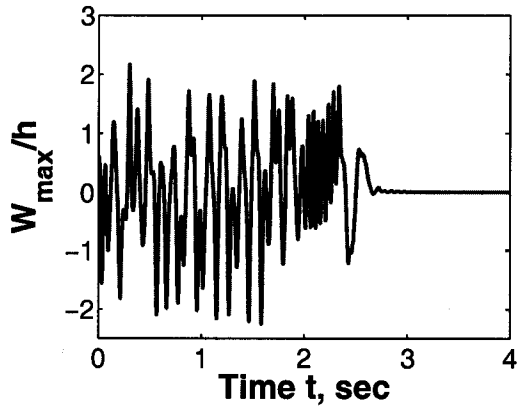

(a) Controlled panel flutter

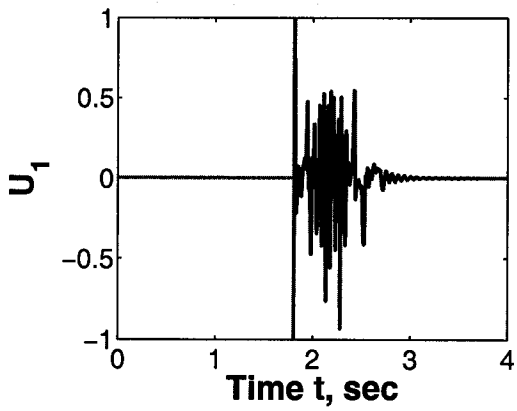

(b) Control input 1

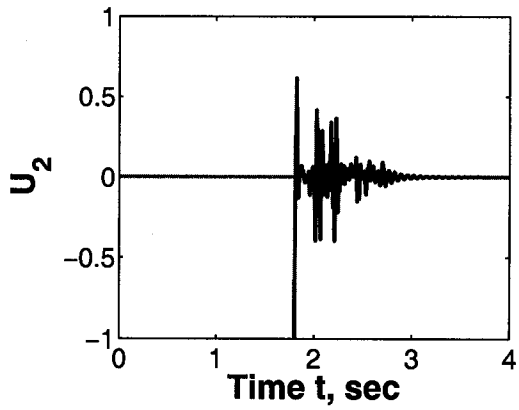

(c) Control input 2

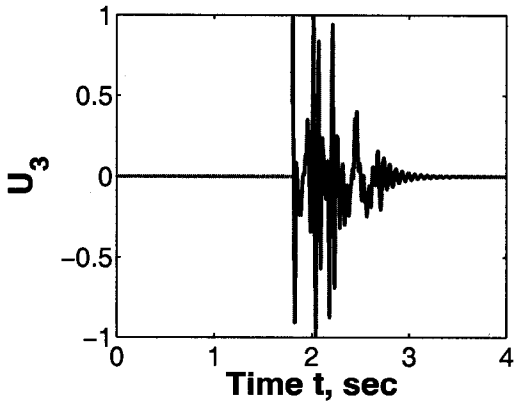

(d) Control input 3

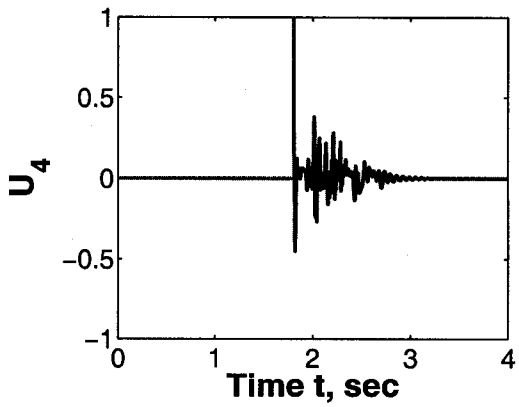

(e) Control input 4

Figure 50 2-D panel flutter suppression ($\lambda = 270$, $\Delta T/\Delta T_{cr} = 8$) for the 4-mode chaotic model using MFC.

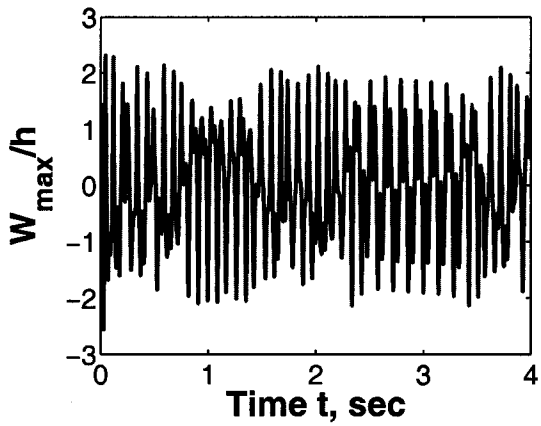

(a) Time history

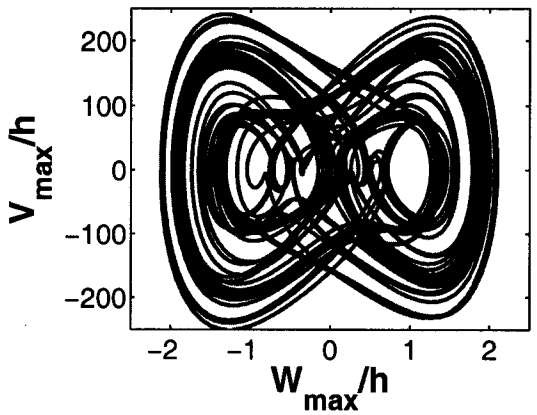

(b) Phase plot

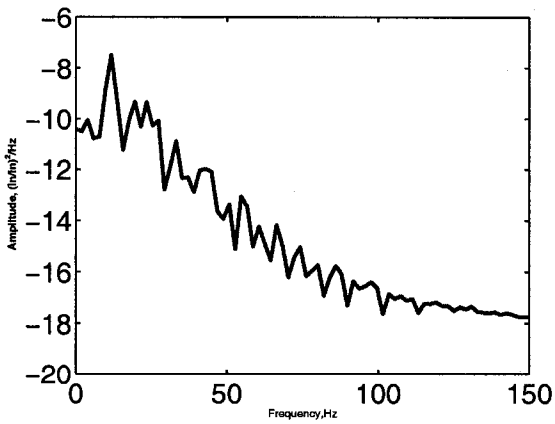

(c) Power spectrum density

Figure 51 Response of the 3-D chaotic panel flutter at $\lambda = 440$ and $\Delta T/\Delta T_{cr} = 8$ using 4 modes.

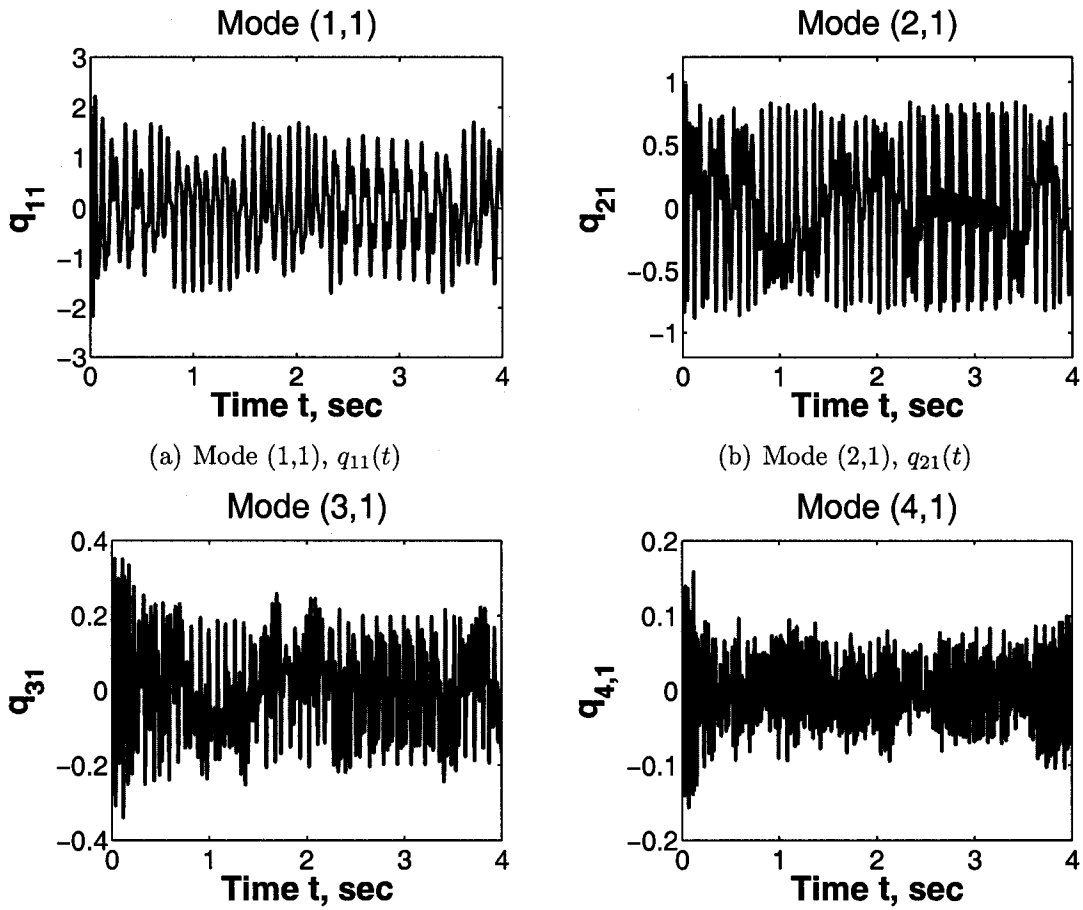

(a) Mode (1,1), $q_{11}(t)$

(b) Mode (2,1), $q_{21}(t)$

(c) Mode (3,1), $q_{31}(t)$

(d) Mode (4,1) $q_{41}(t)$

Figure 52 Time histories of the 4 modes for the 3-D chaotic panel flutter at $\lambda = 440$ and $\Delta T/\Delta T_{cr} = 8$.

3-D Panel Flutter Suppression with PZT5A and MFC

The control results are shown in Figs. 54–56.

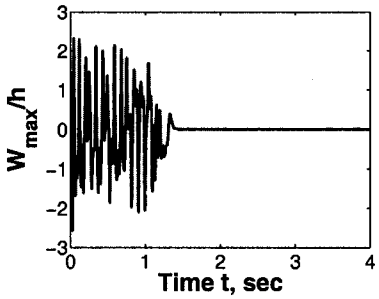

Figure 53 3-D panel flutter ($\lambda = 440$, $\Delta T/\Delta T_{cr} = 8$) suppression for the 4-mode chaotic model using PZT5A.

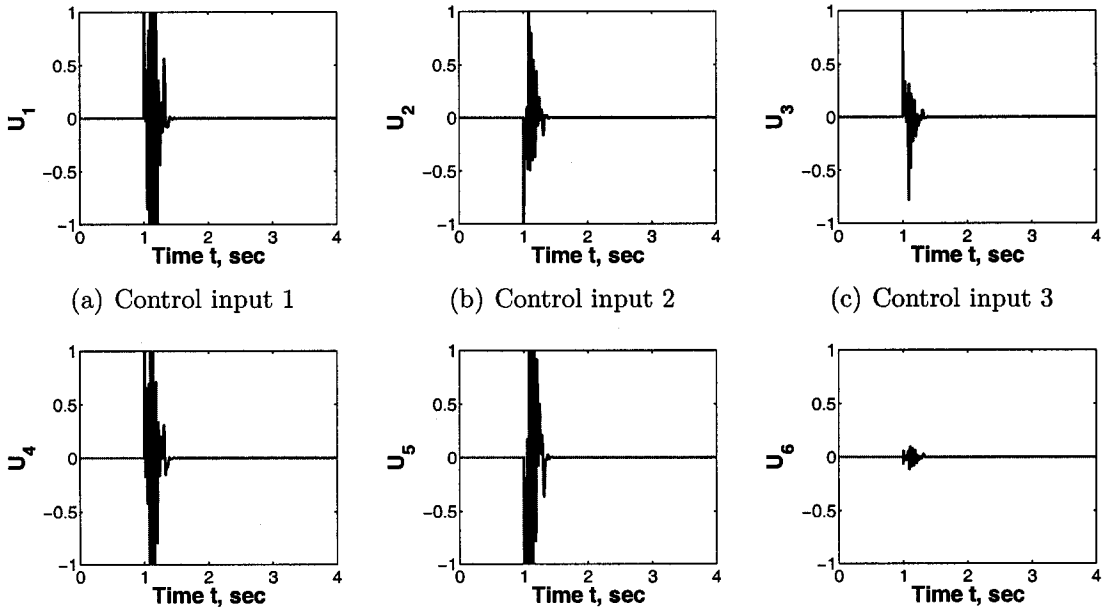

(a) Control input 1 (b) Control input 2 (c) Control input 3

(d) Control input 4 (e) Control input 5 (f) Control input 6

Figure 54 Control inputs for the 4-mode 3-D chaotic panel flutter at $\lambda = 440$ and $\Delta T/\Delta T_{cr} = 8$ using PZT5A.

From all the results of panel flutter suppression, LQR/EKF is a very efficient controller for suppression flutter all three cases: LCO, thermal static post-buckling deflections and chaotic motions. NFCG and NKFEG norm are also effective for the optimal placement of actuators and sensors. MFC is more efficient in flutter suppression than PZT5A. When both MFC and PZT5A give good control performance, a smaller number of MFC is needed. For static deflection and chaotic motion suppression, the estimation is very important because those two cases, thermal loads will increase the difficulty of control and estimation. Also the multiple modes will make the estimation more difficult especially more than one mode is the dominant one. So more actuators and sensors are needed in the control of those two cases than LCO case.

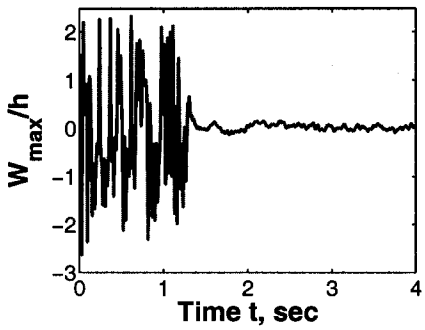

Figure 55 3-D panel flutter ($\lambda = 440$, $\Delta T/\Delta T_{cr} = 8$) suppression for the 4-mode chaotic model using MFC.

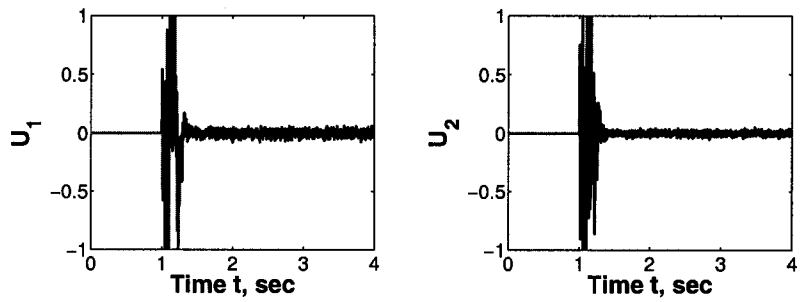

(a) Control input 1

(b) Control input 2

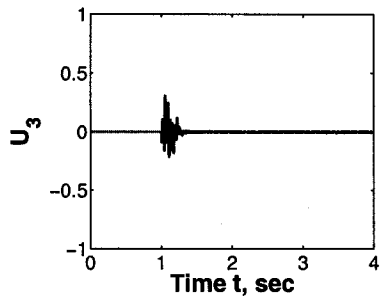

(c) Control input 3

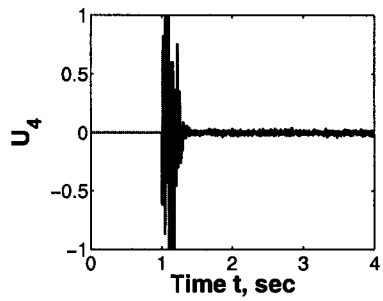

(d) Control input 4

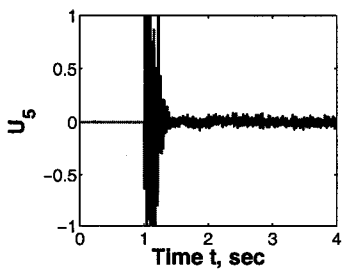

(e) Control input 5

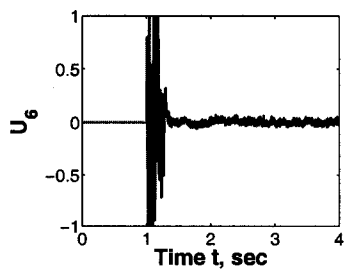

(f) Control input 6

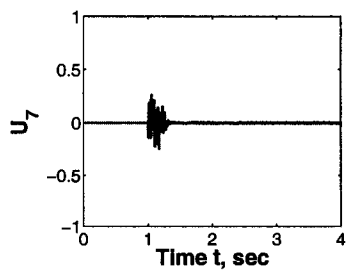

(g) Control input 7

Figure 56 Control inputs for the 4-mode 3-D chaotic panel flutter at $\lambda = 440$ and $\Delta T/\Delta T_{cr} = 8$ using MFC.

CHAPTER VII

CONCLUSIONS AND FUTURE WORK

VII.1 Conclusions

Linear Quadratic Regulator(LQR) with Extended Kalman Filter (EKF) is used to suppress the nonlinear large amplitude free vibrations and panel flutter with or without thermal stresses. For the free vibration suppression case, the results indicate that by linearizing the system in every time step, the EKF can provide a state estimation for the LQR control based on good initial state estimations. However, if the free vibration is changed due to unknown causes, the initial state estimation may be not good, then the LQR/EKF control approach results in bad performance in the suppression of the free vibration. In this paper, a simple modal frequency identification algorithm is proposed. It can identify the changed modal frequency and update the accurate initial state estimation needed for EKF. From the beam and composite plate examples studied, the adaptive LQR/EKF controller is efficient in vibration suppression even when the unknown sudden changes happened. For the placement of the self-sensing actuators, the NFCG, H_2 and NKFEG norm methods are employed and compared for optimal location selection. PZT5A self-sensing actuators are studied. The results show that both NFCG and H_2 norm can give efficient control. But different method should be chosen considering the number of inputs/ouput. The inputs/outputs are fewer, the connection of self-sensing actuators is simpler, so the method resulting in smaller number of inputs/outputs will be preferred to apply. The adaptive control of free vibration of beams and composite plates is a learning

process for a more practical application: panel flutter suppression.

For panel flutter suppression case, LQR/EKF controller can achieve good performance. A 2-D and a composite 3-D panel are considered. When there are no thermal loads, the panel presents limit cycle oscillation, which is similar to free vibration case. But for free vibration case, the first mode occupies more than 95 percentage of the whole motion, so when the first mode of the motion is estimated or controlled, the whole vibration is easy to be handled. But in panel flutter case, the first mode occupies around 50 percent of the whole motion, other modes' motions need to be considered; also aerodynamic force should be considered in the control process, so more control efforts are needed in panel flutter suppression. Since every modes should be considered, more sensors are needed in estimation of panel flutter. But aerodynamic damping will make panel flutter converge to some particular motions no matter what initial states it has, which also makes the estimation states from EKF converge to real states much faster than free vibration when sensors supply enough information. So LQR/EKF can give good control performance for panel flutter.

When there are thermal loads on the panels, they become stiffer and produces thermal post-buckling. Limit cycle oscillation(including periodic motions), static deflections and chaotic motions happen under the condition. Controlling of static responses and chaotic motions of panel flutter is studied and performed successfully in this thesis. From the results, it is proved that MFC is more efficient in the suppression than PZT5A since fewer MFC's are needed to control the same condition. Estimation of motions is very important in the control of static and chaotic responses case. EKF has the same nonlinear structure as the original system and uses linear approximation

over smaller ranges of state space, so it has good robustness. Although the estimation is not so actually tracking with the original motion, it is enough for motion control. And control settling time is depend on the estimator, the faster it converges to real motion, the faster the motion can be controlled.

VII.2 Future Work

After suppressing free vibration and panel flutter with or without thermal loads successfully, more practical aspects need to be considered in this problem.

First, for free vibration case, thermal loads can also be considered. For panel flutter case, flow angle during flight can be considered. Although analysis results for above cases has been discussed in some literature, but control of those conditions still needed to be developed.

Second, for panel flutter, when flow angle, dynamic pressure λ and thermal loads change, adaptive or other intelligent controller can be designed to solve such problems. Since under changing thermal stresses, panel flutter's motion will change between LCO, periodic and chaotic motions, which makes controller's design more challengeable. But it is also a very practical problem which will take place in flight.

Third, other efficient optimal actuator and sensor location method needs to be developed. NFCG and NKFEG norm methods work well in this research, but they are suitable for linear feedback compensator. When nonlinear compensator is designed, such as fuzzy and neural controller, it's hard to apply feedback gains to calculate NFCG or NKFEG norms. So more general method is needed to be derived.

Fourth, other finite element model such as triangle element can be tried to model

the system and find the optimal locations of actuators and sensors. Since angle and shape of actuators and sensors can be considered when using triangle element or other irregular element, maybe better control performance can be obtained by a different angle or shape.

Finally, experimental validation is needed to verify the LQR/EKF and system ID method in suppression of free vibration and panel flutter with or without thermal effects.

BIBLIOGRAPHY

[1] Zhou, R. C., Lai, Z. H., Xue, D. Y., Huang, J. K., and Mei, C., "Suppression of Nonlinear Panel Flutter with Piezoelectric Actuators Using Finite Element Method," *AIAA Journal*, Vol. 33, No. 6, 1995, pp. 1098–1105.

[2] Zhou, R. C., Mei, C., and Huang, J.-K., "Suppression of Nonlinear Panel Flutter at Supersonic Speeds and Elevated Temperatures," *AIAA Journal*, Vol. 34, No. 2, 1996, pp. 347–354.

[3] Park, J.-S. and Kim, J.-H., "Suppression of Aero-thermal Large Deflections and Snap-through Behaviors of Composite Panels Using Macro Fiber Composite Actuators," *Smart Materials and Structures*, Vol. 13, No. 6, 2004, pp. 1448–1459.

[4] Moon, S.-H. and Kim, S.-J., "Suppression of Nonlinear Composite Panel Flutter with Active/Passive Hybrid Piezoelectric Networks Using Finite Eelement Methods," *Computers and Structures*, Vol. 59, No. 4, 2003, pp. 525–533.

[5] Woinowsky-Krieger, S., "The Effect of an Axial Force on the Vibration of Hinged Bars," *Journal of Applied Mechanics*, Vol. 17, No. 1, 1950, pp. 35–36.

[6] Chu, H. N. and Herrmann, G., "Influnce of Large Amplitudes on Free Flexural Vibrations of Rectangular Elastic Plates," *Journal of Applied Mechanics*, Vol. 23, No. 4, 1956, pp. 532–540.

[7] Srinivasan, A. V., "Large Amplitude-Free Oscillation of Beams and Plates," *AIAA Journal*, Vol. 3, No. 10, 1965, pp. 1951–1952.

[8] Srinivasan, A. V., "Nonlinear Vibrations of Beams and Plates," *Int. J. Nonlinear Mechanics*, Vol. 1, No. 3, 1966, pp. 179–191.

[9] Ray, J. D. and Bert, C. W., "Nonlinear Vibratinos of a Beam with Pinned Ends," *Journal of Engineering for Industry*, Vol. 91, No. 4, 1969, pp. 997–1004.

[10] Bennett, J. A. and Eisley, J. G., "A Multiple Degree-of-Freedom Approach to Nonlinear Beam Vibrations," *AIAA Journal*, Vol. 8, No. 4, 1970, pp. 734–739.

[11] Pandalai, K. A. V. and Sathyamoorthy, M., "On the Modal Equtions of Large Amplitude Flexural Vibration of Beams, Plates, Rings and Shells," *Int. J. Nonlinear Mechanics*, Vol. 8, No. 3, 1973, pp. 213–218.

[12] Mei, C., "Nonlinear Vibration of Beams by Matrix Displacement Method," *AIAA Journal*, Vol. 10, No. 3, 1972, pp. 355–357.

[13] Mei, C., "Finite Element Displacement Method for Large Amplitude Free Flexural Vibrations of Beams and Plates," *Computers & Structures*, Vol. 3, No. 1, 1973, pp. 163–174.

[14] Mei, C., "Finite Element Analysis of Nonlinear Vibration of Beam Columns," *AIAA Journal*, Vol. 11, No. 1, 1973, pp. 115–117.

[15] Burgreen, D., "Free Vibrations of a Pin-Ended Column with Constant Disturbance Between Pin Ends," *Journal of Applied Mechanics*, Vol. 18, No. 2, 1951, pp. 135–139.

[16] Evensen, D. A., "Nonlinear Vibrations of Beams with Various Boundary Conditions," *AIAA Journal*, Vol. 6, No. 2, 1968, pp. 370–372.

[17] Nayfeh, A. H., Mook, D. T., and Lobtiz, D. W., "Numerical-perturbation method for the nonlinear analysis of structural vibrations," *AIAA Journal*, Vol. 12, No. 9, 1974, pp. 1222–1228.

[18] Raju, I. S., Rao, G. V., and Raju, K. K., "Effect of Longitude or Inplane Deformaiton and Inertia on the Large Amplitude Flexural Vibrations of Slender Beams and Thin Plates," *Journal of Sound and Vibration*, Vol. 49, No. 3, 1976, pp. 415–422.

[19] Bhashyam, G. R. and Prathap, G., "Galerkin Finite Element Method for Nonlinear Beam Vibrations," *Journal of Sound and Vibration*, Vol. 72, No. 2, 1980, pp. 191–203.

[20] Srirangaraja, H. R., "Nonlinear Free Vibrations of Uniform Beams," *Journal of Sound and Vibrations*, Vol. 175, No. 3, 1994, pp. 425–427.

[21] Dumir, P. C. and Bhaskar, A., "Some Erroneous Finite Element Formulatios of Nonlinear Vibrations of Beams and Thin Plates," *Journal of Sound and Vibration*, Vol. 123, No. 3, 1988, pp. 517–527.

[22] Singh, G. and Rao, G. V., "Large-Amplitude Free Vibrations of Beams—A Discusion on Various Formulaitons and Assumptions," *Journal of Sound and Vibration*, Vol. 142, No. 1, 1990, pp. 77–85.

[23] Pillai, S. R. R. and Rao, B. N., "On Nonlinear Free Vibrations of Simply Supported Unifrom Beams," *Journal of Sound and Vibration*, Vol. 159, No. 3, 1992, pp. 527–531.

[24] Shi, Y., Lee, R. Y. Y., and Mei, C., "Finite Element Method for Nonlinear Free Vibrations of Composite Plates," *AIAA Journal*, Vol. 35, No. 1, 1997, pp. 159–166.

[25] Chladni, E. F. F., *Entdeckungen uber die Theorie des Klanges*, Leipzig, 1787.

[26] von Karman, "Festigkeitsprobleme im maschinenbau," *Encyklopaedie der Mathematischen Wissenschaften*, 1910.

[27] Rao, S. R., Sheikn, A. H., and Mukhopadhyay, M., "Large-Amplitude Finite Element Flexural Vibration of Plates/Stiffened Plates," *The Journal of the Acoustical Society of America*, Vol. 93, No. 6, 1993, pp. 3250–3257.

[28] Chia, C. Y., "Geometrically Nonlinear Behavior of Composite Plates: a Review," *Applied Mechanics Reviews*, Vol. 41, No. 12, 1988, pp. 439–451.

[29] Alhazza, K. A. and Alhazza, A. A., "A Review of the Vibrations of Plates and Shells," *The Shock and Vibration Digest*, Vol. 36, No. 5, 2004, pp. 377–395.

[30] A. Harada, Y. K. and Yamada, G., "Reduced-Order Nonlinear Modal Equations of Plates Based on the Finite Element Method," Eighth International Conference on Recent Advances in Structural Dynamics, Southampton, England, July 2003.

[31] Saha, K. N., Misra, D., Pohit, G., and Ghosal, S., "Large Amplitude Free Vibration Study of Square Plates Under Different Boundary Conditions Through a Static Analysis," *Journal of Vibration and Control*, Vol. 10, No. 7, 2004, pp. 1009–1028.

[32] Mei, C., Mace, B. R., and Jones, R. W., "Hybrid Wave/Mode Active Vibration Control," *Journal of Sound and Vibration*, Vol. 247, No. 5, 2001, pp. 765–784.

[33] Halkyard, C. R. and Mace, B. R., "Feedforward Adaptive Control of Flexural Vibration in a Beam Using Wave Amplitude," *Journal of Sound and Vibration*, Vol. 254, No. 1, 2002, pp. 117–141.

[34] Elliott, S. J. and Billet, L., "Adaptive Control of Flexible Waves Propagating in a Beam," *Journal of Sound and Vibration*, Vol. 163, No. 2, 1993, pp. 295–310.

[35] Meirovitch, L., Baruh, H., and Öz, H., "A Comparison of Control Techniques for Large Flexible Systems," *Journal of Guidance*, Vol. 6, No. 4, 1983, pp. 302–310.

[36] Inman, D. J., "Modal Decoupling Conditions for Distributed Control of Flexible Structures," *Journal of Guidance*, Vol. 7, No. 6, 1984, pp. 750–752.

[37] Inman, D. J., "Active Modal Control for Smart Structures," *Philosophical Transactions: Mathematics, Physical and Engineering Sciences*, Vol. 359, No. 1778, Jan. 2001, pp. 205–219.

[38] Zhang, J. F., "Optimal Control For Mechanical Vibration Systems Based on Second-Order Matrix Equations," *Mechanical Systems and Signal Processing*, Vol. 16, No. 1, 2002, pp. 61–67.

[39] Wang, D.-A. and Huang, Y.-M., "Robust Vibration Control of a Beam Using the H_∞-Based Controller with Model Error Compensator," *Journal of Sound and Vibration*, Vol. 254, No. 5, 2002, pp. 877–895.

[40] Xie, S. L., Zhang, X. N., Zhang, J. H., and Yu, L., "H_∞ Robust Vibration Control of a Thin Plate Covered with a Controllable Constrained Damping Layer," *Journal of Vibration and Control*, Vol. 10, No. 1, 2004, pp. 115–133.

[41] Abdel-Motagaly, K. and Mei, C., "On the Control of Nonlinear Free Vibrations of a Simply Supported Beam," *The 39th AIAA/ASME/ASCE/AHS/ASC Structures, Structural Dynamics and Materials Conference*, Long Beach, CA, April 1998, pp. 3266–3278.

[42] Yu, Y. G. and Zhang, S. C., "Adaptive Backstepping Sychronization of Uncertain Chaotic System," *Choas Solitons and Fractals*, Vol. 21, No. 3, 2004, pp. 643–649.

[43] de Abreu, G. L. C. M. and Ribeiro, J. F., "A Self-organizing Fuzzy Logic Controller for the Active Control of Flexible Structures Using Piezoelectric Actuators," *Applied Soft Computing*, Vol. 1, No. 4, 2002, pp. 271–283.

[44] de Abreu, G. L. C. M. and Ribeiro, J. F., "On-Line Control of a Flexible Beam Using Adaptive Fuzzy Controller and Piezoeletric Actuators," *Revista Controle & Automação*, Vol. 14, No. 4, 2003, pp. 377–383.

[45] Hossian, M. A., Madkour, A. A. M., Dahal, K. P., and Yu, H., "Intelligent Active Vibration Control for a Flexible Beam System," Proceedings of the IEEE SMC UK-RI Chapter Conference 2004 on intelligent Cybernetic Systems, Londonderry, UK, Sept. 2004, pp. 85–89.

[46] Bailey, T. and and, J. E. H., "Distributed Piezoelectric-Polymer Active Vibration Control of a Cantilever Beam," *Journal of Guidance, Control and Dynamics*, Vol. 8, No. 5, 1985, pp. 605–611.

[47] Burke, S. E. and Hubbard, J. E., "Active Vibration Control of a Simply Supported Beam Using a Spatially Distributed Actuator," *IEEE Control System Magazine*, Vol. 7, No. 4, 1987, pp. 25–30.

[48] Anderson, E. H. and Hagood, N. W., "Simutaneously Piezoelectric Sensing/Actuation: Analysis and Application to Controlled Structures," *Journal of Sound and Vibration*, Vol. 174, No. 5, 1994, pp. 617–639.

[49] Demetriou, M. A., "Optimal Switching Policy of Smart Actuators in Flexible Structures," *Smart Structures and Materials 2001: Modeling, Signal Processing, and Control*, edited by V. S. Rao, Vol. 4326 of *Proceedings of the SPIE's Annual International Symposium on Smart Structures and Materials and NDE for Health Monitoring and Diagnostics*, Newport Beach, CA, March 2001, pp. 220–231.

[50] Narayanan, S. and Balamurugan, V., "Finite Element Modelling of Piezolaminated Smart Structures for Active Vibration Control with Distributed Sensors and Actuators," *Journal of Sound and Vibration*, Vol. 262, No. 3, 2003, pp. 529–562.

[51] Dimitriadis, E. K., Fuller, C. R., and Rogers, C. A., "Piezoelectric Actuators for Distributed Noise and Vibration Excitation of Thin Plate," Proceedings of

the 8th ASME Conference on failure prevention, reliability and stress analysis, Montreal, Canada, 1989, pp. 223–233.

[52] Chandrashekhara, K. and Agarwal, A. N., "Active Vibration Control of Laminate Composite Plates Using Piezoelectric Devices: a Finite Element Approach," *Journal of Intellegent Material Systems and Structures*, Vol. 4, No. 4, 1993, pp. 496–508.

[53] Caruso, G., Galeani, S., and Menini, L., "Active Vibration Control of an Elastic Plate Using Multiple Piezoelectric Sensors and Actuators," *Simulation Modelling Practice and Theory*, Vol. 11, No. 5, 2003.

[54] Moita, J. M. S., Correia, I. F. P., Soares, C. M. M., and Soares, C. A. M., "Active Control of Adaptive Laminated Structures with Bonded Piezoelectric Sensors and Actuators," *Computers and Structures*, Vol. 82, No. 17, 2004.

[55] Bent, A. A. and Hagood, N. W., "Improved Performance in Piezoelectric Fiber Composites Using Interdigitated Electrodes," Vol. 2441 of *SPIEs 1995 Symposium on Smart Structures and Materials*, San Diego, CA, Feb. 1995, pp. 196–212.

[56] Williams, R. B. and Inman, D. J., "An Overview of Composite Actuators with Piezoceramic Fibers," Proceedings IMAC-XX: Conference on Structural Dynamics, Westin Los Angeles Airport Hotel, Los Angeles, CA, Feb. 2002.

[57] Wilkie, W. K., Inman, D. J., Lioyd, J. M., and High, J. W., "Anisotropic Piezcomposite Actuator Incorporating Machine PMN-PT Single Crystal Fibers," Vol. 1889 of *The 45th AIAA/ASCE/AHS/ASC Structures, Structural Dynamics & Materials Conference*, Palm Springs, CA, April 2004.

[58] Jha, A. K. and Inman, D. J., "Sliding Mode Control of a Gossamer Structure Using Smart Materials," *Journal of Vibration and Control*, Vol. 10, No. 8, 2004, pp. 1199–1220.

[59] Sodano, H. A., Park, G., and Inman, D. J., "An Investigation Into the Performance of Macro-Fiber Composites for Sensing and Structural Vibration Applications," *Mechanical Systems and Signal Processing*, Vol. 18, No. 3, 2004, pp. 683–697.

[60] Schultz, M. R. and Hyer, M. W., "A Morphing Concept Based on Unsymmetric Composite Lamminate and Piezoceramic MFC Actuators," Vol. 1806 of *45th AIAA/ASME/ASCE/AHS/ASC Structures, Structural Dynamics & Materials Conference*, Palm Springs, CA, April 2004, pp. 1–13.

[61] Abdel-Motagaly, K., *Finite Element Analysis and Active Control for Nonlinear Flutter of Composite Panes Under Yawed Supersonic Flow*, Ph.D. thesis, Department of Aerospace Engineering, Old Dominion University, Norfolk, VA, Dec. 2001.

[62] Gawronski, W. K., *Actuator and Sensor Placement for Structral Testing and Control*, chap. 8, Acedemic Press Inc., San Deigo, CA, 1996, pp. 223–272.

[63] Wang, S. Y., Quek, S. T., and Ang, K. K., "Optimal Placement of Piezoelectric Sensor/Actuator Pairs for Vibration Control of Composite Plates," *Smart Structures and Materials 2002: Modeling,Signal Processing, and Control*, edited by V. S. Rao, Vol. 4693 of *proceedings of SPIE*, San Diego, CA, March 2002, pp. 461–471.

[64] D. Halim, S. R. M., "An Optimization Approach to Optimal Placement of Collocated Piezoelectric Actuators and Sensors on a Thin Plate," *Mechatronics*, Vol. 13, No. 1, 2003, pp. 27–47.

[65] Demetriou, M. A. and Grigoriadis, K. M., "Collocated Actuator Placement in Structural Systems Using an Analytical Bound Approach," Proceedings of the 2004 American Control Conference, Boston, MA, 2004, pp. 1604–1608.

[66] Demetriou, M. A., "A Numerical Algorithm for the Optimal Placement of Actuators and Sensors for Flexible Structures," Proceedings of the 2004 American Control Conference, Chicago, Illinois, June 2000, pp. 2290–2294.

[67] Fahroo, F. and Demetriou, M. A., "Optimal Actuator/Sensor Location for Active Noise Regulator and Tracking Control Problem," *Journal of Computational and Applied Mathematics*, Vol. 114, No. 1, 2000, pp. 137–158.

[68] Beven, J. S., "Piezoceramic Actuator Placement for Acoustic Control of Panels," Tech. Rep. CR-2001-211265, NASA, Old Dominion University, Norfolk, Virginia, Dec. 2001.

[69] Maxwell, N. D. and Asokanthan, S. F., "Optimally Distributed Actuator Placement and Control for a Slewing Single-Link Flexible Manipulator," *Smart Materials and Structures*, Vol. 12, No. 2, 2003, pp. 287–296.

[70] Dowell, E. H., "Panel Flutter: A Review of the Aeroelastic Stability of Plates and Shells," *AIAA Journal*, Vol. 8, No. 3, 1970, pp. 385–399.

[71] Mei, C., Abdel-Motagaly, K., and Chen, R., "Review of Nonlinear Panel Flutter at Supersonic and Hypersonic Speeds," *Applied Mechanics Review*, Vol. 52, No. 10, 1999, pp. 321–332.

[72] Abdel-Motagaly, K., Duan, B., and Mei, C., "Nonlinear Response of Composite Panels Under Combined Acoustic Excitation and Aerodynamic Pressure," *AIAA Journal*, Vol. 38, No. 9, 2000, pp. 1534–1542.

[73] Guo, X. and Mei, C., "Using Aeroelastic Modes for Nonlinear Panel Flutter at Arbitrary Supersonic Yawed Angle," *AIAA Journal*, Vol. 41, No. 2, 2003, pp. 272–279.

[74] Azzouz, M. S., Guo, X., Przekop, A., and Mei, C., "Nonlinear Flutter of Cylindrical Shell Panels Under Yawed Supersonic Flow Using FE," *The 45th AIAA/ASME/ASCE/AHS/ASC Structures, Structural Dynamics and Materials Conference*, No. 2043, AIAA, Palm Springs, CA, April 2004, pp. 1–18.

[75] Duan, B. and Mei, C., "Nonlinear Response of Thermal Protection System at Supersonoic Speeds," No. 1659 in 42nd AIAA/ASME/ASCE/AHS/ASC Structures, Structral Dynamics, and Materials Conference and Exhibit, AIAA, AIAA, Seatle, WA, April 2001.

[76] Cheng, G., Lee, Y. Y., and Mei, C., "Flow Angle, Temperature, and Aerodynamics Damping on Supersonic Panel Flutter Stability Boundary," *Journal of Aircraft*, Vol. 40, No. 2, 2003, pp. 248–255.

[77] Cheng, G. and Mei, C., "Finite Element Modal Formulation for Hypersonic Panel Flutter Analysis with Thermal Effects," *AIAA Journal*, Vol. 42, No. 4, 2004, pp. 687–695.

[78] Sadri, A. M., Wright, J. R., and Wynne, R. J., "LQG Control Design for Panel Fluttre Suppression Using Piezoelectric Actuators," *Smart Materials and Structures*, Vol. 11, No. 6, 2002, pp. 834–839.

[79] Kim, D., Han, J., and Lee, I., "Application of Fiber Optic Sensor and Piezoeletric Actuator to Flutter Suppression," *Journal of Aircraft*, Vol. 41, No. 2, 2004, pp. 409–411.

[80] Duan, B., Abdel-Motagaly, K., Guo, X., and Mei, C., "Suppression of Supersonic Panel Flutter and Thermal Deflection Using Shape Memory Alloy," No. 1513 in 44th AIAA/ASME/ASCE/AHS Structures, Structural Dynamics, and Materials Conference, Norfolk, 7–10 April 2003, pp. 1–10.

[81] Bogner, F. K., Fox, R. L., and Schmit, L. A., "The Generation of Inter-Element Compatible Stiffness and Mass Matrices by the Use of Interpolation Formulas," Tech. Rep. AFFDL-TR-66-80, Wright-Patterson AFB, OH, 1966.

[82] Azzouz, M. S., Mei, C., Bevan, J. S., and Ro, J. J., "Finite Element Modeling of MFC/AFC Actuators and Performance of MFC," *Journal of Intelligent Materials Systems and Structures*, Vol. 12, No. 9, 2001, pp. 601–612.

[83] Bevan, J. S., *Analysis and Testing of Plates with Piezoelectric Sensors And Actuators*, Master's thesis, Department of Aerospace Engineering, Old Dominion University, Norfolk, VA, 1997.

[84] Guo, X., *Shape Memory Alloy Applications on Control of Thermal Buckling, Panel Flutter and Random Vibration of Composite Panels*, Ph.D. thesis, Old Dominion University, Norfolk, VA, May 2005.

[85] Grewal, M. S. and Andrews, A. P., *Kalman Filtering: Theory and Practice Using MATLAB*, chap. 5, John Wiley & Sons, Inc., New York, 2nd ed., 2001, pp. 175–184.

[86] Chen, C.-W., Juang, J.-N., and Huang, J.-K., "Adaptive Linear System Identification and State Estimation," *Control and Dynamic Systems: Advances in Theory and Applications*, edited by C. T. Leondes, Vol. 57 of *Multidisciplinary Engineering Systems: Design and Optimization Techniques and Their Application*, Academic Press, Inc., 1993, pp. 331–368, an invited chapter.

[87] Hsiao, M.-H., Huang, J.-K., and Cox, D. E., "Iterative LQG Controller Design Through Closed-Loop Identification," *ASME Journal of Dynamic Systems, Measurement, and Control*, Vol. 118, No. 2, 1996, pp. 366–372.

[88] Przekop, A., *Nonlinear Response and Fatigue Estimation of Aerospace Curved Surface Panels to Acoustic and Thermal Loads*, Ph.D. thesis, Old Dominion University, Norfolk, VA, Dec. 2003.

[89] Dormand, J. R. and Prince, P. J., "A Family of Embedded Runge-Kutta Formulae," *Journal of Computational and Applied Mathematics*, Vol. 6, No. 1, 1980, pp. 19–26.

VITA

Qinqin Li

Department of Aerospace Engineering

Old Dominion University

Norfolk, VA 23529

EDUCATION

- M.S., Aerospace Engineering, Old Dominion University, Norfolk, Virginia, Aug. 2005 (Expected)

  Thesis Title: Active Control of Large Amplitude Nonlinear Free Vibrations and Nonlinear Supersonic Panel Flutter of Beams and Composite Plates Using Piezoelectric Self-sensing Actuators

  Advisor: Prof. Chuh Mei

- First-year graduate student, Navigation, Guidance and Control, Civil Aviation University of China, Tianjin, P.R. China, Sep. 2002-July 2003

  Advisor: Prof. Ke-Qiang Hua

- B.E., Electrical Engineering and Automation, Civil Aviation University of China, Tianjin, P.R. China, July 2002

PUBLICATION

- "Active control of nonlinear free vibration of beams and composite plates using piezoelectric self-sensing actuators," AIAA, 46th Structures, Structural Dynamics and Materials Conference, Austin, Texas, Apr. 18th-21st, 2005, AIAA-2005-2120.

PROFESSIONAL ACTIVITIES

- "Active control of nonlinear free vibration of beams and composite plates using piezoelectric self-sensing actuators," Research Day, Hampton Roads Region in Virginia, Norfolk, Virginia, Apr. 6th, 2005.
- "Fuzzy logic control of large amplitude nonlinear supersonic panel flutter using piezoelectric actuation," Research Day, Hampton Roads Region in Virginia, Norfolk, Virginia, Apr. 6th, 2005.
- "Shape memory alloy applications on control of thermal buckling and supersonic panel flutter of composite panels," Research Day, Hampton Roads Region in Virginia, Norfolk, Virginia, Mar. 23rd and 24th, 2004.
- "Non-linear flutter of cylindrical shell panels under supersonic flow using finite elements," Research Day, Hampton Roads Region in Virginia, Norfolk, Virginia, Mar. 23rd and 24th, 2004.

Typeset using LaTeX.